Diogo Miguel Vieira Alves de Carvalho

Licenciado em Ciências de Engenharia Civil

Simplified analysis of RC beam and beam-column elements under blast loading

Dissertação para obtenção do Grau de Mestre
em Engenharia Civil - Perfil Estruturas

Orientador: Professora Doutora Ildi Cismașiu
Faculdade de Ciências e Tecnologia, Universidade Nova de Lisboa

Co-orientador: Professor Doutor Corneliu Cismașiu
Faculdade de Ciências e Tecnologia, Universidade Nova de Lisboa

Júri:

Presidente: Professor Doutor Válter José da Guia Lúcio
Professor Associado da Faculdade de Ciências e Tecnologias da Universidade Nova de Lisboa

Arguente: Professor Doutor Hugo Rebelo
Professor Auxiliar na Universidade Lusófona

Vogal: Professora Ildi Cismașiu
Faculdade de Ciências e Tecnologia, Universidade Nova de Lisboa

NOVA SCHOOL OF SCIENCE & TECHNOLOGY

Novembro de 2021

Acknowledgments

The following is a list of the people helped materialize the work present in this dissertation, through technical guidance, support and attention.

To my advisor, Professor Ildi Cismașiu, for providing me the opportunity to learn and work with her with ever present availability to answer any questions or solve any issues. I wish to express my deepest gratitude for her patience and attention.

To my co-advisor, Professor Corneliu Cismașiu, for the invaluable advice in all matters related to the development of this dissertation.

To Professor Jin-Song Pei of the School of Civil Engineering and Environmental Science of the University of Oklahoma for her invaluable help in the implementation of the solving scheme.

To all the Professors in the Civil Engineering department at FCT-UNL, who ensured my successful growth as a student.

To my parents and grandparents, for all the love and for allowing me to grow freely and learn from my mistakes, however many.

To my girlfriend, Daniela, for the perpetuate love and affection. This work would not be made possible had not been for her.

Abstract

The present work aims to provide a non-linear numerical tool capable of analysing the structural response of reinforced concrete beam and beam-column elements when subjected to blast loads.

The increasing frequency of explosion events, stemming from terrorist attacks resorting to improvised explosive devices, or from accidental misuse of hazardous substances has shined a new light on the topic of blast resistant structural design. Recently, many studies have been conducted to better understand how to improve the design of blast resistant solutions in newly constructed buildings, as well as to provide retrofitting reinforcement solutions to pre-existing ones. Columns are a key structural component in any building, supporting its weight and transferring it to the foundations. If many of these elements fail when subjected to a blast event, then the structure's load bearing capacity may be compromised, initiating its progressing collapse and endangering the lives of the people inside.

The work featured in the present dissertation entails the development of a simplified numerical tool that analyses structural elements subject to blast loads, using single-degree-of-freedom systems with equivalent properties. The numerical estimates are then compared with experimental data found in the literature to assess the quality of the numerical predictions.

Both beam and beam-column output results differ no more than 25% from experimental the data. The possible sources of this discrepancy are investigated and it's concluded that the numerical model developed herein proves to be a good preliminary analysis tool for the estimate of the structural response of beams and beam-columns, when subjected to blast loads.

Keywords:

Beam, Beam-column, Non-linear dynamic analysis, Simplified SDOF numerical models, Blast load

Resumo

O presente trabalho visa o desenvolvimento de um modelo numérico não-linear simplificado capaz de analisar a resposta estrutural de vigas e pilares (vigas-coluna) de betão armado, quando sujeitos a cargas explosivas.

A frequência crescente de explosões, decorrentes de ataques terroristas com recurso a engenhos explosivos improvisados ou produzidas acidentalmente, quando substâncias perigosas são manuseadas de forma negligente ou derivadas da fraca manutenção de equipamentos, direcionou a atenção da comunidade científica para o tópico de projeto de estruturas resistentes a ações explosivas. Recentemente, muitos estudos têm sido conduzidos a fim de entender como melhorar o comportamento de soluções construtivas face a ações explosivas, bem como fornecer soluções de reforço a elementos estruturais pré-existentes. Os pilares são componentes estruturais fulcrais em qualquer edifício, suportando o seu peso, transferindo-o para as fundações. Se muitos desses elementos cederem quando submetidos a uma explosão, a capacidade portante da estrutura poderá ser comprometida, bem como a vida das pessoas que a utilizam.

O trabalho apresentado nesta dissertação envolve o desenvolvimento de um modelo numérico simplificado com o objetivo de analisar elementos estruturais, tais como vigas e pilares sujeitos a cargas explosivas, através de sistemas equivalentes de um grau de liberdade. Os resultados do modelo numérico são então comparados com dados experimentais encontrados na literatura, para avaliar as qualidades das simulações.

Os resultados obtidos, tanto para vigas como para pilares, não diferem mais que cerca de 25% dos dados experimentais. As possíveis fontes para esta discrepância são investigadas e conclui-se que o modelo numérico aqui desenvolvido revela-se como uma boa ferramenta para a estimativa da resposta estrutural deste tipo de elementos, quando submetidos a cargas explosivas.

Palavras chave:

Viga, Pilar, Análise dinâmica não linear, Modelos simplificados de 1 GDL, Carga explosiva

Contents

List of figures

List of tables

List of abbreviations, acronyms and symbols

Abbreviations

TNT Trinitrotoluene

Acronyms

DIF Dynamic Increase Factor

FCT Faculdade de Ciências e Tecnologia

IED Improvised Explosive Devices

RC Reinforced Concrete

SDOF Single-degree-of-freedom

SIF Strength Increase Factor

SBEDS Single-Degree-of-Freedom Blast Effects Design Spreadsheets

UFC Unified Facilities Criteria

UNL Universidade Nova de Lisboa

Symbols

α_e Homogenization factor

β Non-dimentional parameter resulting from the ratio between the top and bottom reinforcement areas; Coefficient that accounts for the duration of the loading

γ Safety coefficient; Specific heat ratio

δ Non-dimensional time

ε Nominal strain

$\dot{\varepsilon}$ Strain rate

η Non-dimensional length

ζ Distribution coefficient

θ Support rotation

μ Ductility ratio

$\phi(x)$ Normalized deflection shape function

ξ Damping ratio

ω Natural frequency; Mechanical reinforcement ratio

a Distance between the top of the cross-section to the compressed reinforcement's centroid

$A_{s,tot}$ Total area of longitudinal reinforcement

A_s Area of tensioned steel bars

A'_s Area of compressed steel bars

b Width; Exponential decay factor

c Damping coefficient

C_0 Ambient sound velocity

d Effective depth

e Eccentricity

e_0 Specific energy in undisturbed air

E_c Young's modulus of concrete

e_{EXP} Explosive specific energy

e_s specific energy in disturbed air

E_s Young's modulus of steel

e_{TNT} TNT's specific energy

F External excitation force

f_{ctm} Average tensle strength of concrete

f_c Yield strength of concrete

f_{dc} Dynamic strength of concrete

f_{dsu} Dynamic ultimate strength of steel

f_{dsy} Dynamic yield strength of steel

f_{su} Ultimate strength of steel

f_{sy} Yield strength of steel

h Height of the cross-section

I_g Moment of inertia of the gross cross-section

i_s Shock wave's positive phase's impulse

i_s^- Shock wave's negative phase's impulse

k Stiffness; Scaling constant; slenderness ratio

K_D Damping factor

k_I Uncracked stiffness

K_{LM} Load-mass factor

K_L Load factor

K_M Mass factor

K_R Resistance factor

L Element's span

L_0 Buckling length

L_{min} Minimum distance from the maximum displacement point on the element and the support

m Distributed mass

M_b Balance bending moment

M_{cr} Cracking bending moment

M_e Mass of the equivalent system

M_o Yield or ultimate bending moment in a cross-section without an acting axial load

M_{total} Total mass

M_y Bending moment at yield

N Axial load

p External distributed load

P Load

P_0 Pressure in undisturbed air

P_a atmospheric pressure

P_b Balance axial load

P_{max} Maximum allowed axial load

P_r Peak reflected overpressure

P_{so} Peak incident overpressure

P_{so}^- Nevative peak incident overpressure

P_s Pressure in disturbed air

$P_{\delta,i}$ Equivalent lateral load resulting from $P - \delta$ effects from time step i

R Offset distance

r Radius of gyration

R Resisting force

R_{cr} Cracking resistance

R_y Yield resistance

S Strength increase factor

t Time

t_0^+ Shock wave's positive phase's duration

t_0^- Shock wave's negative phase's duration

t_A Shock wave's arrival time

t_E time for the cross-section to yield

T_n Natural period

u Displacement

U Shock wave front velocity

u_{cr} Cracking displacement

u_y Displacement at yield

u_y Yield displacement

v_0 Particle velocity in undisturbed air

v_s Particle velocity in disturbed air

W Explosive's mass

W_E Equivalent explosive weight in TNT

W_g Bending modulus of the gross cross-section

W_I Uncracked bending moment

x Distance between the point of interest and the free edge

x_I and x_{II} Neutral axis positions of uncracked and cracked reinforced concrete cross-section

y Space-state variable vector

Z Scaled distance

$\bar{x}$ Distance from the neutral axis to the farthest fiber

Chapter 1

Introduction

1.1 Background

Since pre-historic times, Man has erected structures to provide him and his community with shelter against the elements. As Mankind evolved as a species, its needs for shelter became more demanding; as structures became larger in size, more thought needed to be put into their construction so as to not only provide people residing in them with comfort but also a sense of security that comes from a structurally sound construction. Up until the 20th century, regular, non-military structures needed only to be constructed with environmental loads in mind; wind, rain, gravity or earthquakes, for instance. In the recent decades however, due to attacks across the globe and casual mishandling of high explosive material, strategic civil engineering structures must be designed to withstand a new load: the blast wave.

The use of improvised explosive devices (IEDs) by terrorist organizations means that a single individual, with enough knowledge, may cause irreparable damage to infrastructure and human life, disrupting society as whole. On the other hand, gross misuse of explosive material can have equally devastating effects.

On August 4th, 2020, the port of Beirut was devastated by a large explosion, originating from a warehouse in the city's harbor. A cargo of roughly 2,750 tonnes of ammonium nitrate had been stored in the port, with improper safety conditions for the last 6 years. The resulting explosion seen in Figure 1.1(a), produced a shock wave that caused a seismic event of magnitude 3.3 in the surrounding areas [61]. Everything within a 124 m radius from the storage warehouse was instantly vaporized, with structures within 8 km away from ground zero still being damaged by the blast's yield, as Figure 1.1(b) illustrates. Death toll was 204 with more than 6500 others injured and 300 000 people left homeless [53]. The Beirut explosion is known now as one of the largest non-nuclear blasts in history [5], as it destroyed the city, causing a humanitarian crisis, all in the midst of the COVID-19 pandemic. This event represents how negligent handling of high explosive material can very well lead to catastrophe.

Another source of concern is the increasing usage of explosives in terrorist attacks, by employing the aforementioned IEDs. Figure 1.2 illustrates the
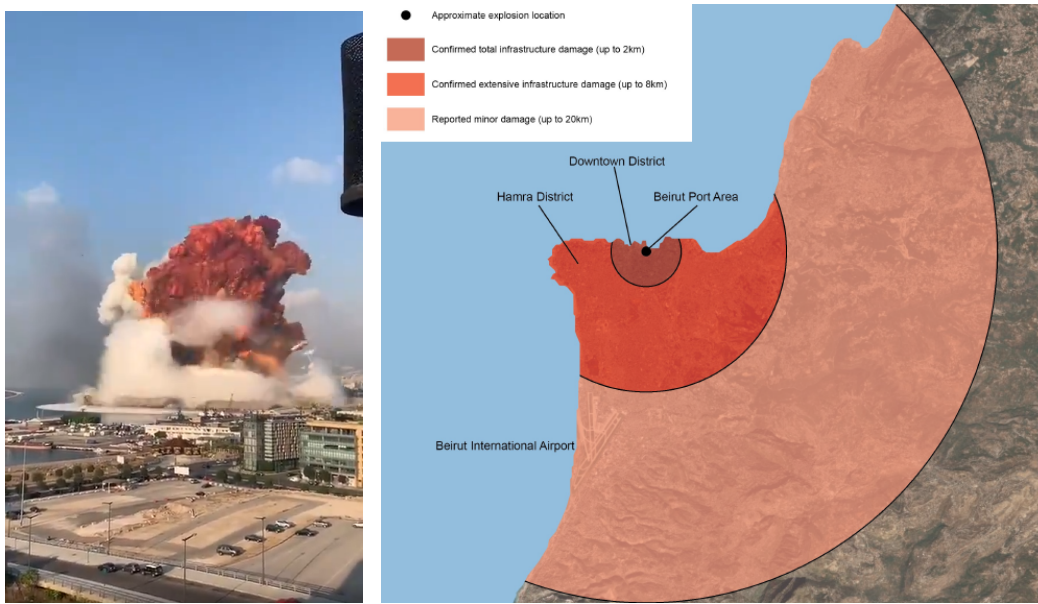
(a) Still frame from video recording of the explosion [7]

(b) Damage map, adapted from [28]

Figure 1.1: Beirut explosion, 2020

increasing frequency of these attacks, showing a significant rise in 2011. The data retrieved from the GTD database [24], accounts for all worldwide attacks that resorted to the use of explosive materials.
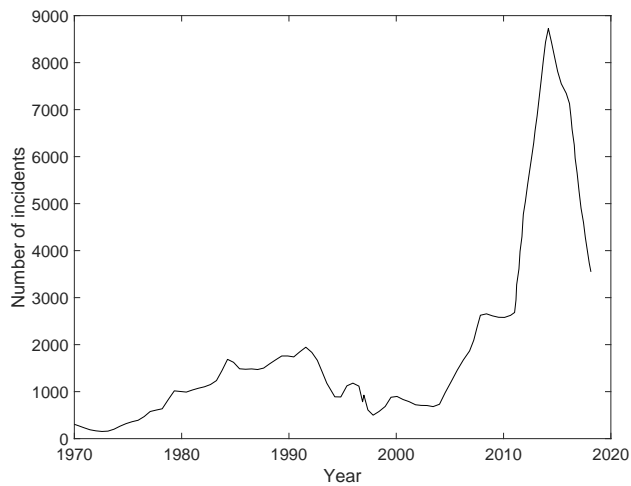
Figure 1.2: IED incidents over time [24]

Perhaps the most egregious example of malicious usage of explosives, at least in US soil, is the 1995 Oklahoma City bombing by two US citizens. On the morning of April 19, 1995, a Ford pickup truck transporting over 2 tons of an ammonium nitrate, nitromethane and diesel fuel mix, known as ANFO, was parked

under the Alfred P. Murrah Federal Building's day care center. After the 5 minute fuse set by one of the perpetrators ended, detonation occurred, killing 168 people and injuring several hundred more [2].

The resulting explosion vaporized about a third of the building as shown on Figure 1.3(b), while also destroying or damaging 324 other buildings in a 3 km radius. Prior to the terrorist airplane attacks of September 9th, 2001, the Oklahoma City bombing was the deadliest terrorist attack on US soil and remains as the deadliest act of domestic terrorism.

(a) Prior to the terrorist attack [58]   (b) Destroyed façade [66]
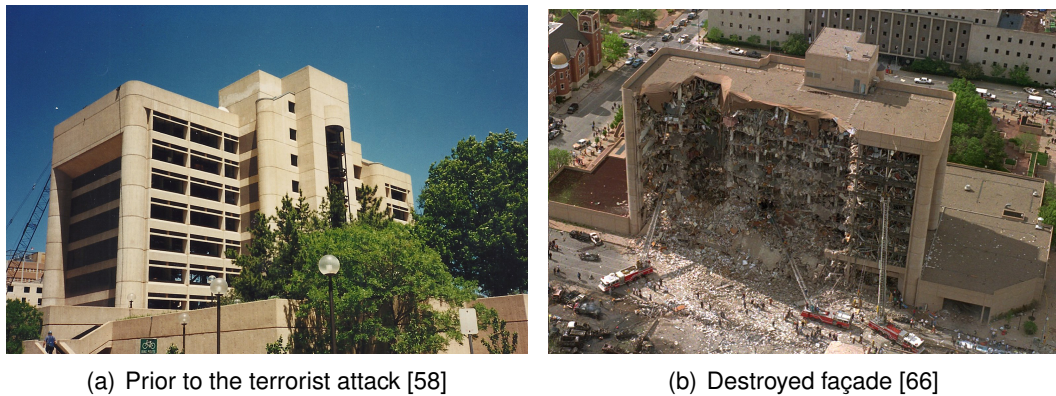
Figure 1.3: A.P.M. building before and after the explosion

The building wasn't designed to resist seismic loads and it's speculated that if that were the case, maybe the damage wouldn't have been so severe [17].

Blast design proves to be vital in strategic buildings, such as service stations, governmental buildings, hospitals, or nuclear plants. Figure 1.4 qualitatively illustrates the different performance of a structure, depending on the design ideals in which its construction was based on, when subjected to a blast load.
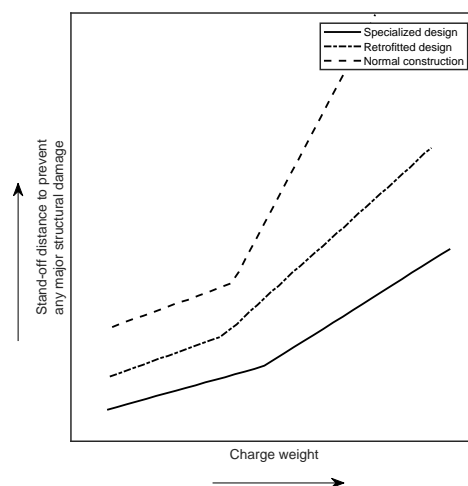
Figure 1.4: Standoff distance effects on building protection, adapted from [42]

One of the principal objectives in designing blast resistant structures is to prevent the progressive collapse of the structure as a whole, initiated by the failure of key structural elements, such as columns or beams. Perhaps the most known example of progressive collapse took place on September 9th, 2001, after the Twin Towers were hit by two airliners each (see Figure 1.5)(a). Following the collision of the aircraft, the two buildings resisted for roughly two hours before progressive collapse was initiated. The phenomena that took place is called "pancaking", as shown in Figure 1.5(b), where a number of structural elements on a given floor fail and cave in onto the floor bellow, which also fails as a result. This process continues until it reaches the ground floor.

(a) After airliner collision   (b) Collapse
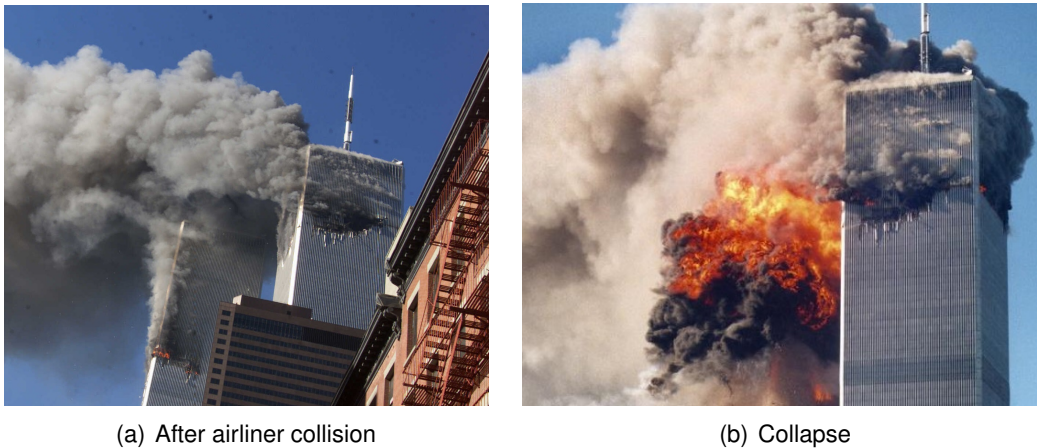
Figure 1.5: World Trade Center terrorist attack

The need for blast resistant design is thus made obvious and quick and reliable pre-design methods need to be employed.

Among the first ones to develop a high interest in the topic of the effects of blast loads on structures we recall B. Hopkinson [26] and C. Cranz [18]. During the decades after World War II, it was important to take blast loads into account for a resistant design in construction projects, especially for strategic buildings. In more recent times, the need for blast resistant design of structures was made evident in several events, particularly in the Middle-East and in South Asia. Examples of such events include the Easter of 2019 Sri Lanka bombings [48], the Beirut US embassy attack in 1983 [46], the November of 2008 Mumbai attacks [59] and the Mariott Hotel attack in Islamabad in 2008 [60], as seen in Figures 1.6(a) through (d).

Major advances in this field were verified in the last decades of the 20th century. Several analytical and experimental studies were conducted to understand the mechanical behavior of structures under blast loads. Out of a large number of publications are recalled Kinney and Graham [33], that published empirical expressions which define the behaviour of blast loads; Henrych and Major (1979) [25] presented the method of computing the peak positive overpressure, positive phase duration and positive phase impulse; Brode (1955) [10] accomplished a numerical integration that concluded in the definition of the dynamic and static pressures, the durations of pressure and velocity, and the

(a) Sri Lanka bombings, 2019 [6]

(b) Mumbai attacks, 2008 [47]

(c) Beirut US Embassy attack, 1983 [64]

(d) Marriott Hotel attack in Islamabad, 2008 [14]

Figure 1.6: Examples of terrorist bombing events

shock values. Kingery and Bulmash proposed the most commonly used set of expressions to model blast loads [32].

The present body of work aims to provide a simplified numerical tool with which to evaluate the preliminary structural response of reinforced concrete beam and beam-column subjected to blast loads. This tool serves as an alternative to more complex analysis tools in that it provides reasonably accurate results in a much shorter time frame.

1.2 Objectives and organization of the thesis

The present dissertation aims to construct a simplified numerical model able estimate the non-linear structural response of beam and beam-column reinforced concrete elements, when subjected to blast loads. This topic is aligned with one of the objectives of the research project PTDC/ECI-EST/31046/2017: PROTEDES - Proteção de Edifícios Estratégicos Contra Explosões/Protection of Strategic Buildings Against Blast Actions funded by Fundação para a Ciência e a Tecnologia (MCTES). The thesis is organized in 5 chapters. They are as follows:

- **Chapter 1** - Introduction

  This chapter provides background on the topic of blast loads and specifies the motivation and objectives of the present study.

- **Chapter 2** - Blast loads

  This chapter outlines relevant aspects regarding the topic of blast loads. It begins with the definition of the explosion phenomenon. It then details how to model it, by including several authors' semi-empirical expressions. It ends with a discussion on the chosen blast load formulation.

- **Chapter 3** - RC Structural response to blast load

  This chapter describes the behaviour of RC elements, when subjected to blast loads, by discussing the materials' response at high strain rates. Following this, the SDOF conversion method is presented, with emphasis on beam and beam-column elements. Next, all steps necessary to construct the equivalent system's resistance-deflection relationship are outlined, with special attention given to beam-column elements by describing the derivation of the moment-axial force diagram. The chapter ends with a discussion on $P - \delta$ effects.

- **Chapter 4** - Numerical implementation

  This chapter describes in detail the relevant aspects pertaining to the implementation of the numerical model, as well as the graphical user's interface that accompanies it. Every function and subroutine needed to run a model is detailed.

- **Chapter 5** - Model validation

  This chapter presents four case studies used to validate the numerical model: two beam and two beam-column elements from the literature are analysed and compared with experimental results. The case studies were chosen to test different support or loading conditions.

- **Chapter 6** - Conclusions and future work

  This chapter offers concluding remarks regarding the present study and proposes further developments.

  The numerical model is accompanied by a user's manual that can be consulted in Appendix A.

Chapter 2

Blast loads

This chapter focuses on the theoretical background on the topic of blast loads. It starts with a discussion on the usual shape of a pressure profile as well as the definition of the various parameters that allow for its definition. Several formulations are presented. This Chapter concludes with the description of the set of empirical formulas used to describe the blast waves in the present study.

2.1 Explosions

An explosion can be defined as a very rapid release of energy by means of deflagration or detonation of solid, fluid or gaseous substances. The resultant energy dissipates quickly and violently through blast waves, propulsion of fragments and thermal radiation [62]. The difference between deflagration and detonation is the speed of the reaction process that initiates the energy's release. Deflagration occurs when the reaction process' speed is less than the speed of sound. On the other hand, if the reaction process is supersonic, the explosion is then classified as a detonation. The priming of a round in the barrel of a firearm constitutes a deflagration event, while demolishing rock fronts in a quarry with the use of TNT is a detonation event.

This dissertation deals exclusively with detonation events on structures and any mention of blast waves and their effects refers to the detonation of explosives.

2.2 Characteristics of blast waves

The most common parameters used to define the blast wave phenomenon, such as the overpressure , impulse and duration times are reviewed. Several blast load formulations are presented next, along with the most common set of expressions used in modelling shock waves.

2.2.1 Scaling law

Among the most important parameters, when defining a shock wave are the distance between the source and the point of interest, and the mass of the explosive. However, such parameters may vary greatly which deems the definition of the characteristics of shock waves a tiresome process.

Therefore, to adequately compare blast scenarios with different characteristics a scaling law is necessary. The most commonly used scaling law, named the "cube-root" scaling law, was proposed by Hopkinson and Cranz [18, 26]. The cube-root scaling law states that in the case of two blast scenarios, as the ones depicted in Figure 2.1, the two scenarios are considered "similar" when an explosive with mass W at a distance R produces the same overpressure at the point of interest as an explosive with mass k^3W at a distance kR. The Hopkinson-Cranz law then defines the scaled distance Z by the following equation:

$$Z = \frac{R}{W_E^{1/3}} \tag{2.1}$$

where W_E is the explosive's equivalent TNT mass. The use of this parameter, as opposed to using the real explosive's mass is done to homogenize the calculation of the scaled distance, using a reference explosive type.
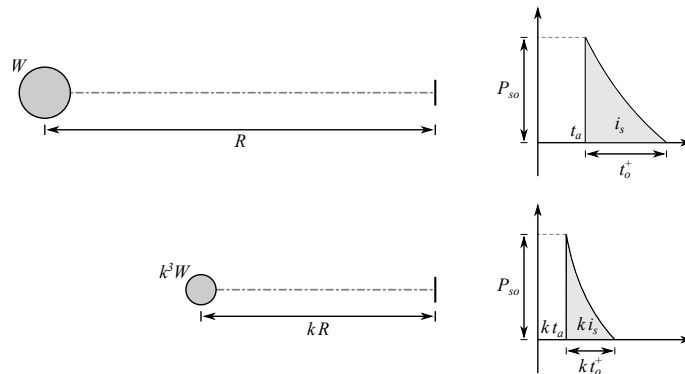
Figure 2.1: Hopkinson-Cranz scaling law, adapted from [52]

The explosive's equivalent TNT mass is given by the following equation:

$$W_E = \frac{e_{EXP}}{e_{TNT}} W_{EXP} \tag{2.2}$$

where e_{EXP} and W_{EXP} are the explosive's specific energy and mass, respectively and e_{TNT} is the specific energy of TNT.

2.2.2 Blast wave parameters

Blast waves are modeled by a pressure profile where the resultant pressure from the detonation of the explosive material is plotted against time, as seen in Figure 2.2. After the time t_A it takes the shock front to reach the point of

interest the local atmosphere suffers an instantaneous rise of pressure P_{so}, which decays at an exponential rate until it reaches ambient pressure again at time t_0^+, the positive phase's duration. What follows is the blast wave's negative phase characterized by a maximum negative pressure P_{so}^- and duration t_0^-, until standard atmospheric pressure is resumed. Integrating the blast wave's function in its positive and negative phases outputs the impulse i_s for the positive phase and i_s^- for the negative phase, respectively. A quick glance at Figure 2.2 establishes the difference in magnitude between both stages. This difference, coupled with the notion that the suction phenomena produced during the negative phase aids in reestablishing equilibrium after the detrimental effects of the positive phase, often means it's conservative to ignore the negative phase of the explosion. However, in cases where the negative phase's impulse surpasses its positive counterpart, it may no longer be acceptable to forgo taking the negative phase into account [52]. The present study will only account for the positive phase of the pressure profile.
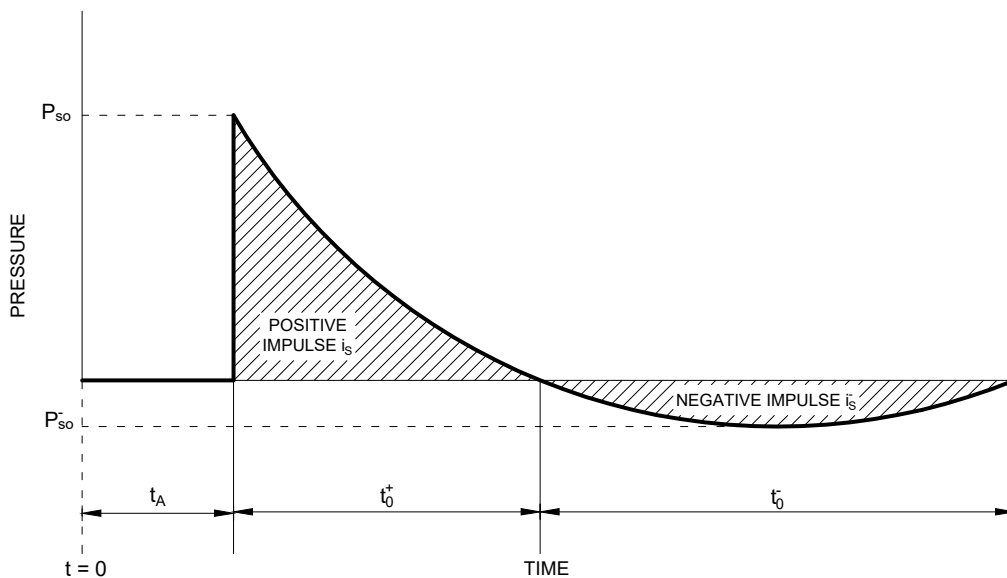
Figure 2.2: Idealized pressure profile shape for explosions, adapted from [62]

Numerous expressions have been proposed in the literature for the definition of the blast wave profile's positive phase.

The simplest form assumes the linear decay given in equation (2.3).

$$P(t) = P \left(1 - \frac{t}{t_0}\right) \tag{2.3}$$

where t_0 can take the value of t_0^+, thus preserving the positive phase's duration or it may take the value of $2i_s/P_{so}$, conserving the impulse i_s. Either of these procedures may prove to be advantageous when measuring the structural response of an element subjected to blast loads. Particularly, in cases where the impulse's duration is shorter than the structure's natural period, with ratios $t_0^+/T_n \leq 1/4$, the dynamic response is essentially controlled by the shock wave's impulse, rather than the shape of the pressure profile [16]. In such cases, it's acceptable to approximate

the pressure profile as a triangular shape [62].

A more precise definition of the pressure profile is given by the modified Friedlander's equation, also published in [4], defined as follows:

$$P(t) = P\left(1 - \frac{t}{t_0^+}\right) e^{-\frac{b\,t}{t_0^+}} \tag{2.4}$$

where b is the dimensionless blast wave decay coefficient.

By integrating equation (2.4) the impulse is obtained as shown in equation (2.5). The same procedure can be done with equation (2.3).

$$i_s = \int_0^{t_0^+} P(t)\,dt = \frac{P_{so}\,t_0^+}{b}\left[1 - \frac{1 - e^{-b}}{b}\right] \tag{2.5}$$

The definition of the blast wave decay factor b may be done with empirical formulations, such as those in [4]. However a more reliable and accurate approach, recommended in [33], is to equate equation (2.5) to i_s and iteratively solve for b. This process implies the previous determination of the impulse i_s via empirical expressions.

2.3   Empirical characterization of blast wave parameters

Several authors have investigated the topic of blast wave characterization with the derivation of expressions that compute the wave's overpressure, impulse and duration.

Early case studies include the works of Brode [10] in 1955, in which equation (2.6) for incident overpressure P_{so} is proposed.

$$P_{so} = \begin{cases} \dfrac{6.7}{Z^3} + 1 & , P_{so} > 10 \text{ bar} \\[3mm] \dfrac{0.975}{Z} + \dfrac{1.455}{Z^2} + \dfrac{5.85}{Z^3} - 0.019 & , 0.1 < P_{so} < 10 \text{ bar} \end{cases} \tag{2.6}$$

where Z [m/kg$^{1/3}$] is the scaled distance.

Similar expressions for the blast wave parameters were proposed by Henrych [25] in 1979, by publishing a series of semi-empirical set of equations derived by data fitting to experimental results. Much like in Brode's research, most of these expressions are piece-wise in nature, given the impracticality of curve fitting the experimental results with a single function. According to Henrych, the overpressure P_{so}, expressed in bars, is given by equation (2.7).

$$P_{so} = \begin{cases} \dfrac{14.072}{Z} + \dfrac{5.540}{Z^2} - \dfrac{0.357}{Z^3} + \dfrac{0.00625}{Z^4} & , 0.05 < Z < 0.3 \\[3mm] \dfrac{6.194}{Z} - \dfrac{0.326}{Z^2} - \dfrac{2.132}{Z^3} & , 0.3 < Z < 1 \\[3mm] \dfrac{0.662}{Z} + \dfrac{4.050}{Z^2} - \dfrac{3.228}{Z^3} & , 1 < Z < 10 \end{cases} \tag{2.7}$$

The expressions for the positive phase's impulse in bar·ms, proposed by Henrych are present in equation (2.8).

$$i_s = \begin{cases} \left(66.3 - \dfrac{111.5}{Z} + \dfrac{62.9}{Z^2} - \dfrac{10.04}{Z^3} \right) W^{1/3} & , 0.4 < Z \le 0.75 \\[3mm] \left(-3.22 - \dfrac{21.1}{Z} + \dfrac{21.6}{Z^2} - \dfrac{8.01}{Z^3} \right) W^{1/3} & , 0.75 < Z \le 3.0 \end{cases} \tag{2.8}$$

Henrych also proposed numerous expressions to estimate the positive phase's duration t_0^+. One of the simplest, albeit less precise is as follows.

$$t_0^+ = 1.5 W^{1/6} R^{1/2} \tag{2.9}$$

In 1985, Kinney and Graham published a book which covered, among many other topics related to blast waves, the characterization of blast wave parameters [33].

Kinney and Graham proposed equation (2.10) to estimate the incident overpressure P_{so}:

$$P_{so} = \frac{808 \left[1 + \left(\dfrac{Z}{4.5} \right)^2 \right] P_a}{\sqrt{1 + \left(\dfrac{Z}{0.048} \right)^2} \sqrt{1 + \left(\dfrac{Z}{0.32} \right)^2} \sqrt{1 + \left(\dfrac{Z}{1.35} \right)^2}} \tag{2.10}$$

where P_a is the atmospheric pressure. The positive phase's duration t_0^+ in ms and impulse i_s in bar·ms are given by equations 2.11 and 2.12, respectively.

$$t_0^+ = \frac{180 \sqrt{1 + \left(\dfrac{Z}{100} \right)^3} W_E^{1/3}}{\sqrt{1 + \left(\dfrac{Z}{40} \right)} \sqrt[6]{1 + \left(\dfrac{Z}{285} \right)^5}) \sqrt[6]{1 + \left(\dfrac{Z}{50000} \right)}} \tag{2.11}$$

where W_E is the explosive's equivalent TNT mass in kg.

$$i_s = \frac{0.067\sqrt{1 + \left(\dfrac{Z}{0.23}\right)^4}}{Z^2\sqrt[3]{1 + \left(\dfrac{Z}{1.55}\right)^3}} \qquad (2.12)$$

However, the most ubiquitous set of expressions used in blast analysis are the Kingery & Bulmash [32] semi-empirical polynomials, proposed in 1984. The proposed expressions were obtained by fitting to experimental results obtained from tests that took place in Canada in the 50's and 60's by using higher order polynomials and prove to be valid from scaled distances in the range $0.067 \leq Z \leq 39.97\,\text{m/kg}^{1/3}$. The Kingery & Bulmash method accounts for two distinct blast scenarios; the first is a spherical free airburst, in which the shock front retains its energy, suffering no reflection from its source to the point of interest; the second being a hemispherical surface burst, that suffers amplification by reflection, assuming the surface to be perfectly flat and rigid, magnifying its intensity. The use of this method is recommended by the US Dept. of Defence's UFC-340-02 manual [1] for the design of blast resistant structures, being employed as well by programs such as ABAQUS [56], AUTODYN [15] and LS-DYNA [35] for blast load analysis.

Given the nature of the proposed expressions, their use proves to be laborious. Thus, in 1994, Swisdak [57] presented a simpler set of expressions that output blast wave parameters with a 1% error, comparing to the polynomials proposed by Kingery and Bulmash [32]. In [57] the author details the polynomial coefficients that calculate the blast wave parameters. Each expression may have up to seven coefficients, from A to G. The equations have the following shape:

$$\begin{aligned} Function =\ & exp\big[A + B\,\ln(Z) + C\,\ln^2(Z) + \\ & + D\,\ln^3(Z) + E\,\ln^4(Z) + F\,\ln^5(Z) + G\,\ln^6(Z)\big] \end{aligned} \qquad (2.13)$$

where $Function$ represents the blast wave parameter to be calculated.

Computing the blast wave parameters via the Kingery & Bulmash method consists on finding the corresponding polynomial constants published in [57] and calculating the desired parameter.

However, if a graphical method is preferable, both UFC 3-340-02 [1] and the SBEDS Design Guide [62] provide figures with all parameters represented as a function of the scaled distance Z, as seen in Figure 2.3. In this case, all the designer needs to do is draw a vertical line to the corresponding Z value and all blast wave parameters are readily available.
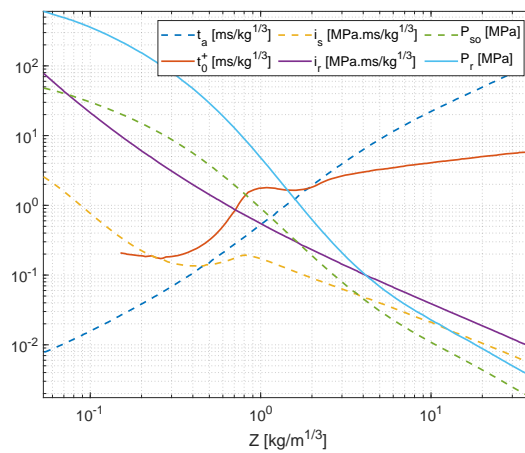
(a) Free-air burst parameters
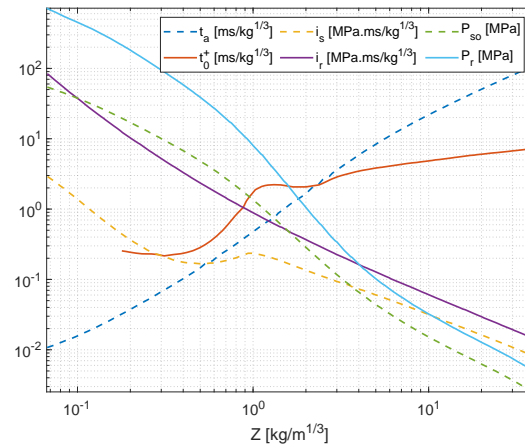
(b) Surface burst

Figure 2.3: Positive phase shock wave parameters [1]

2.3.1 The Rankine-Hugoniot relations

The Rankine-Hugoniot (R-H) relations are a set of expressions that define the conservation of mass, momentum and energy across a shock front that describe the relationship between states within the shocked air and the undisturbed air. The propagation of a shock wave travelling at velocity U, with pressure P, density ρ and particle velocity v through undisturbed air is illustrated in Figure 2.4 in a single dimension. The subscripts "0" and "s" indicate undisturbed air and disturbed air, respectively. It's worth noting that despite this being the most common graphic representation of the R-H relations, these can be applied in any number of dimensions.

Equations 2.14 through 2.16 define the conservation of mass, momentum and energy as a shock wave propagates.
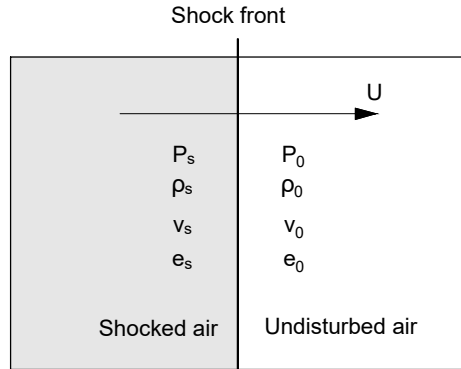
Figure 2.4: Properties of air travelling through a shock front at velocity U

$$\rho_s(U - v_s) = \rho_0 U \tag{2.14}$$

$$P_s - P_0 = \rho_0 U v_s \tag{2.15}$$

$$\frac{1}{2}\rho_0 \, U v_s^2 + \rho_0 U(e_s - e_0) = P_s v_s \tag{2.16}$$

2.4   Shock wave attenuation

The idealized representation of a shock wave in the form of equation (2.4) is a good approximation of reality, however it fails to account for the deformability of the element and its dimensions. As previously mentioned, shock wave profiles are usually simulated by assuming that the surface on which the wave is impinged on is infinite and perfectly rigid. However, if the element subjected to a shock wave is deemed as non-rigid, fluid-structure interactions must be considered. Additionally, if the surface of the element is finite, clearing effects must also be accounted for [54].

2.4.1   Reflection of blast waves

The study of the effects of incident blast waves may be conducted by assuming the shock wave is reflected on surfaces such as the ground or the targeted element. In this case, the shock wave's overpressure P_r is amplified, resulting in an also amplified impulse i_r, as Figure 2.5 illustrates. The pressure profile's positive and negative phases' durations remain unaltered.

To compute P_r one may resort to the Rankine-Hugoniot relations. Firstly, computing the air's density ρ_s with equation (2.17).

$$\rho_s = \rho_0 \frac{2\gamma + (\gamma + 1)P_r/P_a}{2\gamma + (\gamma - 1)P_r/P_a} \tag{2.17}$$

where P_a is the ambient pressure, ρ_0 is the ambient density and γ is the specific
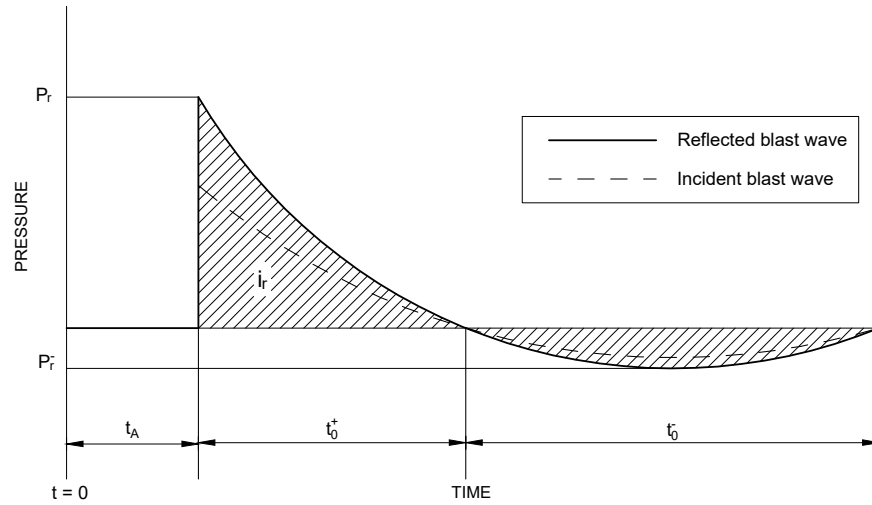
Figure 2.5: Reflected pressure time history

heat ratio. As stated in [43], by considering the air as an ideal gas, γ is equal to 1.4, which proves to be a good approximation for incident overpressure values of up to 2 MPa. All expressions relating to the calculation of P_r from this point on will be simplified assuming γ as equal to 1.4.

With γ equaling 1.4, equation (2.17) is simplified:

$$\rho_s = \rho_0 \frac{7 + 6P_{so}/P_a}{7 + P_{so}/P_a} \tag{2.18}$$

The particle velocity v_s is computed with equation (2.19).

$$v_s = \frac{5P_{so}}{7P_a} \frac{C_0}{\sqrt{1 + \frac{6P_{so}}{7P_a}}} \tag{2.19}$$

where C_0 is the ambient sound velocity.

Next, considering the magnitude of the dynamic pressure q, computed as follows:

$$q = \frac{1}{2}\rho_s v_s^2 \tag{2.20}$$

The shock wave's reflected pressure P_r is computed by equation (2.21).

$$P_r = 2P_{so} + 2.4q = 2P_{so}\frac{7 + 4P_{so}/P_a}{7 + P_{so}/P_a} \tag{2.21}$$

2.4.2 Fluid-structure interaction

The fluid-structure interaction effects take place when a blast load is imparted on a flexible structural element. As the structure deflects, there occurs an attenuation of the reflected impulse.

The way this attenuation is accounted for comes in the form of a correction in the reflected overpressure P_r and depends on the air density at the shock front ρ_s, the wave's propagation velocity U and the particle velocity v_s, as equation (2.22) relays.

$$P(t) = P_r - \rho_s U v(t) \tag{2.22}$$

The resulting P_r is the one used as the pressure P in equation (2.4).

2.4.3   Clearing effects of blast waves

As discussed previously, if a blast wave is simulated as being applied on a target with finite dimensions, clearing effects must be considered. Blast wave clearing takes place the instant the shock front encounters a target's free edges. At this instance, while the reflected shock front begins to reflect away from the element's surface, the incident shock front proceeds freely past the free edge, causing diffraction around it. The pressure differential associated with this phenomenon leads to the creation of a rarefaction wave that travels along the loaded surface, which begins at the boundaries and propagates towards the center of the target surface. The rarefaction wave reduces the pressure imparted on the surface which in turn reduces the total positive impulse acting on the target, as illustrated in Figure 2.6.
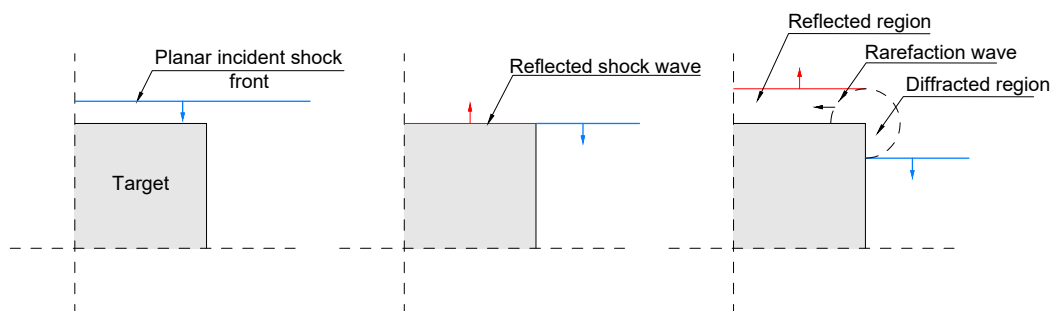
Figure 2.6: Blast wave diffraction around a finite target resulting in propagation of a rarefaction clearing wave, adapted from [54]

Hudson [27] conducted a study on this topic and presented the spacial and temporal distribution of a rarefaction wave originating from the impact of a planar blast wave on a rigid target with finite dimensions. The method assumes that the rarefaction wave is weak i.e that it propagates along the loaded surface at the ambient sound velocity C_0 and that the blast wave is planar, which means the target's lateral dimensions are sufficiently small in comparison with the standoff distance and the target's depth is large enough such that no clearing waves propagate from the back of the target at the time of loading.
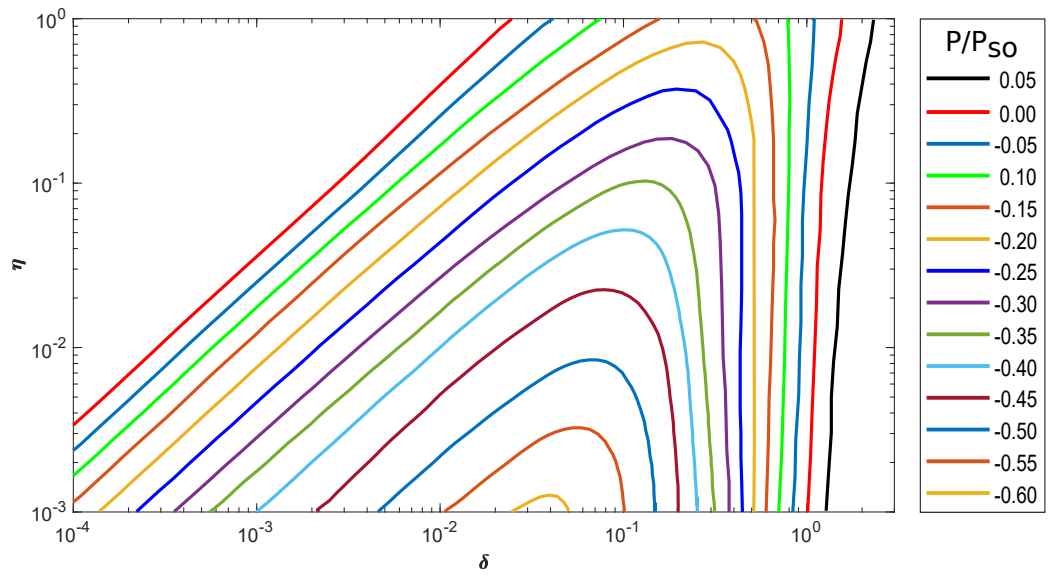
Figure 2.7: Spacial and temporal distribution of rarefaction wave, adapted from [27]

The proposed method describes the relief pressure P normalized against the peak incident overpressure, as a function of two non-dimensional length η and non-dimensional time δ, as shown in Figure 2.7.

These parameters are computed as follows in equations 2.23 and 2.24.

$$\eta = \frac{x}{C_0 t_0^+} \tag{2.23}$$

where x is the distance between the point of interest and the free edge.

$$\delta = \frac{t}{t_0^+} - \eta \tag{2.24}$$

Chapter 3

RC structural response to blast load

The following chapter describes how blast loading affects reinforced concrete structural elements, particularly beam and beam-column elements. A brief review of the mechanical properties of concrete and reinforcement steel when under dynamic loading is given first. Next, a simplified method which converts the aforementioned concrete elements to SDOF systems is presented. In the last section of this chapter, all steps necessary to materialize a resistance curve will be detailed.

3.1 Performance criteria

The assessment of structural element response to blast loads is done in order to guarantee it falls within the specified deformation criteria. The ASCE/SEI-11 [20] proposes two parameters to gauge the deformation. These parameters are the ductility ratio , μ, and the element's maximum rotation, θ_{max}. The ductility ratio is defined as the ratio between the maximum displacement in the response , u_{max}, and the maximum elastic displacement, u_y, as illustrated in equation (3.1).

$$\mu = \frac{u_{max}}{u_y} \tag{3.1}$$

The maximum support rotation depends on the maximum displacement and the minimum distance from the maximum displacement point on the element and the support, L_{min}, given by equation (3.2).

$$\theta_{max} = \arctan\left(\frac{u_{max}}{L_{min}}\right) \tag{3.2}$$

These parameters are then compared with the the maximum allowed values for each deformation category, present in Table 3.1. The ASCE/SEI-11 Standard [20] proposes four distinct deformation hazard categories ranging from superficial to hazardous damage.

Additionally, as proposed in [21], performance criteria may also be assessed by evaluating the deformation energy of the element, the support

19

Table 3.1: Deformation criteria, adapted from [20]

Element Type	Superficial		Moderate		Heavy		Hazardous	
	μ_{max}	θ_{max}	μ_{max}	θ_{max}	μ_{max}	θ_{max}	μ_{max}	θ_{max}
Flexural elements								
Single reinforced beam	1	-	-	2°	-	5°	-	10°
Double-reinforced beam without shear reinforcement	1	-	-	2°	-	5°	-	10°
Double-reinforced beam with shear reinforcement	1	-	-	4°	-	6°	-	10°
Combined flexure and compression								
Single reinforced beam-column	1	-	-	2°	-	2°	-	2°
Double-reinforced beam-column without shear reinforcement	1	-	-	2°	-	2°	-	2°
Double-reinforced beam-column with shear reinforcement	1	-	-	4°	-	4°	-	4°

reactions and/or by checking the ultimate limit states.

3.2   Material mechanical behavior

When a structural element is subjected to a blast load the materials composing it suffer high strain rates. Both yield and ultimate strengths of the materials increase resulting in a higher load bearing capacity. Figure 3.1 outlines several strain rate magnitudes that arise from different imposed loads. An estimation of the increase in mechanical capacity can be attained via experimentation, with devices such as the Split Hopkinson Tensile Bar, which can be used in both compression and tensile tests. The estimated dynamic strengths are then divided by the material's static strength, resulting in a dynamic increase factor (DIF).

Quasi-static   Earthquake   Impact   Explosion

10^{-6} 10^{-5} 10^{-4} 10^{-3} 10^{-2} 10^{-1} 10^{0} 10^{1} 10^{2} 10^{3} 10^{4}
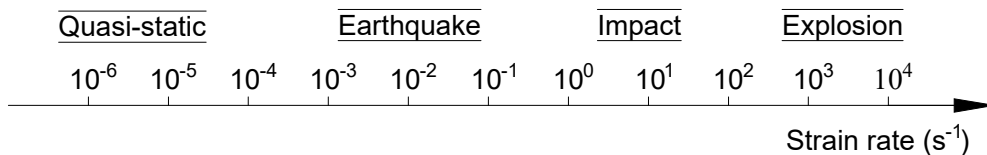
Strain rate (s^{-1})

Figure 3.1: Variation in strain rate depending on load, adapted from [45]

Numerous authors [9, 13, 34, 38, 39] have conducted experiments on the increase in strength on both concrete and reinforcement steel under dynamic load. The authors of these studies established that the increase in strength for concrete follows a bi-linear progression when plotted versus strain rate in a log-log plot, seen in Figure 3.2(a), with two noticeable branches. In the first branch of this function,

up to strain rates of about 25 s^{-1}, the DIF dependency on strain rate is moderate. In the second branch however, the slope increases and DIFs estimated by various authors suffer significant change over a small strain rate interval, substantiating the claim that concrete has a higher load bearing capacity under dynamic loads.

In [13], the authors conclude that reinforcement steel's dynamic capacity follows a linear progression as strain rates rise, seen in Figure 3.2(b). It has been observed that the steel's dynamic yield strengths increase by up to 45%, for strain rates of about 100 s^{-1}, while ultimate resistance sees a rise of 10%, for the same strain rate value. The expression for the reinforcement steel's DIF is given by equation (3.3).

$$DIF = \left(\frac{\dot{\varepsilon_s}}{10^{-4}} \right)^{\alpha} \tag{3.3}$$

where $\alpha = 0.074 - 0.040 f_{sy}/414$ for the yield state and $\alpha = 0.019 - 0.009 f_{su}/414$ for the ultimate state, as proposed by Malvar & Crawford in [39].

(a) Concrete (b) Steel
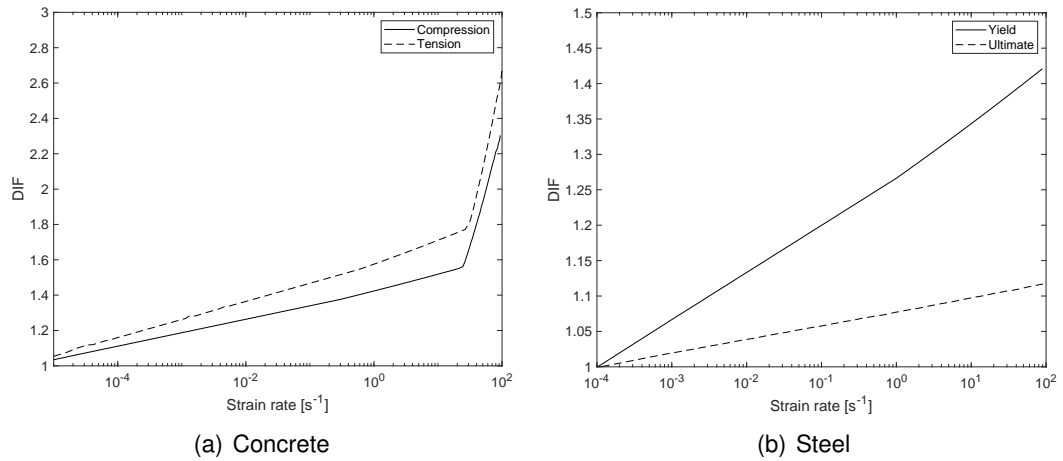
Figure 3.2: Dynamic increase factors for concrete and steel [22, 39]

When the load originates from an explosive, two distinct groups of DIFs may be considered, according to the Design Manual PDC TR-06-01 [62]. The far-range group, for scaled distances bigger than 1.2 kg/m$^{1/3}$, contains DIFs of smaller magnitude, while the opposite is true for DIFs in the close-range group. DIFs for both concrete and steel, in both design-ranges are given in Table 3.2.

Within the confines of the present study, the choice of DIFs may occur in two different ways: either choose the DIF from Table 3.2, depending on the blast scenario to be analysed or estimate it iteratively based on the method proposed in SBEDS [62].

3.2.1 Iterative estimation of dynamic increase factors

The use of DIFs in dynamic analysis may be done simply by using the factors in Table 3.2. However, these factors can be estimated by an iterative estimation

Table 3.2: Concrete and reinforcement steel DIFs, adapted from [62]

Stress type	Far-range design			Close-range design		
	Rebar		Concrete	Rebar		Concrete
	f_{dy}/f_y	f_{du}/f_u	f_{dc}/f_c	f_{dy}/f_y	f_{du}/f_u	f_{dc}/f_c
Bending	1.17	1.05	1.19	1.23	1.05	1.25
Bending and axial	1.16	1.03	1.16	1.19	1.20	1.12

method.

This method relies on the time it takes the section to yield, meaning that the estimation process requires multiple analyses to be performed. To begin the estimation, values for the initial estimated DIFs are set to 1 and the dynamic yield strain of the material, ε_y, is computed resorting to equation (3.4).

$$\varepsilon_y = \frac{DIF}{E} f_y \tag{3.4}$$

where E and f_y are the material's Young's modulus and yield strength. Then, a SDOF analysis is performed to assess the time t_E that it takes the element to yield, allowing for the calculation of the average strain rate, $\dot{\varepsilon_y}$, of the material, as follows:

$$\dot{\varepsilon_y} = \frac{\varepsilon_y}{t_E} \tag{3.5}$$

The resulting strain rate is then used to compute a new DIF which is then compared with the previous. If the difference between two consecutive values is around 5-10% [62], then the process may stop. If the difference is above the tolerance, the newly computed DIF is used in equation (3.4), and a new iteration step is performed.

3.3 Strength increase factors

The US Design Guides [1] and [62] recommend an additional constant to be added in the calculation of the materials' dynamic strengths which is the strength increase factor (SIF). Three different SIFs are proposed, henceforth denoted by the letter 'S'.

Two SIFs are proposed for concrete: the concrete aging factor S_a and the static increase factor S_e. The first accounts for the increase in strength of aged concretes and assumes the value of 1.1. The second takes into account the fact that concrete strengths exceed the specified minimums by roughly 10% and equals to 1.1.

For steel a single SIF is proposed, the static increase factor S_e, equaling to 1.1. The reason for this is that the actual static strength of reinforcement steel is almost always 10% greater than the specified values [62].

The Design Codes [1, 62] indicate that the SIF for steel should only be applied to the dynamic yield strength.

In cases where the strength of these materials is determined by experimental testing, and therefore more precise values for these properties are

available, the SIFs for the tested materials are set to 1.

3.4 Equivalent single-degree-of-freedom analysis

In dynamic analysis it's common to use approximate methods to evaluate the structural response as they prove to be time efficient and return relatively accurate results when compared to more rigorous dynamic analyses.

One such approximate method is the equivalent single-degree-of-freedom method [8]. The use of this method is recommended in design manuals such as SBEDS [62] and UFC-3-340-02 [1] to design blast resistant structural elements.

Often, most systems with distributed properties may be reduced to a SDOF system by equating relevant displacement at a significant point in the real structure to the displacement in the reduced system [8]. Examples of structural systems that allow for this conversion can be seen in Figure 3.3.

(a) Beam to SDOF conversion   (b) Frame to SDOF conversion
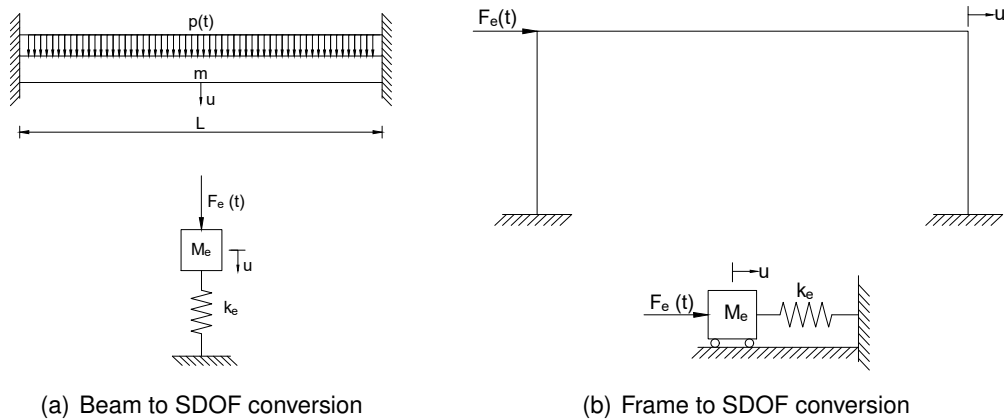
Figure 3.3: Examples of conversion to an SDOF system

The equation of motion for dynamic systems is written as follows:

$$m\ddot{u}(t) + c\dot{u}(t) + ku(t) = F(t) \tag{3.6}$$

in which m, c and k are the system's distributed mass, damping and stiffness, respectively and $\ddot{u}$, $\dot{u}$ and u are the the acceleration, velocity and displacement, respectively and $F(t)$ is the externally applied force. In case of time-invariant systems with linear elastic behavior the coefficients m, c and k are constant, while the variables $\ddot{u}$, $\dot{u}$ and u are time-dependent.

In [8], Biggs describes the inherent difficulty in handling the plastic behaviour of structural elements. A fixed-fixed beam with three stages of deformation is exemplified in Figure 3.4. The first stage being purely elastic; the second is elastoplastic and takes place when the section yields at the supports and plastic hinges are formed; and the third is purely plastic.

Since each of the three different stages is defined by different deflection shapes, it's impossible to identify shapes that remain meaningful throughout the
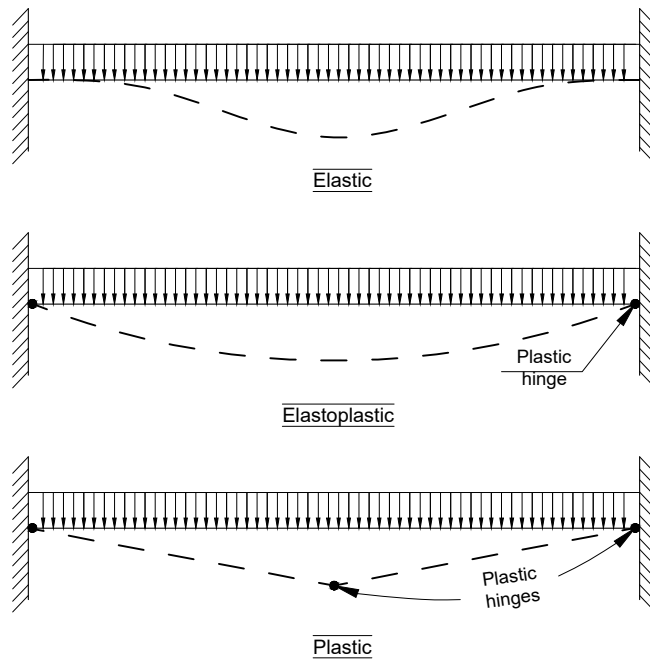
Figure 3.4: Stages of fixed-fixed beam response. Adapted from [8]

entire response [8], as shown in Figure 3.4. Thus, to circumvent this problem, each stage is handled independently.

Regarding the effects of damping, both UFC-3-340-02 [1] and SBEDS [62] assume that its contribution to the analysis can be ignored, as it has very little effect on the first peak of response, which is usually the only relevant cycle of response. Nevertheless, damping may still be considered in the analysis.

3.5 Transformation factors

The conversion to a SDOF system is accomplished through transformation factors, denoted by K_i, where i stands for M, R, L, D or LM or the mass, resistance, load, damping and mass-load transformation factors, respectively. These factors transform the real mass, damping and stiffness into their respective equivalent parameters M_e, C_e, K_e and $F_e(t)$.

The equation of motion for a SDOF system is the following:

$$K_M M_{total}\, \ddot{u} + K_D\, c\, \dot{u} + K_R\, k\, u = K_L F(t) \tag{3.7}$$

Mass transformation factor

The equivalent mass is computed as $M_e = K_M M_{total}$, where the mass factor, denoted K_M, is determined by setting the kinetic energy done by the equivalent mass M_e equal to the kinetic energy done by the total mass M_{total} of the real component, resulting in the following expression:

$$K_M = \frac{M_e}{M_{total}} = \frac{\int_0^L m\,\phi_i(x)^2\,dx}{\int_0^L m\,dx} \tag{3.8}$$

in which m is the element's distributed mass, L is the span of the element, $\phi(x)$ is the normalized deflection shape function with respect to the point of maximum deflection, $\phi(x) = u(x)/u_{max}$ and the subscript i indicates the deformation stage out of the possible three contemplated in Figure 3.4.

Load transformation factor

The equivalent load is computed as $F_e(t) = K_L F(t)$, where the load transformation factor K_L is derived by equating the external work energy done on the equivalent system by the equivalent external force F_e to the total load F_{total} acting on the real structure. Thus, K_L is calculated by the following expression:

$$K_L = \frac{F_e}{F_{total}} = \frac{\int_0^L p(t)\,\phi_i(x)\,dx}{\int_0^L p(t)\,dx} \tag{3.9}$$

Resistance transformation factor

The resistance transformation factor K_R is calculated by equating the strain energy, defined as work done by resisting force by the equivalent spring in the SDOF system R_{me} with the work done by the resisting force in the real component R_m. Defining resistance in terms of load distribution, that is, assuming the resisting forces have the same spatial distribution as the applied load, and that the component has the same deflection shape as the one used to compute K_L, one can conclude that $K_R = K_L$.

Therefore, the equivalent SDOF equation, when neglecting damping, becomes as follows:

$$K_M M_{total}\ddot{u} + K_L k u = K_L F(t) \tag{3.10}$$

For convenience's sake, the equivalent equation of motion may be written exclusively with the load-mass transformation factor K_{LM}, defined as the ratio K_M/K_L, which turns equation (3.10) into the following:

$$K_{LM} M_{total}\ddot{u} + k u = F(t) \tag{3.11}$$

The equivalent system's natural frequency ω is then given by equation (3.12).

$$\omega = \sqrt{\frac{k}{K_{LM}\,M_{total}}} \tag{3.12}$$

Finally, the natural period of the equivalent SDOF system is then:

$$T = \frac{2\pi}{\omega} \tag{3.13}$$

Damping transformation factor

The damping transformation factor, K_D, is assumed equal to K_L, as suggested in [62]. This is a simplification, so that only a single K_{LM} factor is needed. This procedure is made possible because the damping only contributes a small amount of energy to the response of the SDOF system [62].

If the damping ratio ξ is provided and damping is to be taken into account, the coefficient c is computed by the following expression:

$$c = 2\,\xi\,M_e\,\omega \tag{3.14}$$

3.6   Deflection shape functions

As seen in section 3.5, computing transformation factors depends on deflection shape functions. These in turn depend on the support conditions and on the load distribution along the span of the element. In this dissertation, only distributed loads are considered. These functions are derived from the deflected shape related to the Euler-Bernoulli beam theory and expressed by equation (3.15),

$$EI\frac{d^4 u}{d^4 x} = p \tag{3.15}$$

Their magnitude is set so that $\phi_{max}(x) = 1$. To exemplify the procedure the beam in Figure 3.4 is considered. The shape functions for this beam are:

$$\phi(x) = \begin{cases} \dfrac{16}{L^4}(L^2 x^2 - 2Lx^3 + x^4) & \text{, elastic} \\[2em] \dfrac{16}{5L^4}(L^3 x - 2Lx^3 + x^4) & \text{, elastoplastic} \\[2em] \dfrac{2x}{L} & \text{, plastic, for } x < L/2 \\[0.5em] 2\left(1 - \dfrac{x}{L}\right) & \text{, plastic, for } x > L/2 \end{cases} \tag{3.16}$$

Table 3.3 shows the transformation factors for different boundary conditions, for a uniformly distributed load. In Table 3.3, M_{pl}^m and M_{pl}^s refer to the moment at mid-span and at the support, respectively.

3.7   Resistance-displacement curve

The resistance-displacement relationship is a crucial part in the non-linear analysis as the resistance parameter varies with displacement, as shown in equation (3.17).

Table 3.3: Transformation factors for beams

Support conditions	Strain range	K_L	K_M	K_{LM}	R_m	k
	Elastic	0.64	0.50	0.78	$\dfrac{8M_{pl}^m}{L}$	$\dfrac{384EI}{5L^3}$
	Plastic	0.50	0.33	0.66	$\dfrac{8M_{pl}^m}{L}$	0
	Elastic	0.53	0.41	0.77	$\dfrac{8M_{pl}^s}{L}$	$\dfrac{384EI}{L^3}$
	Elastoplastic	0.64	0.50	0.78	$\dfrac{8}{L}(M_{pl}^m + M_{pl}^s)$	$\dfrac{384EI}{5L^3}$
	Plastic	0.50	0.33	0.66	$\dfrac{8}{L}(M_{pl}^m + M_{pl}^s)$	0
	Elastic	0.58	0.45	0.78	$\dfrac{8M_{pl}^s}{L}$	$\dfrac{185EI}{L^3}$
	Elastoplastic	0.64	0.50	0.78	$\dfrac{4}{L}(2M_{pl}^m + M_{pl}^s)$	$\dfrac{384EI}{5L^3}$
	Plastic	0.50	0.33	0.66	$\dfrac{4}{L}(2M_{pl}^m + M_{pl}^s)$	0

$$K_{LM}M_{total}\ddot{u} + R(u)u = F(t) \tag{3.17}$$

The resistance-displacement curve relates to the material's properties, the element's geometry as well in the type of structural elements to be analysed. As illustrated in Figure 3.5, for a beam with both ends fixed, the curve exhibits three different deformation stages.

The first stage is purely elastic in nature and ends when the concrete's tensile strength is reached and the section cracks. In the second stage, the element withstands loads in a cracked state, with a lower stiffness. It ends when the reinforcement steel's yield strength is reached and the structure can no longer bear load. The third and final stage is purely plastic and ends when the ultimate displacement is reached and the element fails, forming a plastic hinge at mid-span,

as shown in Figure 3.4.

This section will describe the calculations inherent to all three stages assuming they refer to a fixed beam or beam-column element. The calculations for other boundary conditions may be found in [8].
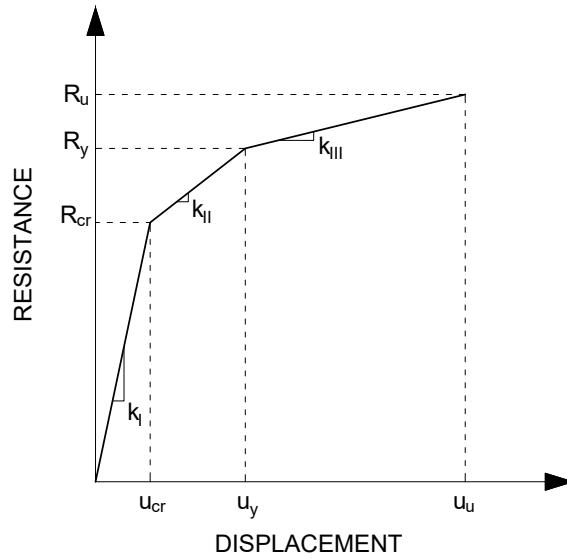
Figure 3.5: Generic Resistance-displacement curve

3.7.1   Uncracked stage (I)

As previously mentioned, this stage is delimited by the cracking load, i.e the maximum load the structure can support until cracking is initiated. This load is accounted for with the cracking moment M_{cr} which is calculated in a simplified fashion, by ignoring the contribution of the reinforcement steel. The cracking moment is thus computed as follows:

$$
M_{cr} = \begin{cases} W_I \left(f_{ctm} - \dfrac{N}{A_I} \right) \cong W_g \left(f_{ctm} - \dfrac{N}{A_g} \right) & \text{, for uniaxial loading} \\[2em] W_I \, f_{ctm} \cong W_g \, f_{ctm} & \text{, for pure bending} \end{cases}
\tag{3.18}
$$

in which A_I and W_I are the uncracked homogenized section's area and bending modulus, respectively; f_{ctm} defines the concrete's average tensile strength; A_g and N are the gross uncracked section's area acting axial load, respectively.

The gross section's bending modulus , W_g, is given by:

$$
W_g = \frac{I_g}{\bar{x}}
\tag{3.19}
$$

where I_g is the gross concrete section's moment of inertia and $\bar{x}$ is the distance from the neutral axis to the farthest tensioned fibre, which for a rectangular section

equals $h/2$.

Uncracked neutral axis distance

Considering a rectangular cross section as shown in Figure 3.6 and the general expression for the determination of the distance to the neutral axis from the top of the section, the uncracked neutral axis distance, x_I, is computed as follows:
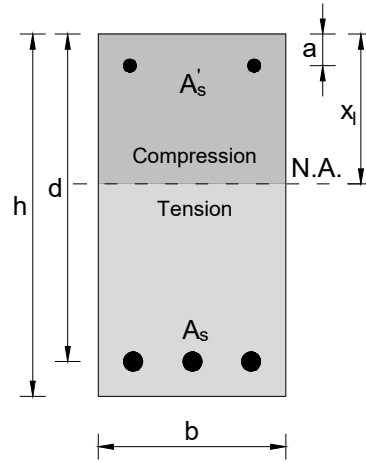
Figure 3.6: Generic RC cross-section, uncracked stage

$$x_I = \frac{\sum A_i d_i}{\sum A_i} = \frac{bh^2/2 + (\alpha_e - 1)(A_s d + A_s' a)}{bh + (\alpha_e - 1)(A_s + A_s')} \tag{3.20}$$

where b is the section's width, h is the section's depth, d is the distance between the top of the cross section to the tensioned reinforcement's centroid, a is the distance between the top of the cross section to the compressed reinforcement's centroid, α_e is the homogenization factor, $\alpha_e = E_s/E_c$ and A_s and A_s' are the bottom and top reinforcement's area, respectively. The area of the steel bars is usually multiplied by α_e and added to the concrete's cross-sectional area. However, this procedure introduces a small error in the computation of the neutral axis distance. To avoid this, the steel's area is multiplied by $(\alpha_e - 1)$ instead, given that the concrete's gross cross-sectional area is being used instead of the net area.

Next, the uncracked section's moment of inertia I_I is computed by the following expression:

$$I_I = \frac{bh^3}{12} + bh\left(x_I - \frac{h}{2}\right)^2 + (\alpha_e - 1)(A_s(d - x_I)^2 + As'(x_I - a)^2) \tag{3.21}$$

It's now possible to calculate the cracking moment M_{cr}. Following this, the limiting resistance for stage I, R_{cr} is computed by using the corresponding expression in Table 3.3.

Finally, the displacement at the end of stage I, u_{cr} is calculated as a

function of the bending stiffness of the element. The displacement that ends stage I is thus,

$$u_{cr} = \frac{R_{cr}}{k_I} = \frac{L^3}{384 E_c I_I} R_{cr} \tag{3.22}$$

For boundary conditions other than both ends fixed, the expressions are given in Table 3.3.

3.7.2 Cracked stage II

After the formation of cracks in the cross section, the concrete is no longer able to resist tensile loads and the tensile stress is sustained exclusively by the steel bars. Thus, the cracked stage is limited by the yielding of the reinforcement bars. Figure 3.7 illustrates the section's stress state in stage II, as the neutral axis is higher and most of the section is subjected to a tensile load.
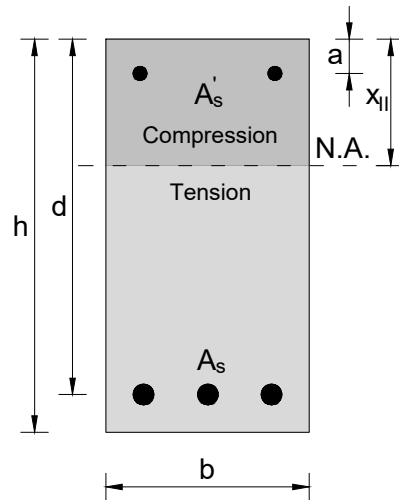
Figure 3.7: Generic RC cross-section, cracked stage

The mechanical reinforcement ratio ω, defined as,

$$\omega = \frac{A_s f_{sy}}{b \, d \, f_c} \tag{3.23}$$

where f_y is the reinforcement steel bars' yield strength and f_c is the concrete's compressive yield strength, and the reduced bending moment μ is given by the following expression,

$$\mu = \omega(1 - 0.5\omega) \tag{3.24}$$

The bending moment M_y, for a rectangular RC cross section, is thus given by the expression:

$$M_y = \mu \, b \, d^2 f_c \tag{3.25}$$

The calculation for the yield resistance R_y is carried out in a similar fashion as the cracking resistance R_{cr}, by switching the acting moment to M_y. The expressions of M_y for different boundary conditions are present in Table 3.3.

Next, the neutral distance for stage II is computed by using equation (3.20), yielding:

$$x_{II} = \frac{-(\alpha_e - 1)(A_s + A_s') + \sqrt{[(\alpha_e - 1)(A_s + A_s')]^2 + 2b(\alpha_e - 1)(dA_s + aA_s')}}{b} \tag{3.26}$$

where β is the ratio between the compression reinforcement area A_s' and the tension reinforcement area A_s. Next, the cracked section's moment of inertia I_{II} is computed:

$$I_{II} = \frac{bx_{II}^3}{3} + (\alpha_e - 1)\left[A_s(d - x_{II})^2 + A_s'(d - a)^2\right] \tag{3.27}$$

To determine the yielding displacement, u_y, the Eurocode 2's [21] methodology is employed, where an intermediate state between a non-cracked section and a fully cracked one is considered for any element predicted to be subjected to loads that would induce cracking.

The expression for u_y is thus:

$$u_y = \zeta a_{II} + (1 - \zeta)a_I \tag{3.28}$$

in which a_I and a_{II} are the deflections for the uncracked and cracked sections, respectively, when M_y is imposed on the element and ζ is the distribution coefficient that takes into account the tension stiffening of the section, computed as follows:

$$\zeta = 1 - \beta\left(\frac{M_{cr}}{M}\right)^2 \tag{3.29}$$

The coefficient β accounts for the duration of the load and M is the pertaining moment. As the goal is to compute the yield displacement and that the load is explosive in nature, β takes a value of 1 and M is the yield moment M_y.

It is then necessary to determine the deflections a_I and a_{II}. This is done in the same way as in equation (3.22), according to Table 3.3, which for a simply supported beam yields:

$$a_I = R_y \frac{5L^3}{384E_c I_I} \tag{3.30}$$

and

$$a_{II} = R_y \frac{5L^3}{384E_c I_{II}} \tag{3.31}$$

3.7.3 Post-yield stage III

The remaining branch to be defined in the resistance curve takes place after the reinforcement bars have yielded and the element can no longer bear any additional load. It ends when the element fails.

In this stage, the ultimate moment M_u and resistance R_u are computed the same way as in section 3.7.2, only substituting the index y to u, denoting the ultimate deformation stage.
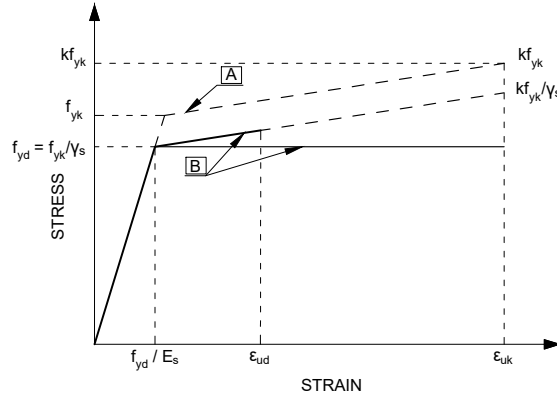
Figure 3.8: Idealized and design stress-strain diagrams for steel [21]

To determine $E_{s,y}$, the slope of the second branch in the design curve (B) in Figure 3.8 is determined by equation (3.32).

$$E_{s,y} = f_{dsy}\frac{\xi - 1}{\varepsilon_y - f_{dsy}/E_s} \tag{3.32}$$

where ξ is the ratio between the reinforcement steel's ultimate dynamic and dynamic yield strengths and ε_y is the steel's yield strain. Note that the strengths at each end of the plastic branch of the design curve (B) are affected by a safety coefficient γ_s which equals 1, since according to EC2 [21], the blast load is accidental, meaning that the the design curve to be used is actually curve (A).

Finally, stage III's stiffness is calculated following the appropriate expression from Table 3.3 and u_u is computed in the same way as equation (3.22), only switching the indexes to R_u and k_{III}.

3.7.4 Bilinearization of the resistance curve

The transformation of the resistance-displacement relationship from a trilinear curve to a bilinear one is done to simplify the solving of the dynamic problem. The idea is to define an equivalent elastic branch, with stiffness k_{eq}, and new equivalent displacement u_{eq} such that:

$$u_{eq} = u_{cr} + u_y\left(1 - \frac{R_{cr}}{R_y}\right) \tag{3.33}$$
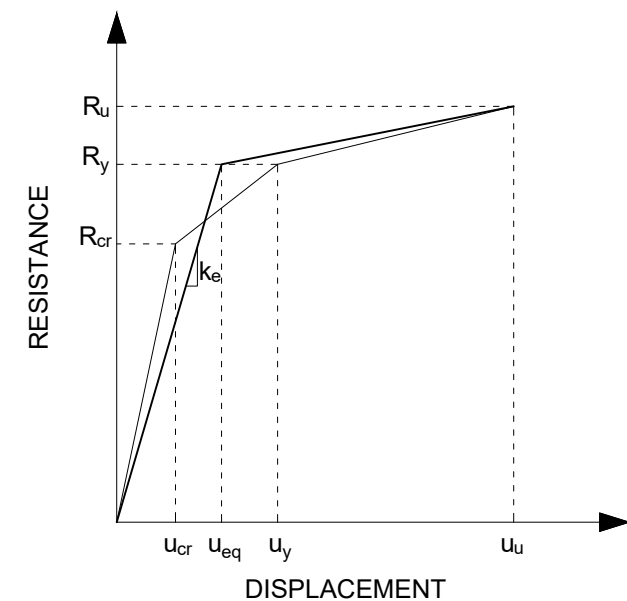
Figure 3.9: Bilinear resistance-displacement curve

which means the yield resistance R_y is retained. This operation ensures that the areas between the original curve and the equivalent one are the same in Figure 3.9.

3.7.5 Applicability of US norms on non-US materials

The formulation used to model reinforced concrete under dynamic loads in the present dissertation comes from US design codes [62, 1] and as such, it accounts for the behaviour of materials (concrete or reinforcement) manufactured in the US.

As such, seemingly anomalous situations may arise where the third branch on the resistance-displacement relation is defined by a softening branch, when applying these norms to cases foreign to the US. This is caused by application of the DIF and SIF coefficients, discussed earlier in this chapter, to the calculation of the materials' dynamic strengths.

In particular, the DIF for steel in yield being always greater than the DIF in the ultimate state, compounded with the fact that the SIF coefficients aren't applied to the steel's ultimate strength, may lead to scenarios where $f_{dsy} > f_{dsu}$ which in turn leads to resistance relationships with a descending plastic branch.

To investigate this behaviour, an example beam was analysed using the program RCBlast [29]. The beam has a cross section of 290 mm by 160 mm and a span of 1.5 m, as shown in Figure 3.10.

The cross section is composed by $2\phi16$ bars on the tensioned face with a yield and ultimate strengths as well as a Young's modulus of 604 MPa, 703 MPa and 210 GPa, respectively. The concrete has a compressive strength, tensile strength and Young's modulus of 53.8 MPa, 4.6 MPa and 44.7 GPa, respectively.

The DIFs used in this analysis were 1.296, 1.223 and 1.130, for the concrete, steel in yield and steel in its ultimate tensile state, respectively. The resulting stress-strain behaviour for concrete and steel are represented in
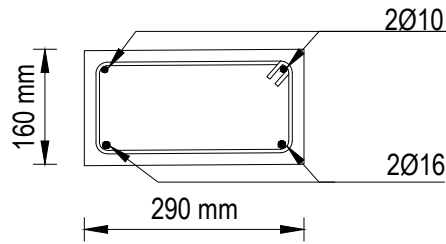
Figure 3.10: Cross-section
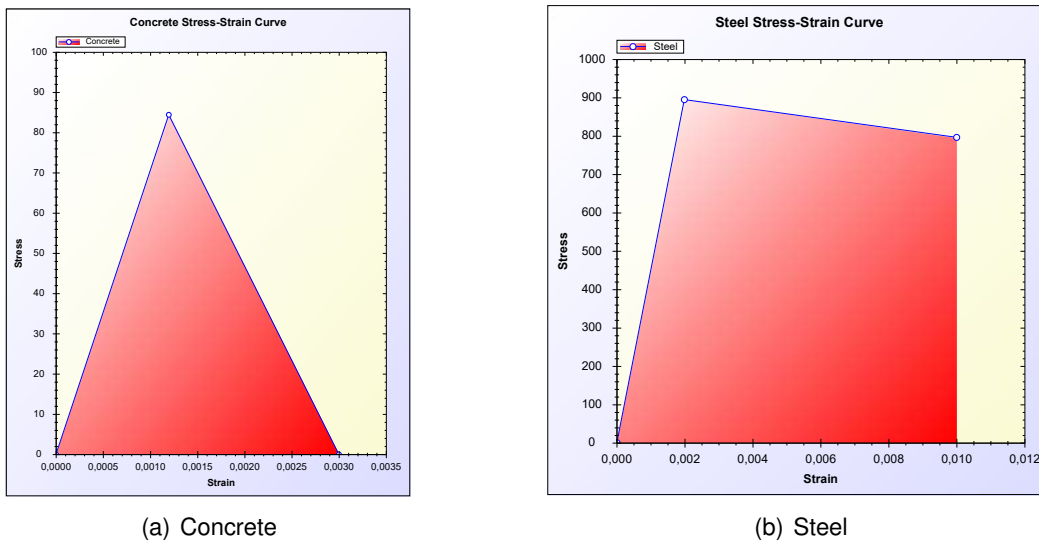
| (a) Concrete | (b) Steel |

Figure 3.11: Stress-strain relations for RCBlast example [29]

Figure 3.11.

The resulting resistance curve is presented in Figure 3.12. Notice the descending plastic branch in Figure 3.11(b), leading to the softening branch of the resistance curve in Figure 3.12.
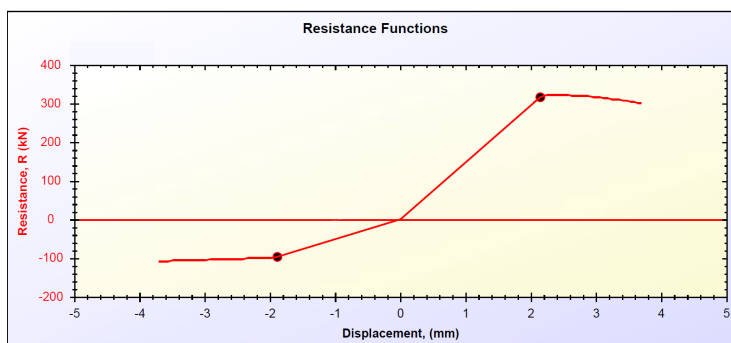
Figure 3.12: Resistance curve for RCBlast example [29]

Given the nonexistence of European or Portuguese blast Design Codes,

the formulations described in the previous sections will be applied.

3.8 Moment-axial force interaction diagram

In case of beam-columns, the contribution of the axial load must be accounted for in the analysis. In the present study, the contribution of the axial load in the element's cross-sectional resistance is evaluated in the form of a bending moment - axial load interaction diagram. Construction of the moment-axial load interaction diagram follows the guidelines provided in the UFC-3-340-02 [1]. To do this, three points and two regions are defined by varying the axial load from 0 to the section's ultimate compressive stress, as shown in Figure 3.13.
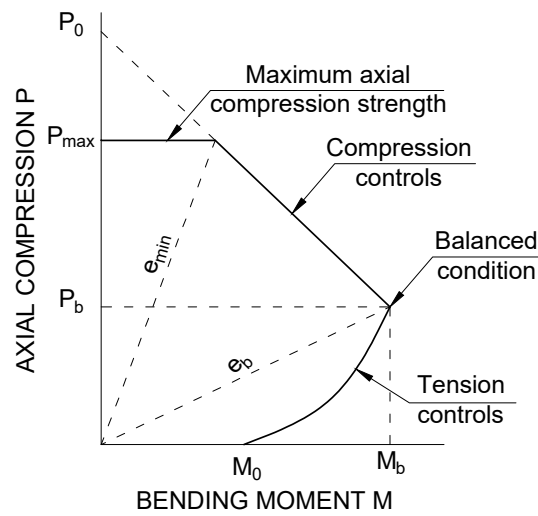
Figure 3.13: Generic P-M diagram, adapted from [1]

The first point is defined as the pure compression point. In this scenario, the element acts exclusively as a column, with no bending moments applied. Thus, the coordinates for the pure compression point in the P-M diagram are $P = P_{max}$ and $M = 0$. P_{max} is calculated as follows.

$$P_{max} = f_{dc}(A_g - A_{s,tot}) + A_{s,tot}f_{dy} \qquad (3.34)$$

where f_{dc} is the concrete's dynamic compressive strength, A_g is the section's gross area, $A_{s,tot}$ is the section's total steel bar area and f_{dy} is the steel bars' dynamic yield strength.

Next is the balanced failure point, where the element is under balanced strain conditions and is achieved when the concrete reaches its limiting strain $\varepsilon_c = 0.003$ at the same time the reinforcement steel reaches its dynamic yield strength f_{dy}. This point's coordinates are the balanced axial load P_b and moment M_b. The point (M_b, P_b) is computed implicitly in the model developed for the present study as the intersection between the compression controls and the tension controls regions.

The balanced conditions point acts as a frontier between stress states: at higher values than P_b, the strength of the section is governed by its compressive strength. Failure for $P > P_b$ is initiated by the crushing of the concrete while the reinforcement has yet to reach its yield tension and may actually be in compression rather than tension [1]. On the other hand, if $P < P_b$, the section's strength is controlled by the reinforcement bars' yield strength. Section failure in this region is initiated by the yielding of the reinforcement bars while the concrete hasn't reached its limiting strain. This means section failure at axial loads less than P_b is a ductile one, while in the compression controls region entails a brittle collapse, being much less desirable. The coordinates for this point are $P = 0$ and M_0, calculated by the expression that follows [62].

$$M_0 = A_s f_{dy} \left(d - \frac{A_s f_{dy}}{2b f_{dc}} \right) \tag{3.35}$$

where A_s is the tensioned steel's area, f_{dy} is the steel dynamic yield strength, d is section's effective depth, b is the section's width and f_{dc} is the concrete's dynamic compressive yield strength.

The interaction diagram progresses in a linear fashion on both regions and its shape depends on the section's eccentricity, $e = M/P$. In the compression controls region and for a rectangular section, the diagram follows the shape provided by equation (3.36).

$$P = \frac{A_s f_{dy}}{\frac{e}{2d - h} + 0.5} + \frac{b h f_{dc}}{\frac{3he}{d^2} + 1.18} \tag{3.36}$$

in which P is the axial load, e is the eccentricity of the applied load, A_s is the tensioned steel's area, f_{dy} is the reinforcement steel's dynamic yield strength, f_{dc} is the concrete's dynamic compressive strength, d is the section effective depth and h is the section's depth.

Reading the diagram from top to bottom, what follows next is the balance point, characterized by the balance eccentricity e_b, calculated by equation (3.37).

$$e_b = 0.2h + \frac{1.54 f_{dy} A_s}{b f_{dc}} \tag{3.37}$$

The tension controls region of the diagram is defined by a straight line from the balanced conditions point to where the axial load reaches a null value and $M = M_0$, as can be seen in Figure 3.14. This procedure is proposed in [62] and is meant as a simplification of the tension controls region, in Figure 3.13. All indexes pertaining to the reinforcement steel's yield strength are now switched to its ultimate strength f_{du} and the diagram construction is repeated, this time to draw an ultimate axial load and moment combination.

Finally, the balance point in the interaction diagram results from the intersection between the compression controls and the tension controls line segments.

By virtue of being exclusively composed of linear functions, the resulting interaction diagram provides more conservative resistant loads P_R and M_R. A more bulbous shaped diagram would provide resistant load values higher than

those calculated by this method, which would imply a higher sectional load bearing capacity, thus being less conservative.
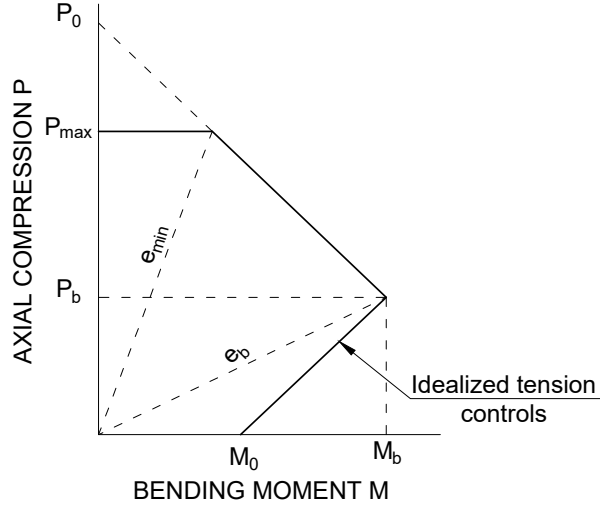
Figure 3.14: Generic idealized P-M diagram

Having the diagrams constructed, the yielding and ultimate bending moments can be discerned from the graphs, and the algorithm may proceed in the exact same fashion as described in sections 3.7.2 and 3.7.3, to compute the resistance-deflection curve.

3.9 P-δ effects

The present study will account for both the resistance of elements subjected to the combination of axial load and moment and the effects of eccentrically axial loaded elements. To accomplish the latter, the axial load is converted into an equivalent lateral distributed load, following the equivalent lateral load method [49].

The additional load to be added to the pre-existing lateral load is computed by the folowing expression:

$$P_{\delta i} = N \left[(u_{i-1} + e) \left(\frac{C}{L^2} \right) \right] b \tag{3.38}$$

where $P_{\delta i}$ is the equivalent lateral load at time step i, b is the element's width, N is the acting axial load, u_{i-1} is the displacement at time step i-1, C is a constant that takes into account the blast load distribution and support locations; for a uniformly loaded beam-column it equals 8, L is the element's span and e is the eccentricity of the applied load, as discussed in Eurocode 2 [21].

The eccentricity e is computed according to the second-order effects section in Eurocode 2 [21], as follows:

$$e = \theta_i \frac{L_0}{2} \tag{3.39}$$

in which L_0 is the element's buckling length and $\theta_i = \theta_0 \, \alpha_h \, \alpha_m$, where in turn:

- $\theta_0 = 1/200$;

- $\alpha_h = 2/\sqrt{L}$;

- $\alpha_m = 1$

Eurocode 2 [21] defines $\alpha_m = \sqrt{0.5(1 + 1/m)}$, where m is the number of vertical members contributing to the total effect, but since there'll only be one element being studied at a given time, $m = 1$ and α_m equals 1.

The buckling length L_0 may take the value of L, $0.5L$ or $0.7L$, depending on whether the element is simply supported, doubly fixed or fixed-simply supported, respectively.

According to the Design Guides PDC-TR-06-01 [62] and UFC-3-340-02 [1], secondary moments originating from an eccentrically applied axial load can be ignored if the following inequality is verified:

$$\frac{kL}{r} \leq 22 \tag{3.40}$$

where the left side is called the *slenderness ratio*, k is the effective length factor based on boundary conditions, L is the column's length and r is the radius of gyration.

Chapter 4

Numerical implementation

This chapter gives the details on the implementation aspects of the SDOF algorithm able to predict the dynamic response of the structural elements under blast-induced shock waves. The program has built-in capabilities to generate resistance functions of RC beam and beam-column elements , blast load functions and to perform SDOF dynamic analysis. Additionally, a Graphical User Interface (GUI) has been created to streamline the use of the program.

The computer application comprises three phases: pre-processing, analysis and post-processing. All routines pertinent to each phase will be described.

4.1 Pre-processing stage

The pre-processing area is where the problem is defined by user input. The end of this stage consists in the generation or loading of two data files: a blast load file and a resistance curve file.

4.1.1 Blast load file

This is the first data input instance numbered **1** in Figure 4.1. The user is prompted with three input choices:

- Direct input of the discrete load values at each time step, by choosing the `Load blast wave function` option. This in turn may be accomplished in two ways; the first option consists in inputting a text (.txt) file containing an n x 1 vector where the first value is the time step `dt` in seconds and the remaining values are the discrete load values at times `dt(i+1)` at the `i`th entry in the input file. The second option involves the input of an n x 2 array consisting of time-load pairs (time in first column and load values in the second);

- The `Load explosive parameters` option. Requires a user input of a .txt file containing a 2x6 array. The first row describes the required input variables and contains the string `dt,eEXP,wEXP,R,width,L`. The variables in this file are: the time step dt [s], the explosive's specific energy `eEXP` [kJ/kg], the

explosive's mass `wEXP` [kg], the blast standoff distance `R` [m] and the element's width and span, `b` and `L` [m]. The model computes the blast load's parameters via the Kingery & Bulmash polynomials which are then used in the modified Friedlander equation to compute the load time history;

- Input of a string function is also an available option, by selecting the `Input custom function`. To use this option, the user must provide a valid string in MATLAB with respect to the time variable `t`.

Additionally, the user is able to select either incident or reflected blast waves in the analysis by activating the button group *Type*, in section **3** in Figure 4.1.
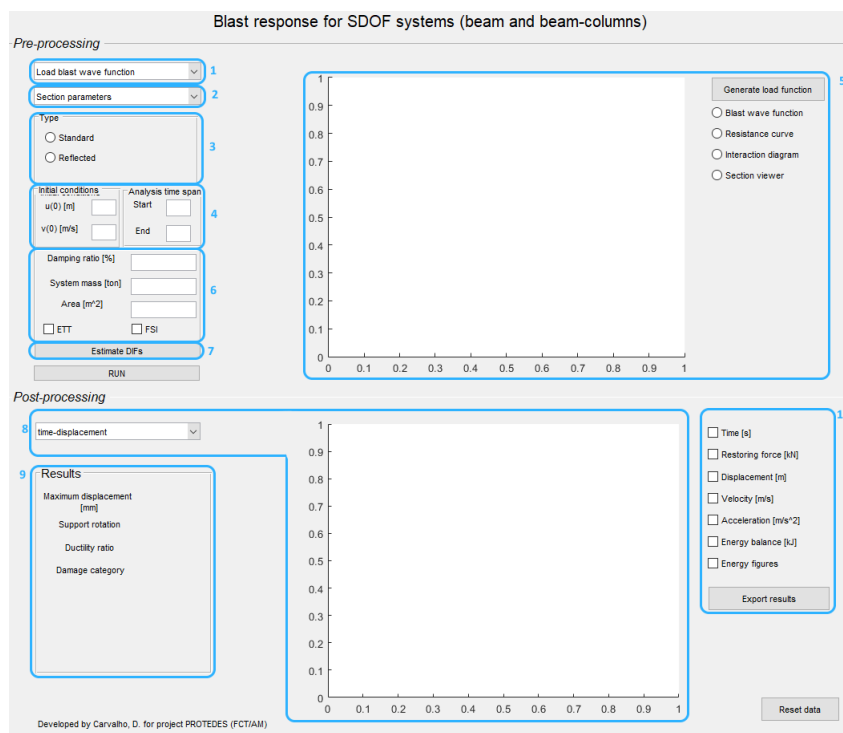
Figure 4.1: Graphical user interface

The solving function in the numerical model interpolates load values for each time step, if the input load function is discretized with respect to time. As such, an adequate time step must be used in order to avoid introducing errors in the analysis. The recommended time step is 10% of the element's natural period. It is only necessary to provide the time step in cases where the input load is an n x 1 vector.

4.1.2 Resistance curve file

For the definition of the resistance curve, two options are available in field **2** in Figure 4.1.

The first, named *Section parameters* implies the input of a file containing the following structure. Again, dummy data is present as an example.

```
SectionProperties.txt
Rows 1 through 13
L,b,h,c,phi_s,phi_t,phi_c,n_t,n_c,fc,fctm,Ecm,Es,
1.98,0.15,0.1,0.02,6.3,11.3,11.3,2,2,58,6.6,34.27,200,

Rows 14 through 25
fy,fys,fyu,N,Z,support,DIFc,DIFsy,DIFsu,spacing, SIFc, SIFs
483,604,675,350,-1,1,1.25,1.315,1.043,5,0,0
```

in which:

- `L` [m] is the element's span;

- `b` [m] is the element's width;

- `h` [m] is the section's depth ;

- `c` [m] is the section's cover;

- `phi_s` [mm] is the transversal reinforcement steel bars' diameter;

- `phi_t` [mm] is the longitudinal tension reinforcement steel bars' diameter;

- `phi_c` [m] is the longitudinal compression reinforcement steel bars' diameter;

- `n_t` is the number of longitudinal tension reinforcement steel bars;

- `n_c` is the number of longitudinal compression reinforcement steel bars;

- `fc` [MPa] is the concrete's static compression yield strength;

- `fctm` [MPa] is the concrete's static tensile yield strength;

- `Ecm` [GPa] is the concrete's Young's modulus;

- `Es` [GPa] is the reinforcement steel's Young's modulus;

- `fy` [MPa] is the longitudinal steel's static yield strength;

- `fys` [MPa] is the transverse steel's static yield strength;

- `fyu` [MPa] is the longitudinal steel's static ultimate strength;

- `N` [kN] is the acting axial force;

- `Z` [m/kg$^{1/3}$] is the scaled distance; Set to -1 if custom DIFs are to be used;

- `support` represents the desired support conditions; Available options are 1, 2, and 3 for simply support, fixed-fixed supports and simple-fixed supports, respectively. If the this variable is set to 0, then the mass transformation factors are both set to 1;

- `DIFc` is the concrete's dynamic increase factor;

- `DIFsy` is the reinforcement steel's dynamic increase factor in yield;

- `DIFsu` is the reinforcement steel's dynamic increase factor in its ultimate state;

- `spacing` [cm] is the spacing of the transverse reinforcement steel;

- `SIFc` is the concrete's strength increase factor; Set to 1 to use this factor, 0 otherwise;

- `SIFs` is the reinforcement steel's strength increase factor; Set to 1 to use this factor, 0 otherwise.

The `SectionProperties.txt` file may be written as a 2 x 25 or a 25 x 2 array. If the explosive parameters aren't available and the blast load function is directly loaded in the GUI, thus, the value of the scaled distance Z is not known, the user must set $Z = -1$ and assign values to the three DIF's in the file in the section properties file.

Following the loading of the section's properties via the "Section properties" option, the routine `behaviour_curve.m` is launched automatically. This function starts by calculating the dynamic capacity of both concrete and steel. Next, it decides weather the the element is acting as a beam ($N = 0$) or a beam-column ($N \neq 0$).

In the case of a beam element, a sectional analysis is carried out to determine the loads and displacements that define the resistance curve. In particular, calculations for the elastic and elastoplastic stages involve determining the distance from the top of the section to the neutral axis x_I and x_{II}, respectively. The uncracked (I) and cracked (II) section's moment of inertia are computed next, to be used in calculating the stiffness k of each phase. The final loads are calculated for each stage using Bigg's methodology. The resulting tri-linear curve is bilinearized.

Conversely, if the element to be analyzed is a beam-column, then the function generates a P-M interaction diagram following the equations described in section 3.8. The resistant moments are evaluated depending on the magnitude of the imposed axial load, and the function proceeds in the same fashion as if the element would be a beam.

Alternatively, if the user chooses to directly input the resistance curve, the file should contain two columns, the first containing displacements [m] and the second the resistant force [kN], as follows:

```
ResistanceCurve.txt
      -0.02,           -300
      -0.01,           -300
       0.0,             0.0
       0.01,            300
       0.02,            300
```
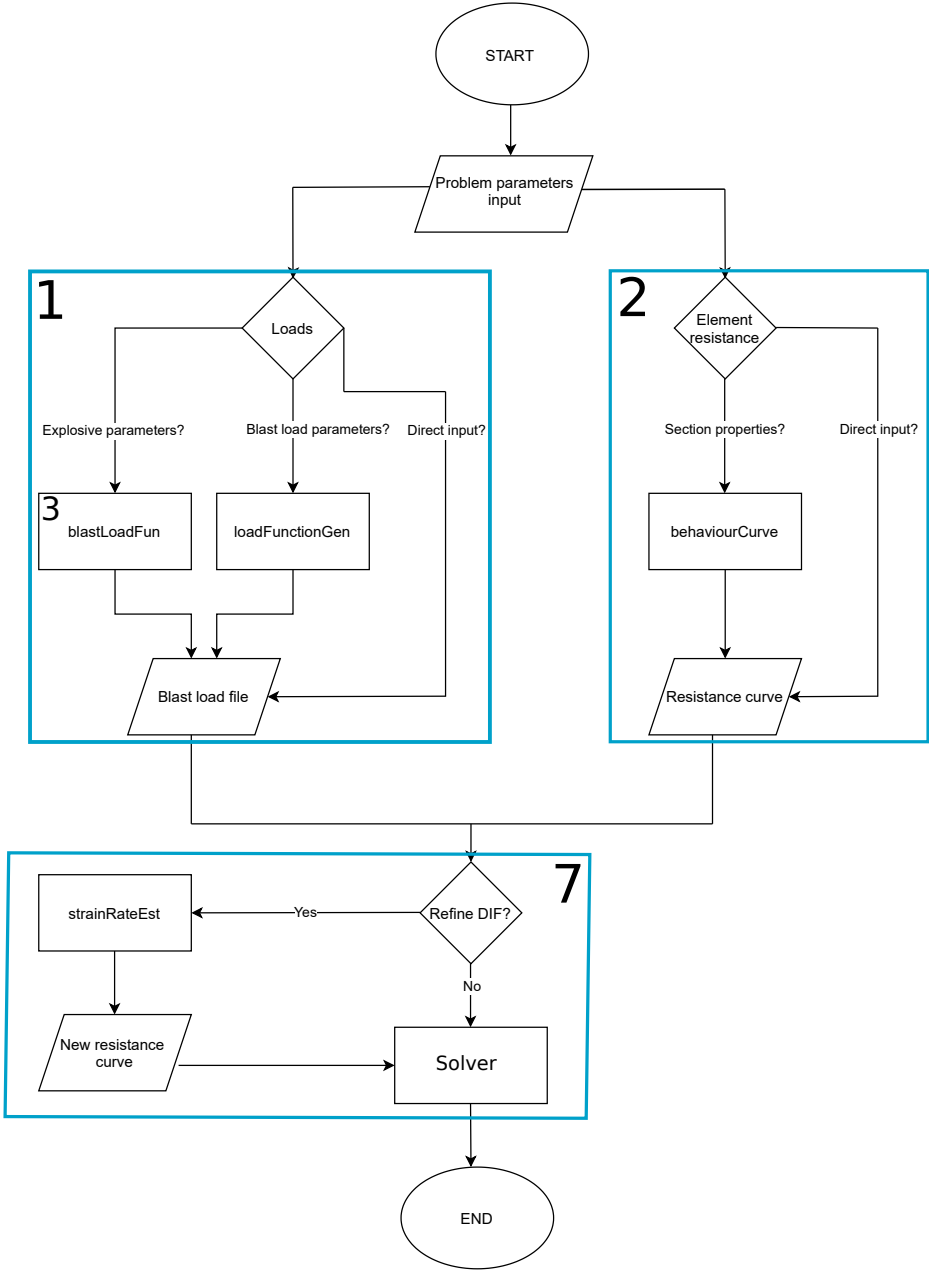
The flowchart of the pre-processing stage is presented in Figure A.2

Figure 4.2: Pre-processing stage flowchart

4.1.3   Initial conditions and other material properties

The solving function requires the input of the system's initial kinematic conditions u_0 and $\dot{u}_0$ and time-span in the section numbered **4** in Figure 4.1.

The remaining material properties not contemplated in the section numbered **2**, such as the damping ratio [%], the element's mass [ton] and shock wave incident area [m^2] are loaded in section **6**.

Additionally, if wave attenuation effects are to be accounted for, the check boxes *ETT* and *FSI* must be ticked for shock wave clearing and fluid structure interactions, respectively.

4.1.4   Visual representation of input files

To visualize the input data, four different sets of pre-processing data can be selected, as seen in Figure A.3.

- Blast wave function - plots the time history of the blast load;

- Resistance curve - plots the displacement-resistance curve;

- Interaction diagram - plots the resultant interaction diagram for beam-column only; Otherwise, the string `No axial load detected. Element acts as a beam` is displayed;

- Section viewer - displays the element's cross-section; If no geometrical parameters were defined, the string `No material properties detected. Section view is unavailable.` is displayed.

4.1.5   Estimation of dynamic increase factors

The estimation of the DIFs is performed via the push-button numbered **7** in Figure 4.1. By clicking this button, the user is prompted with a dialog box which requires a percentual tolerance value as input for the DIF estimation routine. If no value is input and the button *OK* is clicked, the program assumes the default tolerance as 1%. Next, the routine `StrainRateEst` is ran and the DIFs are computed. Following this, the program prompts the user with another dialog box indicating that the routine ran successfully and displaying the newly computed DIFs, as seen in Figure A.4.

The iterative algorithm for computing DIFs is detailed in section 3.2.1 and visually represented in Figure A.5. As the computation of the DIFs relies on the time to yield t_E to compute the strain rates for each material at each iteration, the routine can only run if the element yields.

(a) Input load

(b) Resistance-deflection curve

(c) P-M Interaction diagram

(d) Cross-section viewer
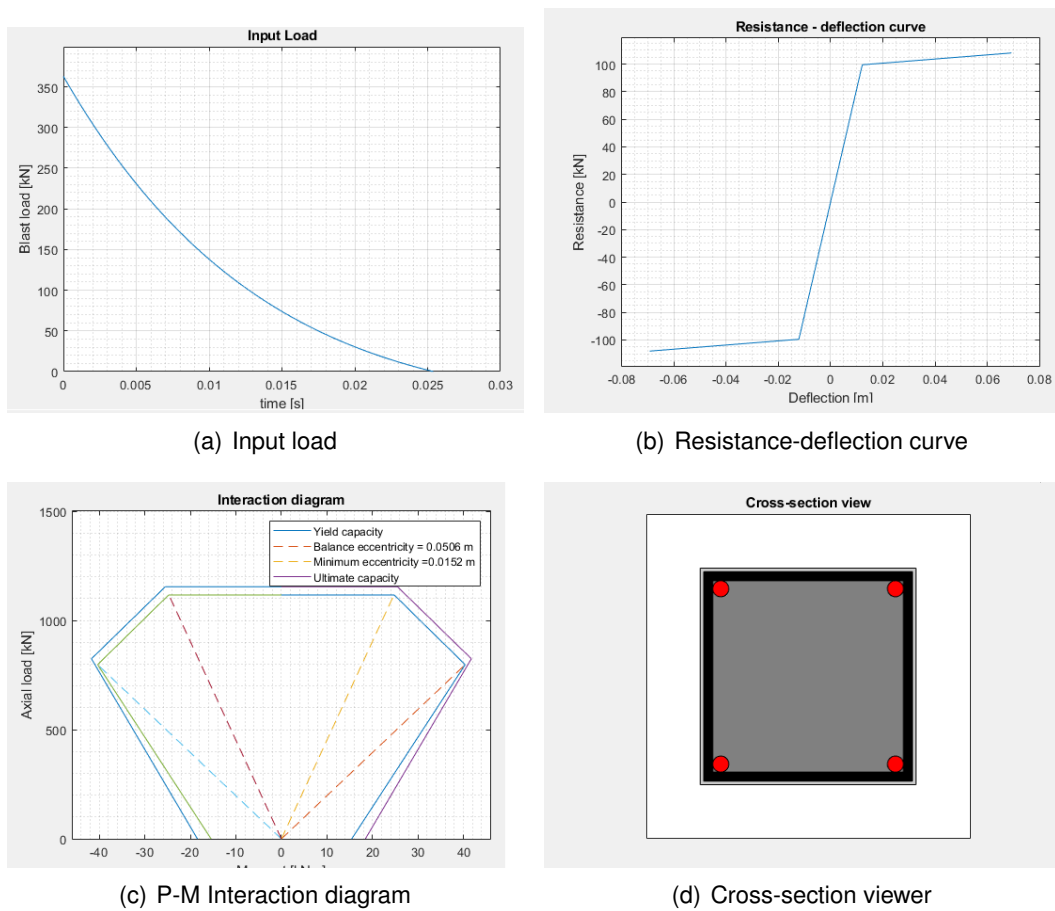
Figure 4.3: Pre-processing graphical visualization options
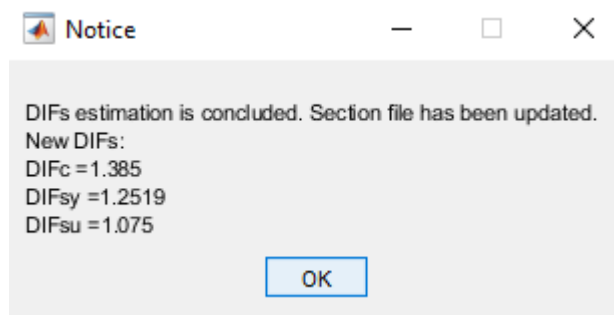
Figure 4.4: Dialog box displayed after running StrainRateEst

4.2 Processing stage

This section briefly introduces some of the methods available for the numerical solution of the nonlinear SDOF equation of motion. It begins by describing the reason why there's a need for numerical integration solutions, the methods that make it possible and ultimately focuses on the integration scheme chosen for the
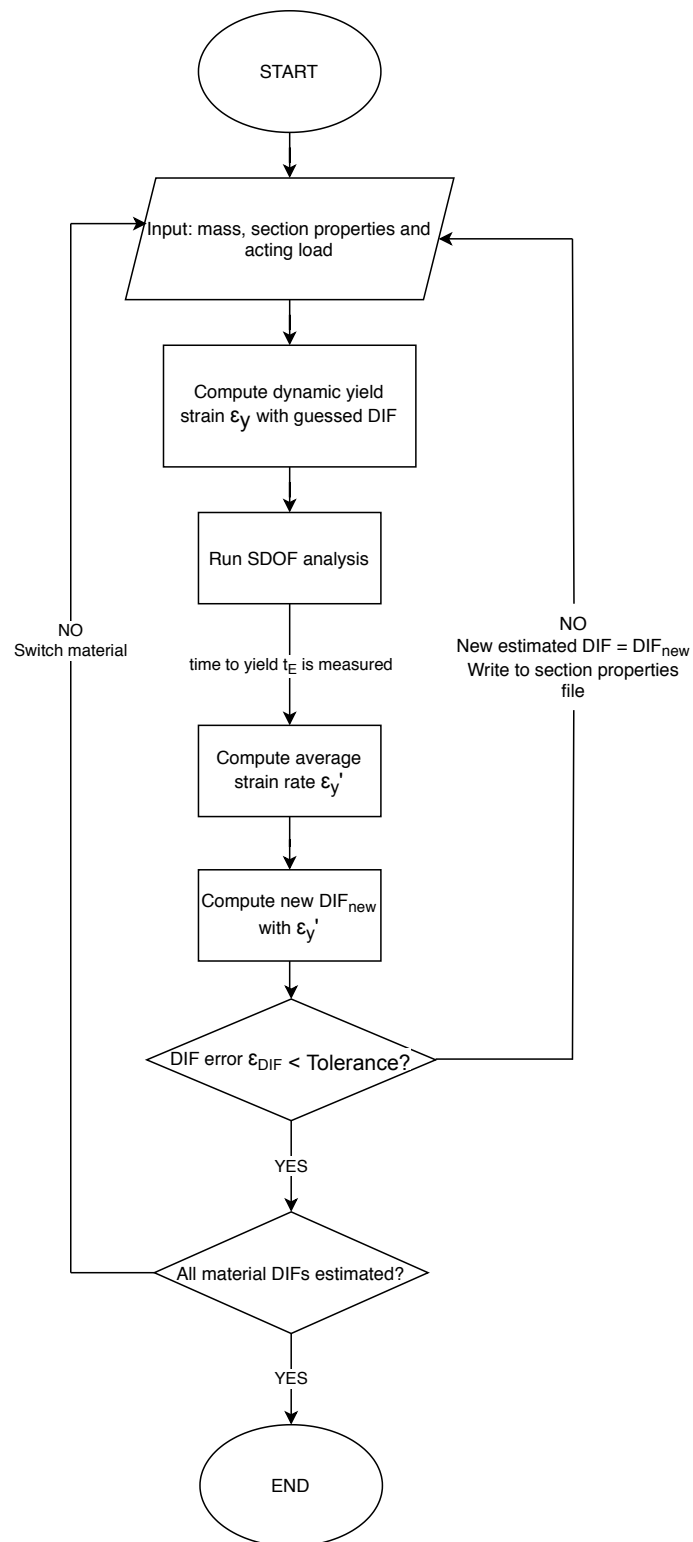
Figure 4.5: DIF estimating routine, `StrainRateEst.m`

present study. Next, the various stages of the function used to perform the SDOF analysis are presented. All the supporting nested functions are described.

4.2.1 Numerical Solution of the equation of motion

Analytical solutions to the equation of motion for an SDOF system can be complex to obtain if the excitation varies indiscriminately with time or if the system is nonlinear. Thus, numerical time-stepping methods are employed instead as they provide a good alternative to the integration of differential equations. The goal of such methods is to solve equation (4.1), by computing displacements that satisfy the equilibrium conditions at each time step.

$$M_e \ddot{u} + c\dot{u} + R(u) = F_e(t) \tag{4.1}$$

Integration schemes fall into one of two categories: implicit and explicit numerical methods. Implicit time-integration techniques are computationally slower per step but are able to utilize significantly larger time steps than the explicit methods, while retaining an appreciable accuracy [31]. In other words, implicit time-stepping methods provide solutions to the equation of motion over longer computational times, while requiring less time steps. The reverse of this is true for explicit methods.

Among the most commonly used methods are the Newmark-β, the Wilson-θ and the central difference methods.

MATLAB ODE solvers

The proprietary software package MATLAB [40] offers a suite of functions capable of solving ODEs. These functions are named `ode`, followed by a number that can be 45, 23, 113, etc. The function to be used depends on the precision requirements as well as the time scale of the equation to be solved. As a rule of thumb, `ode45` should be used as it is the function suite's general-purpose ODE solver.

4.2.2 Adopted integration scheme

The algorithm implemented in the present study used to solve the equation (4.1) was proposed in [30]. This integration scheme makes use of the built-in function in MATLAB ode45, which is based on an explicit adaptive Runge-Kutta formula, developed by Dormand and Price [19].

The complexity in solving equation (4.1) arises from the nonlinearity of the restoring force R, given that bilinear hysteretic models are discontinuous functions of the displacement, u. Thus, the prediction of the response at any given time is dependent not only on state variables at the current time but also at previous time-steps [30].

The use of Runge-Kutta method to integrate equation (4.1) implies the use of space-state variables, since it only deals with first-order ordinary differential equations. Defining **y** as the space-state variable vector:

$$\mathbf{y} = \begin{bmatrix} \dot{u} \\ \ddot{u} \end{bmatrix} = \begin{bmatrix} v \\ \dfrac{F_e(t) - c\dot{u} - R(u)}{M_e} \end{bmatrix} \tag{4.2}$$

where v defines the velocity.

In the present study, the system's restoring force R is a piecewise function of the displacement u, turning the dynamic system into a hybrid one, where it interacts with both continuous and discrete state/algebraic variables [30]. The variables assumed to be continuous are the displacement, velocity and restoring force. The discrete variable is the state flag tag_2 that indicates whether the system is responding elastically or elastoplastically to the external force.

In order to take hardening/softening effects into account the bilinear resistance model can be treated as a "Jenkin's element" and a linear spring connected in parallel [30]. The Jenkin's element is a linear spring that models the linear hysteretic behaviour while the second linear spring enables the system to harden or soften in post-yield responses. The contribution of these elements is illustrated in Figure 4.6.
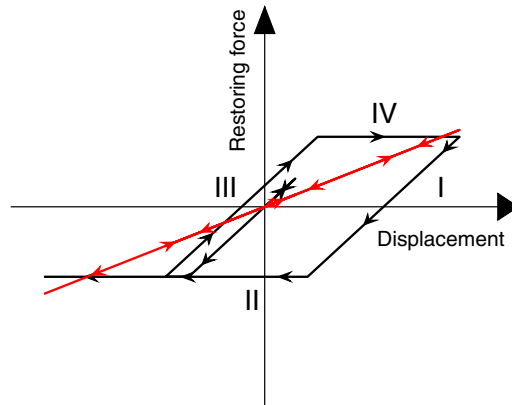

Figure 4.6: Separation of the resistance components in the Jenkin's element (black) and a linear spring (red)

To account for this decomposition of the resistance function, the space-state vector is rewritten as such:

$$\mathbf{y} = \begin{bmatrix} y(1) \\ y(2) \\ y(3) \\ y(4) \\ y(5) \end{bmatrix} = \begin{bmatrix} u \\ \dot{u} \\ p = p_1 + p_2 \\ R_1 \\ R_2 \end{bmatrix} \tag{4.3}$$

where $y(4)$ and $y(5)$ are the contribution of the Jenkin's element and the additional linear spring, respectively. $y(3)$ defines the integral of the restoring force with respect to time and is called *g-momentum*.

Finally, by differentiating the space-state vector:

$$\dot{\mathbf{y}} = \begin{bmatrix} \dot{y}(1) \\ \dot{y}(2) \\ \dot{y}(3) \\ \dot{y}(4) \\ \dot{y}(5) \end{bmatrix} = \begin{bmatrix} \dot{u} \\ \ddot{u} \\ R = R_1 + R_2 \\ \dot{R}_1 \\ \dot{R}_2 \end{bmatrix} = \begin{bmatrix} y(2) \\ \dfrac{F_e(t) - c\,y(2) - y(4) - y(5)}{M_e} \\ y(4) + y(5) \\ (1 - tag_2)(1 - \alpha)ky(2) \\ \alpha ky(2) \end{bmatrix} \tag{4.4}$$

where k defines the elastic stiffness of the system and α is the ratio between the post-yield stiffness and k.

The transition between deformation states is done with modes 1 through 8. The start of the modes is detected via event functions within the `ode45` option set. Three event functions were implemented to do so, encompassing stages I through IV, each representing a different combination of deformation and loading states. Stages I and III indicate that the response is currently elastic and the system is being unloaded and loaded, respectively. Stages II and IV indicate that the response is in the plastic stage in unloading and loading, respectively. Thus, tag_2 equals 0 for stages I and III, and 1 for stages II and IV. The hysteretic formulation can be seen graphically in Figure 4.7(a), while the mode transition diagram is illustrated in Figure 4.7(b).

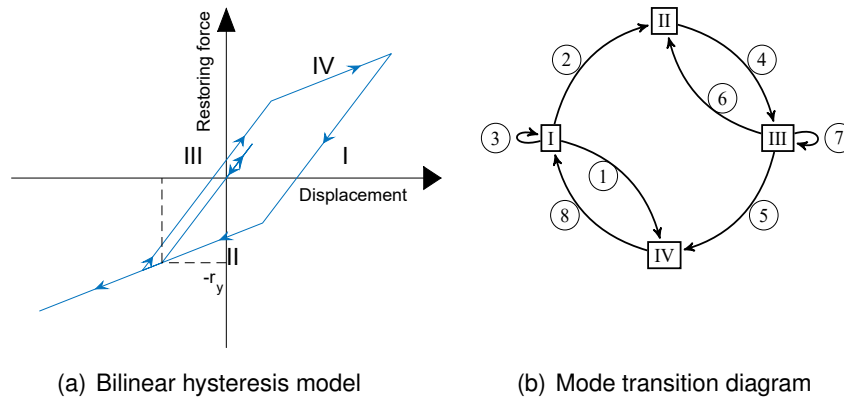(a) Bilinear hysteresis model   (b) Mode transition diagram

Figure 4.7: Representation of the hysteretic model implemented in the numerical model and its mode transition diagram, adapted from [30]

The event functions are handled by the nested function named `EventFun` and the conditions detected by this routine are the following:

$$\begin{aligned} \text{Event 1} &\longrightarrow y(4) - (1 - \alpha^{(+)})R_y^{(+)} = 0 \\ \text{Event 2} &\longrightarrow y(4) + (1 - \alpha^{(-)})R_y^{(-)} = 0 \\ \text{Event 3} &\longrightarrow y(2) = 0 \end{aligned} \tag{4.5}$$

The algorithm was modified to allow for asymmetric

resistance-displacement relationships to be used in simulations. In particular, the modified algorithm is able to simulate equivalent systems with different positive and negative yield loads as well as different post yield stiffness values, as illustrated in equation (4.5) with the superscripts signaled as "$+$" or "$-$".

The solving algorithm makes use of nested functions, removing the necessity for multiple m-files. The validation of the integration scheme is present in Appendix B.

4.2.3   Structure of the solving function

The function that solves the equation of motion is named `Solver.m`. It contains all routines and nested functions necessary to simulate a blast scenario. The main solving scheme is described in Figure A.6.

Within the function `Solver.m`, several supporting sub-routines are present. Those are the following:

- `StructureODE` - Constructs the space-state vector that serves as input in the ode45 function;

- `EventFun` - Contains the event functions that detect changes in the deformation state and indicates ode45 to halt the analysis and reevaluate tag_2;

- `loadIdx` - Only used in cases where the input function is a non-blast load, custom function. Interpolates the input load function and outputs a load value for the desired time-step;

- `fetchParam` - Outputs the blast wave characteristics, provided the input load function is a blast load scenario;

- `load_history` - Outputs the complete load time history;

- `corrected_loads` - Outputs the corrected acting load time history (if load attenuation effects were considered);

- `EnergyBalance` - Computes the energy balance for the response;

- `monoDetect` - Detects whether the input load function is a strictly monotonic function;

- `ELL` - This is the equivalent lateral load function; it receives the previous displacement, the boundary conditions, the element's width and span and the acting axial load as input; outputs an equivalent lateral load at each time step to be added to the main load time history.

4.2.4   Dissipated energies

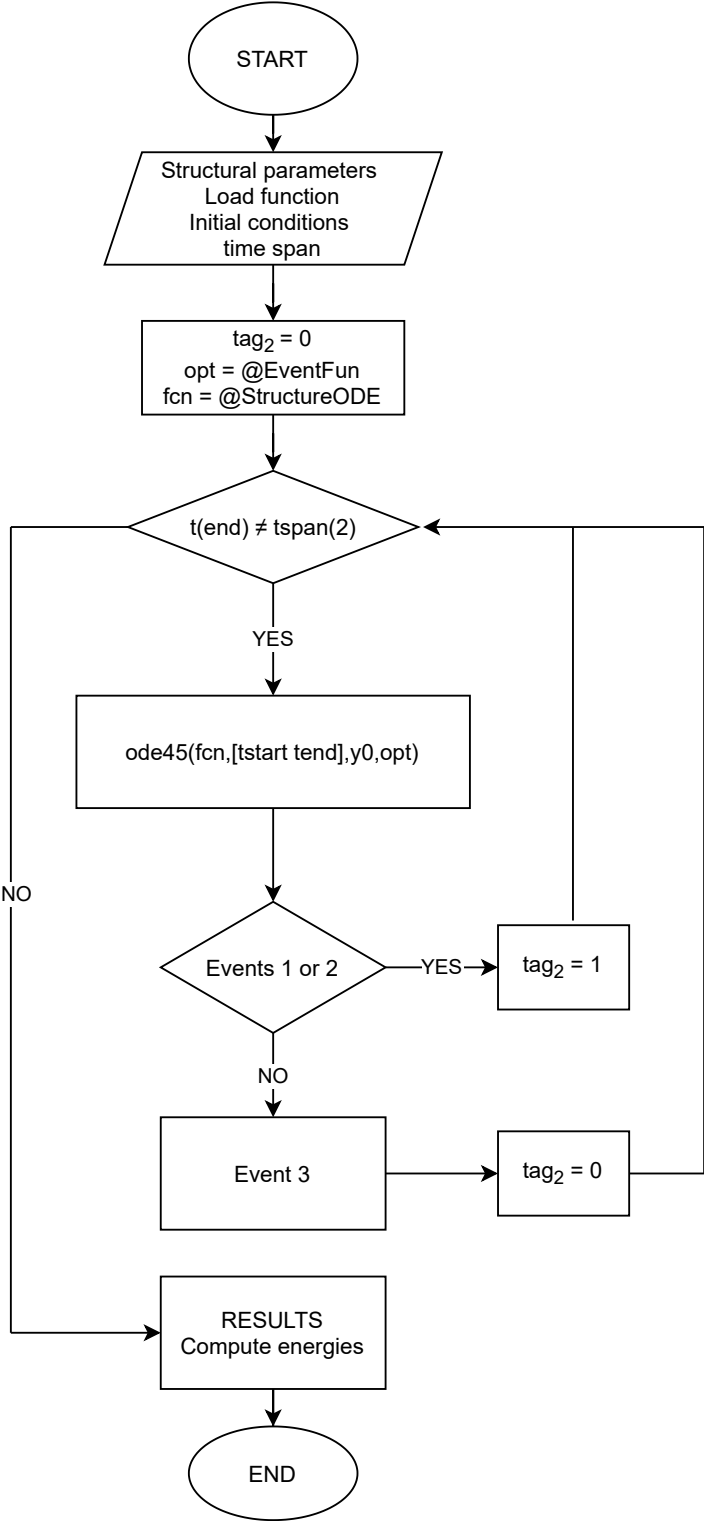When the analysis is concluded, the energy balance is conducted. The computed energies are present in Table A.1.

Figure 4.8: Solving function flowchart

Table 4.1: Energy balance typology and corresponding expressions

Type	Expression $(i > 0)$
Total	$\sum \frac{1}{2}(u_{i+1} - u_i)(p_{i+1} + p_i)$
Elastic	$\frac{1}{2}R^2/k_y$
Kinetic	$\frac{1}{2}M_e v^2$
Visco-elastic	$\sum \frac{1}{2}c\,(u_{i+1} - u_i)(\dot{u}_{i+1} + \dot{u}_i)$
Histeretic	Total - Elastic - Kinetic - Visco-elastic

4.3 Post-processing stage

The software produces three types of outputs: a graphical representation of the evolution of a series of parameter with respect to time, the maximum values of the relevant parameters and solution files for spreadsheet manipulations.

4.3.1 Graphical results

In the numbered section **8** in Figure 4.1 are the available graphical representations of results. Those are as follows:

- `displacement` - plots the displacement time history;

- `velocity` - plots the velocity time history;

- `acceleration` - plots the acceleration time history;

- `displacement-restoring force`;

- `displacement-velocity` - plots the phase plane;

- `Energy time history` - plots the energy balance;

- `Corrected load history` - plots the corrected acting load with shock wave attenuation effects, when available.

4.3.2 Final results

In section number **9** in Figure 4.1, the relevant results regarding the analysis are displayed. Those are:

- `Maximum displacement`;

- `Support rotation`;

- `Ductility ratio` - the ratio between the maximum displacement and the maximum elastic displacement;

- `Damage category`.

These are the most relevant results for the structural design elements intended to sustain blast loads as they allow for the verification of limit states.

4.3.3 Exporting results

In the section numbered **10** in Figure 4.1, the program allows for the exportation of several outputs, generated in the analysis. Those are the following:

- `Time [s]` - prints an n x 1 time vector, where n is the number of time steps;

- `Restoring force [kN]` - prints an n x 1 restoring force vector, where n is the number of time steps;

- `Displacement [m]` - prints an n x 1 displacement vector;

- `Velocity [m/s]` - prints an n x 1 velocity vector;

- `Acceleration [m/s^2]` - prints a n x 1 acceleration vector;

- `Energy balance [kJ]` - prints an n x 5 array containing all computed energies.

- `Energy figures` - prints the energy balance plot to a figure file;

The results are readily available to export by checking the relevant checkboxes and pressing the *Export results* button.

Chapter 5

Model validation

This chapter details the simulations performed with the developed numerical tool to assess its to estimate the structural response of beam and beam-column elements when subjected to blast loads. The simulated results are compared with the experimental data available in the literature.

The validation is based on two sets of experimental data. In the first, the response of equivalent beam and beam-column elements will be compared with numerical data from Biggs [8] and the Design Guide PDC-TR-08-03 problem sheet [63], respectively.

The second set of tests consists in the comparison of the responses obtained from real tests conducted on beam and beam-column elements subjected to shock waves. The data for these tests was obtained by Magnusson [37] and Burrel et. al [12].

The results are evaluated in terms of peak displacement and maximum support rotation. All simulations in the present chapter feature null initial displacements and velocities.

5.1 Case study 1: Fixed-fixed beam

This case study will assess the program's ability to analyse fixed-fixed boundary conditions in beams, by comparing results with those reported in [51]. The results were obtained in [51] by using an abacus derived by Biggs [8] and recommended by the UFC-3-340-02 [1]. The abacus presented in Figure 5.1 is used to compute the maximum response of the structural element, when subjected to a triangular load.

5.1.1 Material and geometric properties

The beam to be analysed is fixed at both ends, Figure 5.2(a), has a 0.4 m by 0.3 m section and a span of 3 m. It possesses equal tensile and compression steel in the form of $3\phi20$ bars. Shear reinforcement is not mentioned in the report, and the failure mode for this case study is assumed to be purely flexural. The steel's yield strength is 435 MPa. The concrete has a compressive strength and Young's modulus of 20 MPa and 33 GPa, respectively.
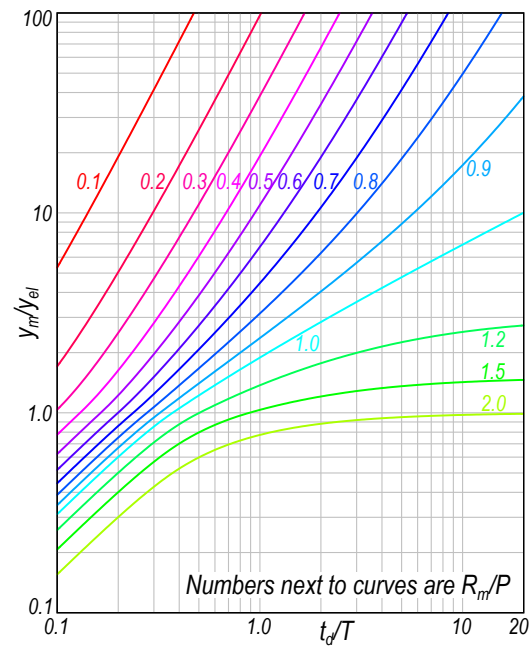
Figure 5.1: Maximum response of undamped elasto-plastic one-degree system due to triangular load pulses [8, 1]

The system's mass, assuming a volumetric weight for concrete of 2.5 ton/m^3, is 0.9 tons.

Since many of the parameters needed by the resistance-deflection algorithm are missing, such as the concrete cover c, the concrete's tensile resistance f_{ctm}, ultimate steel resistance f_{su}, etc., the curve presented will be used directly as input. Its defining points are present in Table 5.1.

Table 5.1: Case study 1 resistance curve points

Deflection [mm]	Resistance [kN]
-1	-494.3
-0.82	-494.3
0	0
0.82	494.3
1	494.3

The value for the ultimate displacement is set to 1 mm just to define the resistance curve as having no post-yield stiffness.

5.1.2 Load conditions

The applied load is triangular with a peak value of 87 kN/m and a duration of 9 ms. A graphical representation is in Figure 5.3(a). This pressure profile is converted to a force by multiplying by the incident area of 3.0 m by 0.4 m, equaling 1.2 m^2. The resulting load history is the one displayed in Figure 5.3(b)
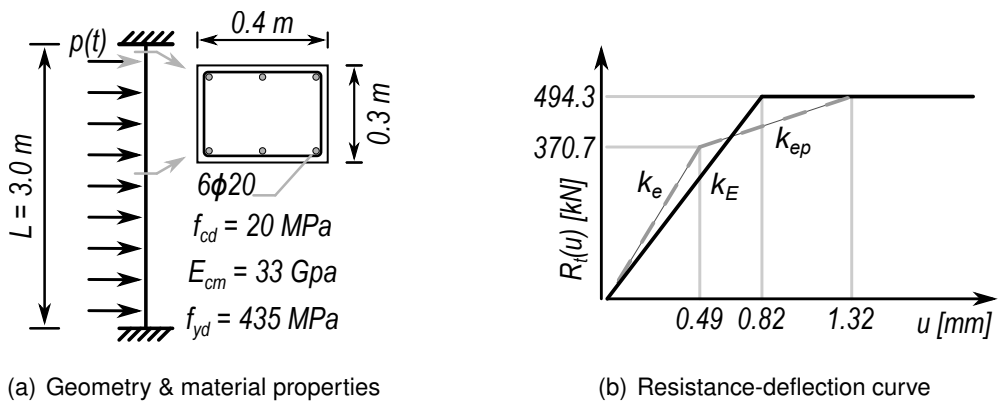
(a) Geometry & material properties

(b) Resistance-deflection curve

Figure 5.2: Longitudinal and cross-section properties of example beam, adapted from [51]

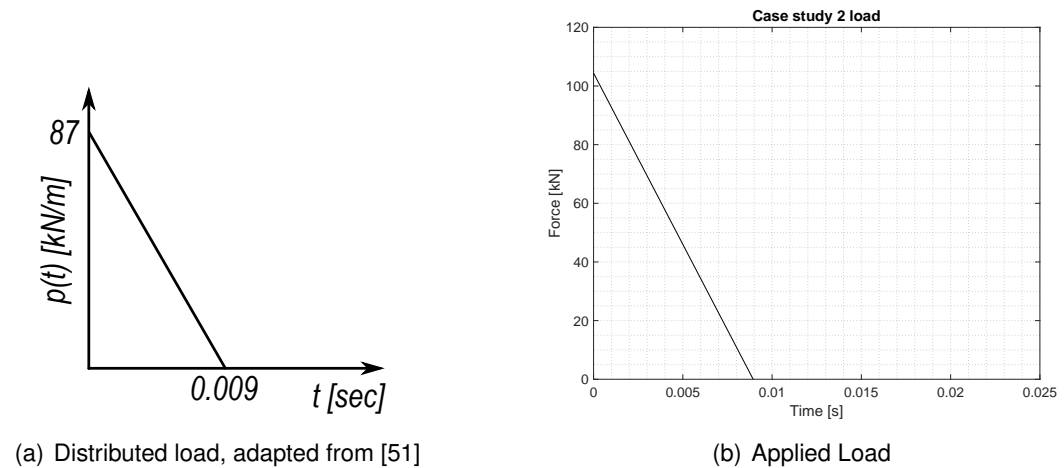(a) Distributed load, adapted from [51]

(b) Applied Load

Figure 5.3: Case study 1 pressure and load

5.1.3 Results

The analysis for the current case study yielded a maximum displacement of 0.286 mm, which when compared with the of 0.285 mm [51] produces a relative error of 0.35%. The displacement time history is illustrated in Figure 5.4(a) and the energy balance is found in Figure 5.4(b).

5.2 Case study 2: Fixed-simply supported column

Case study 2 features a fixed-simply supported column from the US Army's Corps of Engineers Example problems for SBEDS sheet [63].
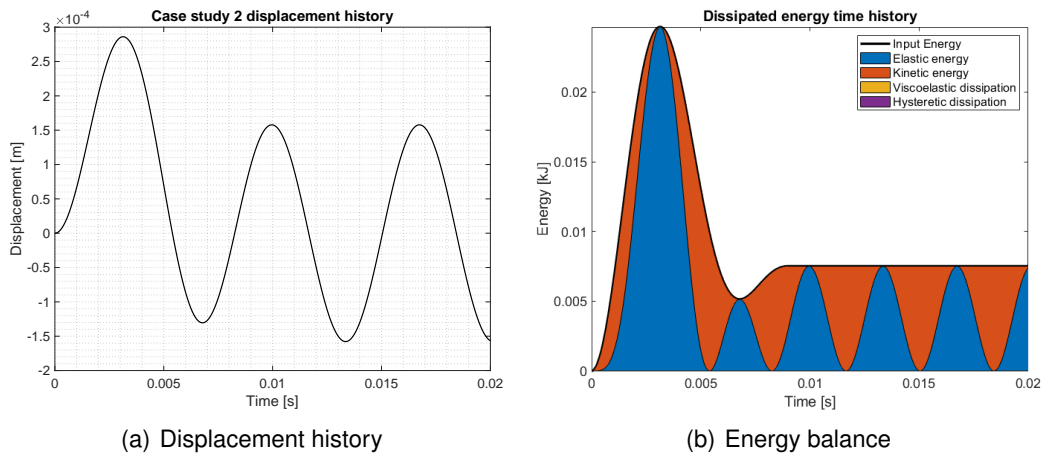
(a) Displacement history   (b) Energy balance

Figure 5.4: Case study 1 results

5.2.1   Material and geometric properties

The problem is described as a column fixed at the bottom and simply supported at the top, part of a single storey building with the columns spaced out 7 m from each other. The column has a square section of 0.46x0.46 mm^2 and a span of 4 m.

The cross-section, displayed in Figure 5.5(b), contains two 19 mm G 415 steel bars at each face, while the shear reinforcement is not mentioned, as failure is assumed to be purely flexural. The steel's yield strength, ultimate strength and Young's modulus are 415 MPa and 620 MPa and 200 GPa, respectively.

Regarding the concrete, it has a compressive strength and Young's modulus of 28 MPa and 23.803 GPa, respectively. There's no mention of the concrete's tensile strength; it was assumed to be equal to 2.9 MPa, as recommended by [21], for $f_c \approx 28$ MPa. The DIFs used in this case study were equal to 1.19, 1.17 and 1.0 for the concrete, steel in yield and the steel's ultimate capacity, respectively. Additionally, damping will not be accounted for in this analysis, thus ξ is set to 0.

5.2.2   Load conditions

The applied lateral load is a triangular pressure profile, with a peak pressure of 20 kPa and positive phase duration of 8 ms, Figure 5.5(a). Additionally, the element is subjected to a 1000 kN axial load, Figure 5.5(c).

5.2.3   Simplified model

The resistance-deflection function pertaining to the equivalent model of case study 2 is displayed in Figure 5.6. The column's interaction diagram is computed, both for the yielding and ultimate resistance stages, according to section 3.8. Both interaction diagrams for case study 2 are presented in Figure 5.7.

(a) Pressure-profile, adapted from [63]   (b) cross-section   (c) Loads imposed on the element
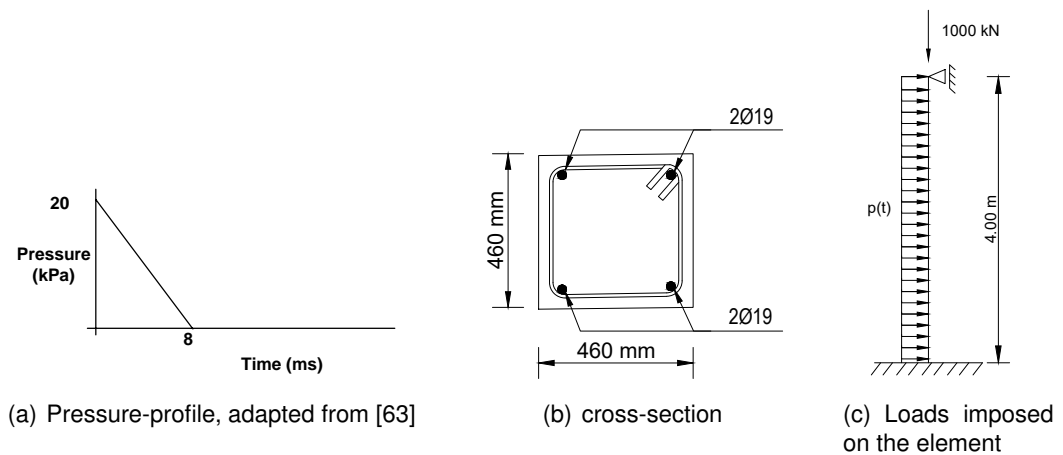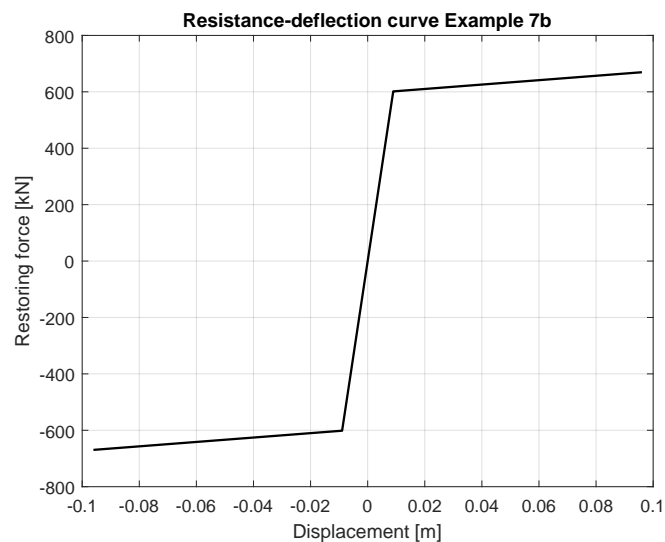
Figure 5.5: SBEDS problem sheet example 7b [63]

Figure 5.6: SBEDS problem sheet example 7b resistance curve

The mass of the system is computed by taking into account a concrete volumetric weight of 2.403 ton/m^3, as proposed for the problem, multiplied by the volume of the element plus 20% of the volume of the slab above it, Figure 5.8. According to the authors, only 20% of the total slab height actually vibrate with the column. The mass of the SDOF system is thus equal to 5.06 tons.

5.2.4 Results

The reference results were obtained with the SBEDS SDOF spreadsheet, which for this problem outputs a maximum displacement of 3.24 mm and a maximum support rotation of 0.09°. The model developed in the present study output a maximum displacement of 3.18 mm, a maximum rotation of the support of 0.09º.
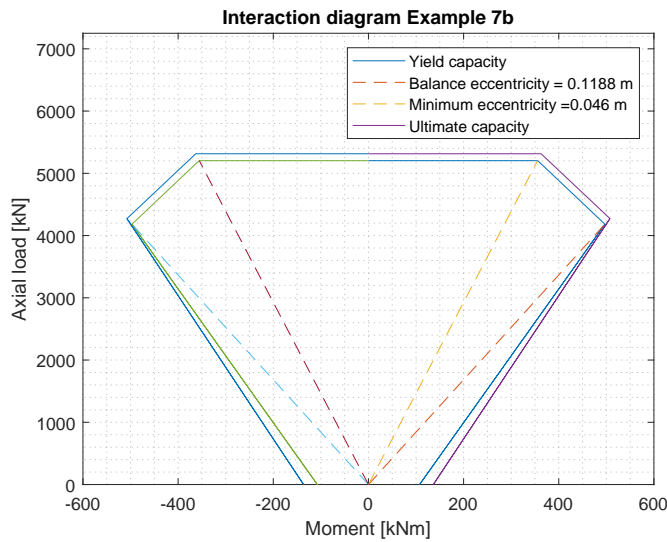
Figure 5.7: SBEDS problem sheet example 7b interaction diagram

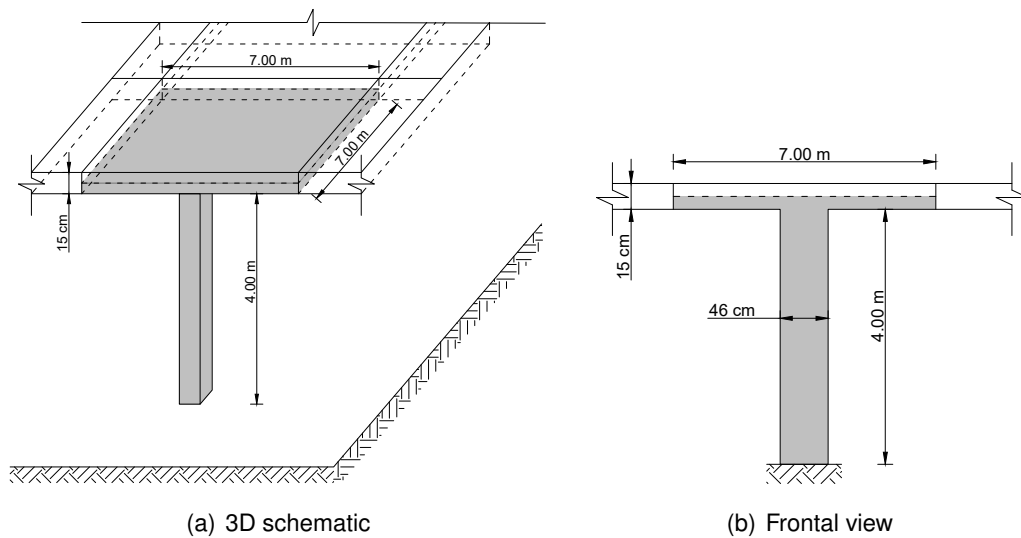

(a) 3D schematic

(b) Frontal view

Figure 5.8: SBEDS problem sheet example 7b total volume representation

A full comparison of the results and the relative errors are presented in Table 5.2. The graphical representation of the response is found in Figure 5.9(a) and (b) for the solved displacement history and energy balance, respectively.

Table 5.2: SBEDS problem sheet example 7B results

Parameter	Present study	SBEDS	Error [%]
u_{max} [mm]	3.18	3.24	1.9
θ_{max} [°]	0.09	0.09	0.0

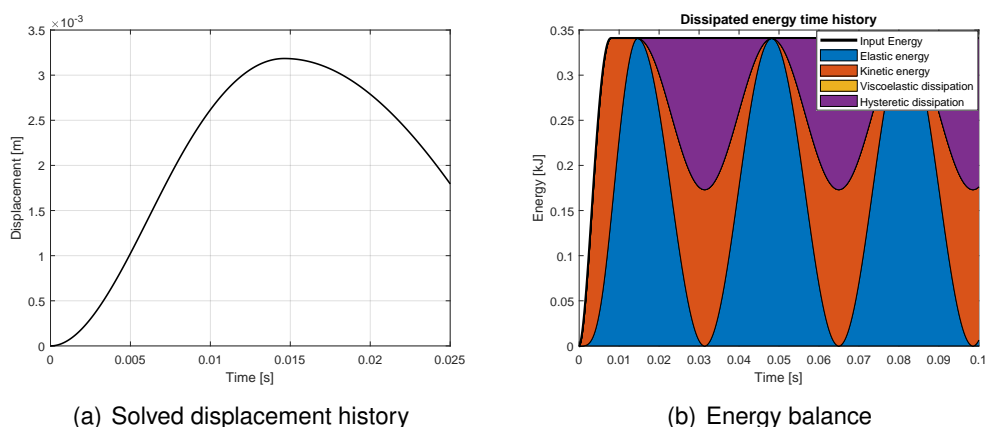(a) Solved displacement history

(b) Energy balance

Figure 5.9: SBEDS problem sheet example 7b response and energy balance

Table 5.2 illustrates a slight discrepancy between results. This difference may arise from the total mass calculations, where the author recommends the mass to account for an additional 20% of the above slab's mass whilst describing a 7 m horizontal span, while not mentioning the slab's dimension parallel to the load, seen in Figure 5.8, assumed as 7 m.

5.3 Case study 3: Magnusson's beams

The third benchmark test is taken from an experimental campaign performed by Magnusson [37]. The goal with the experimental campaign was to evaluate the performance of high-strength reinforced concrete beams when subjected to both quasi-static and blast loads.

The experimental campaign consisted of 14 reinforced concrete beams with 3 different combinations of concrete grade: beam B40, with concrete grade K40, beam B100 with concrete grade K100 and beam B200 with concrete grade K200. The numeral after 'K' refers to the nominal compressive cube strength in MPa.

This case study's purpose is to assess the developed numerical model's capability to predict the structural response of simply supported beam elements with imposed blast loads. The beams considered in this section are the B40 and B100(16) beams.

5.3.1 Specimen's properties

All specimens were reinforced with the same configuration of steel bars, with $5\phi16$ bars for tensile reinforcement and $2\phi10$ bars for compression reinforcement. The concrete section was confined by $\phi8$ stirrups, with a 20 cm spacing. The bars' diameter was measured before construction. Uniaxial tensile tests were carried out on the steel bars and their properties are summarized in Table 5.3.

All specimens shared the same geometry, both transversal and

Table 5.3: Magnusson beam steel properties

ϕ_{nom} [mm]	ϕ_{obs} [mm]	f_{sy} [MPa]	f_{su} [MPa]	E_s [GPa]
		Steel		
16	15.37	604	703	210
8	8.27	501	597	205

longitudinal. The cross-section was 290 mm in width and 160 mm in height, with a 25 mm concrete cover. Longitudinally, all elements had a length of 1.72 m with a 1.5 m free span length between supports.

Concrete cubes were tested on the same day as the experiments. The results of these tests are listed in Table 5.4. The detailing of both the longitudinal and the cross-section are present in Figure 5.10.

Table 5.4: Magnusson beam concrete's mechanical properties

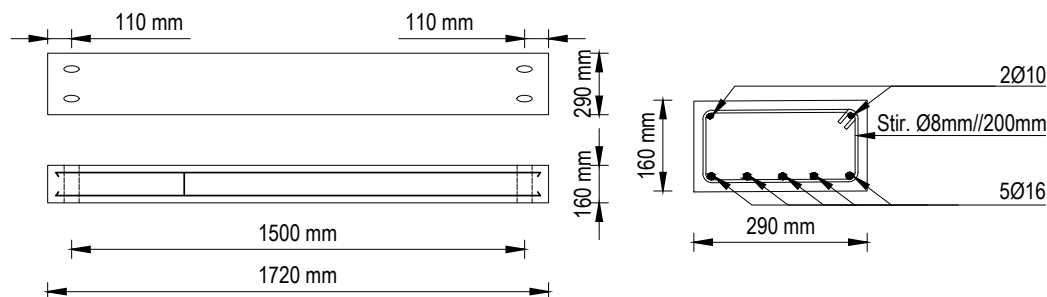| Specimen	f_c [MPa]	f_t [MPa]	E_c [GPa]
	Concrete		
B40	53.8	4.6	44.7
B100(16)	101.0	5.40	41.7

Figure 5.10: Geometrical and reinforcement detailing of B40 and B100(16) beams, adapted from [37]

The blast load was induced in a shock tube at the Swedish National Defence Research Institute, in Märsta. The tube , represented in Figure 5.11 has an internal section of 1.6 m in height and 1.2 m in width and is used to simulate short duration shock waves originating from air blasts. The explosive charge is positioned 80 cm from the ground, at the center of the tube's cross-section, at a distance of 10 m from the specimen. According to the authors, at this distance the reflected pressure can be considered as a uniformly distributed load [37].

The supports that hold the beam in place can be considered as rigid with negligible horizontal displacements and the beam may be considered as being simply supported, given the bolt's low flexural strength. The tranverse displacement time history at mid-span was measured by a deflection gauge. Support reactions were also recorded resorting to two load cells with a maximum capacity of 1000 kN. Two pressure gauges, positioned on each side of the specimens allowed for the
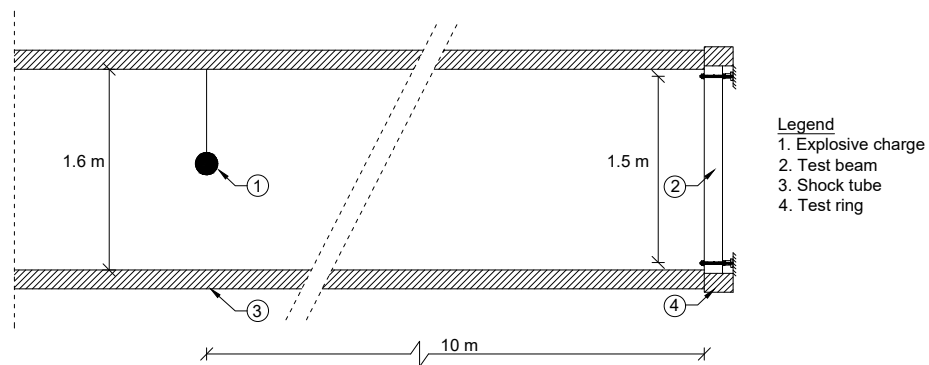
measurement of the reflected pressure.

Figure 5.11: Experimental set-up of the beam and explosive charge within the tube, adapted from [37]

5.3.2 Test setup

Four blast scenarios will be considered; two imparted on B40 specimens and two on B100(16) specimens. These were selected as they either induced failure by bending or no failure at all. After generating the idealized load time histories, by using the parameters recorded in the test in the modified Friedlander equation, it was found that the approximated load profiles imparted a bigger impulse on the equivalent specimens. As such, new load time histories were computed to match the recorded impulses.

The specifications for each of the blast scenarios is presented in Table 5.5. Column 3 in Table 5.5 contains the impulses indicated by the authors, while column 4 presents the impulses obtained by integrating the pressure time histories, recorded after the tests. The initial idealized, adjusted idealized and measured pressure profiles may be found on Figure 5.12.

Table 5.5: Blast load characteristics

Beam nº	P_r [kPa]	$i_r^{(measured)}$ [kPas]	$i_r^{(used)}$ [kPas]	t_0^+ [ms]
B40-D1	650	3.76	3.23	23
B40-D3	780	4.70	4.78	22
B100(16)-D1	998	5.33	4.70	25
B100(16)-D2	1459	6.44	6.32	20

5.3.3 SDOF properties for B40 and B100(16) beams

The equivalent model is defined in accordance with the procedures outlined in chapters 2 and 3. The construction of the blast load file is done by inputting the blast wave parameters in the modified Friedlander equation. The load is then converted from pressure units into force by multiplying it with the section's width and height.

(a) B40-D1   (b) B40-D3

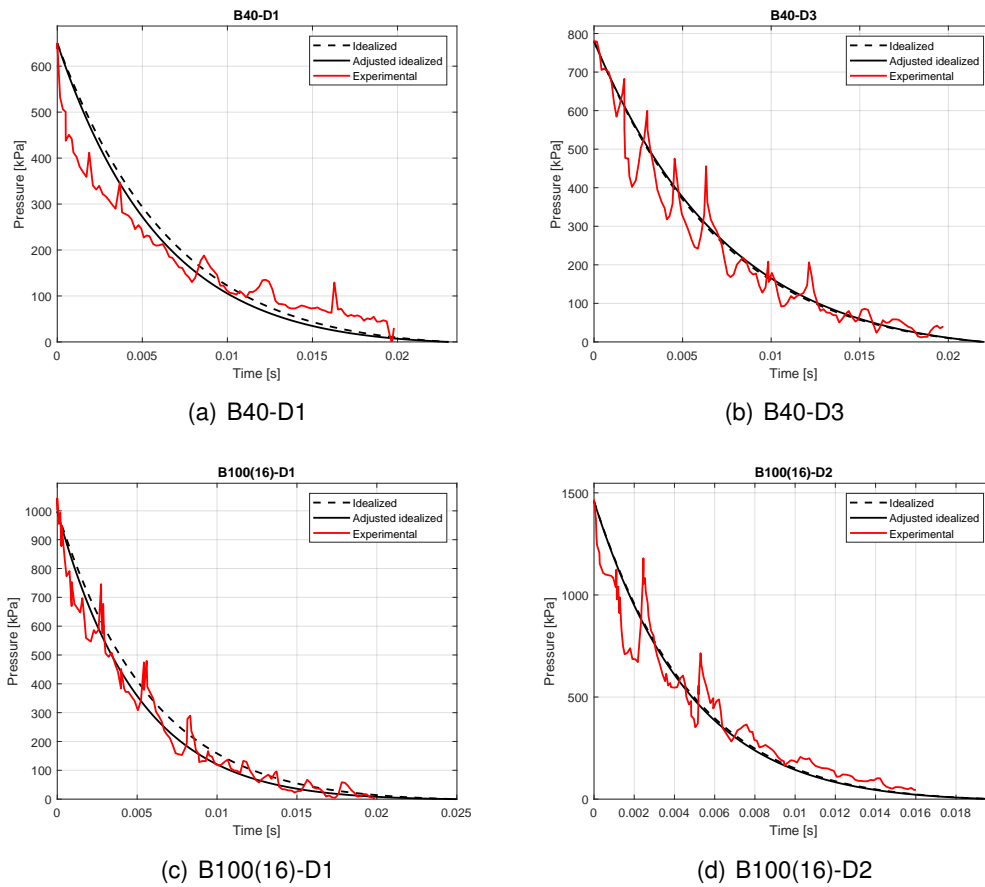(c) B100(16)-D1   (d) B100(16)-D2

Figure 5.12: Idealized, adjusted idealized and measured pressure time histories for blasts on specimens B40 and B100(16), measured data adapted from [37]

The resistance-displacement relation was constructed based on the geometric and material properties in each beam's corresponding file. The dynamic increase factors for concrete, steel in yield and ultimate steel strength, which after running the DIF estimation routine, resulted in the values present in Table 5.6. Since the mechanical properties of both the concrete and the reinforcement steel were obtained from tests, all SIFs are set to 1. Additionally, the damping ratio, ξ, equals zero as recommended in [62, 1].

Table 5.6: Dynamic increase factors for beams B40-D1 and B40-D3

Beam nº	DIF_c	DIF_{sy}	DIF_{su}	E_{dyn}/E_{sta}
B40-D1	1.351	1.230	1.068	1.100
B40-D3	1.381	1.265	1.078	1.100
B100(16)-D1	1.410	1.27	1.080	1.290
B100(16)-D2	1.430	1.27	1.080	1.310

The resulting resistance curves are presented in Figure 5.13.
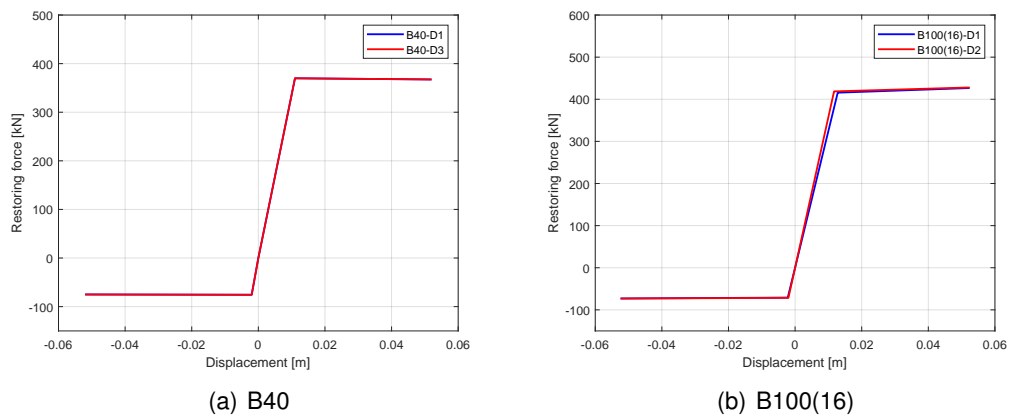
(a) B40

(b) B100(16)

Figure 5.13: Resistance curves for B40 and B100 beams

5.3.4 Simulated results

Four blast scenarios were considered. Two acting on B40 beams and the other two on B100(16) beams. A summary of the recorded responses is present in Table 5.7. A graphical comparison between the experimental and numerical results , with and without load attenuation effects for the four blast scenarios is illustrated in Figure 5.14. The energy balance and force-displacement (hysteretic loops) from numerical simulations are presented in Figure 5.15 and 5.16, respectively.

Table 5.7: Experimental [37] and simulated responses for Magnusson beams

Specimen	Attenuation effects	u_{max} [mm]	u_{exp} [mm]	Error [%]
B40-D1	No	10.56	9.40	10.98
	Yes	8.65		7.98
B40-D3	No	13.03	12.00	7.90
	Yes	11.05		7.92
B100(16)-D1	No	15.49	18.60	16.72
	Yes	13.11		29.52
B100(16)-D2	No	24.57	25.40	3.27
	Yes	18.06		28.90

5.3.5 Discussion

The algorithm revealed an appreciable adequacy in evaluating the response of beams when subjected to blast loads and proves to be accurate enough to provide good early-design stage results. A maximum error of 14% and 28% were recorded for the upper and lower bound limits, respectively, where the upper and lower
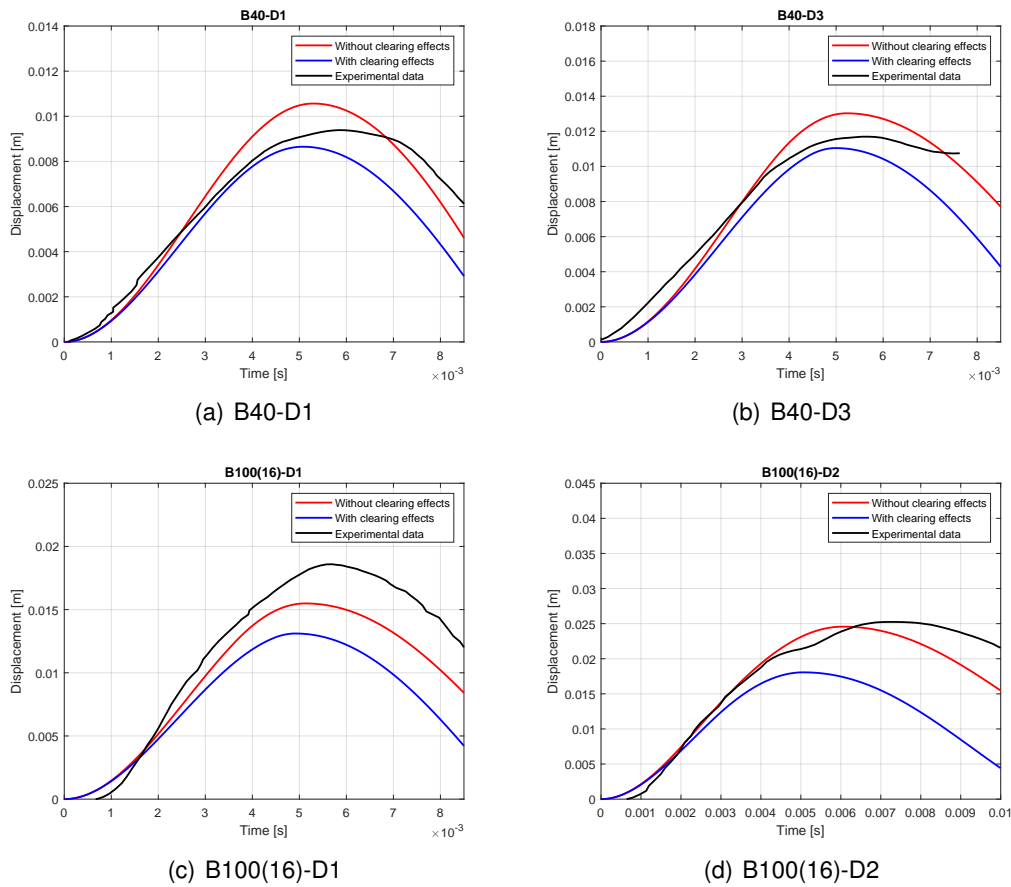
Figure 5.14: Algorithm results vs Magnusson experimental data of B40 and B100 beams, adapted from [37]

limits were computed with and without blast wave attenuation effects, respectively. The only case where the experimental data isn't delimited the upper and lower simulated results is in the simulation on beam B100(16)-D1. A possible source for the discrepancy recorded in this case study is the use of an idealized load time history, which, even when adjusted, fails to perfectly replicate the recorded pressure time histories. The idealized load profiles provide a good approximation to the ones recorded in [37], though noticeable disparities between the two introduce errors in the analysis. A quick analysis of Figures 5.12 and 5.14 reveals a load duration and natural period of 23 ms and 5.5 ms, on average, respectively. Thus, the ratio $t_0^+/T_n \approx 4 >> 1/4$ which means the loading is not impulsive and its shape over time must be carefully accounted for.

5.4   Case study 4: Burrel columns

The fourth case study will focus on a set of tests performed in 2014 by Burrel and coworkers [12] which were conducted in order to study the performance of steel fiber-reinforced concrete (SFRC) columns under shock wave and axial loads. This

(a) B40-D1

(b) B40-D3

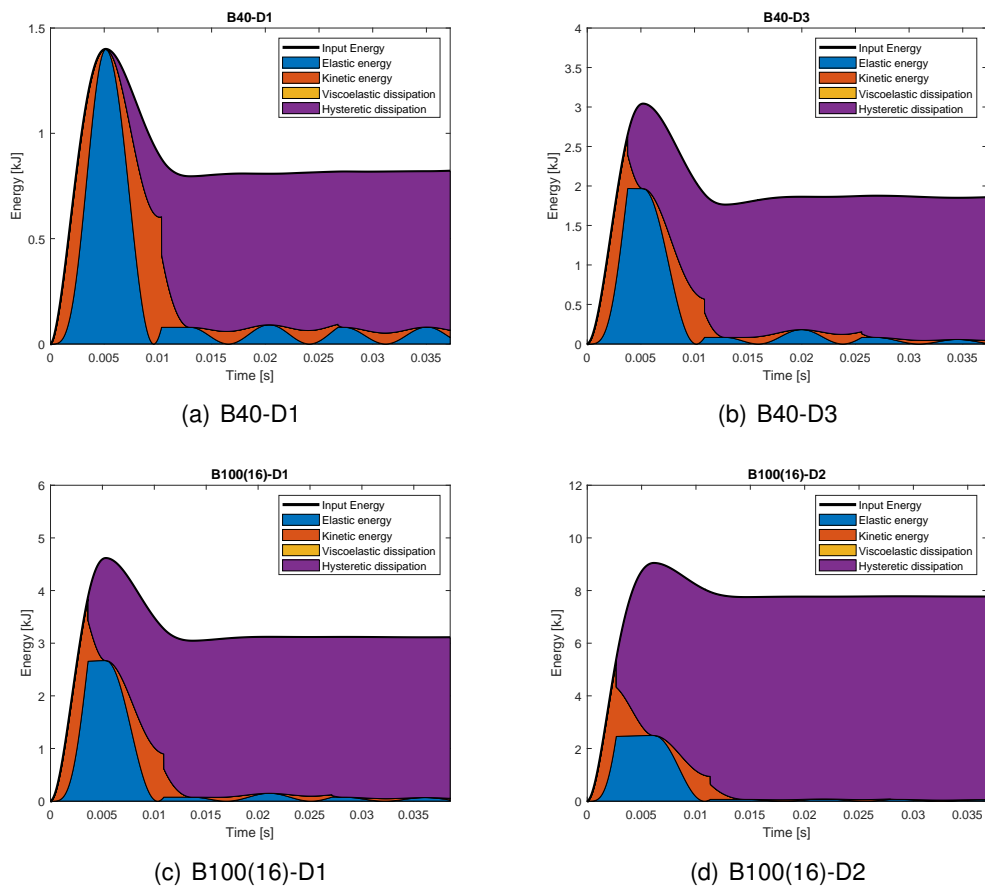(c) B100(16)-D1

(d) B100(16)-D2

Figure 5.15: Energy balance of Magnusson beams

case study aims to assess the performance of column analyses performed with the program developed within this dissertation.

In the test campaign 28 columns were tested, 7 of which were not fiber-reinforced to serve as control specimens. This study will focus on column SCC-0%-75, following the author's notation, under three distinct shock load scenarios. The notation SCC, refers to self-consolidating concrete, 0% means that there are no steel fibers incorporated in the the concrete and 75 refers to the spacing of shear reinforcement, in mm.

5.4.1 Specimen's properties

Column SCC-0%-75 has the geometric characteristics illustrated in Figure 5.17, having a square section of 152 mm by 152 mm, 5 mm of concrete cover and spanning 2.468 m. The reinforcement consists of 2x10M (ϕ = 11.3 mm) steel bars as longitudinal reinforcement on each face and 6.3 mm stirrup for shear reinforcement.

The mechanical properties of both concrete and reinforcement steel were obtained from mechanical tests. The concrete had a compressive strength, tensile
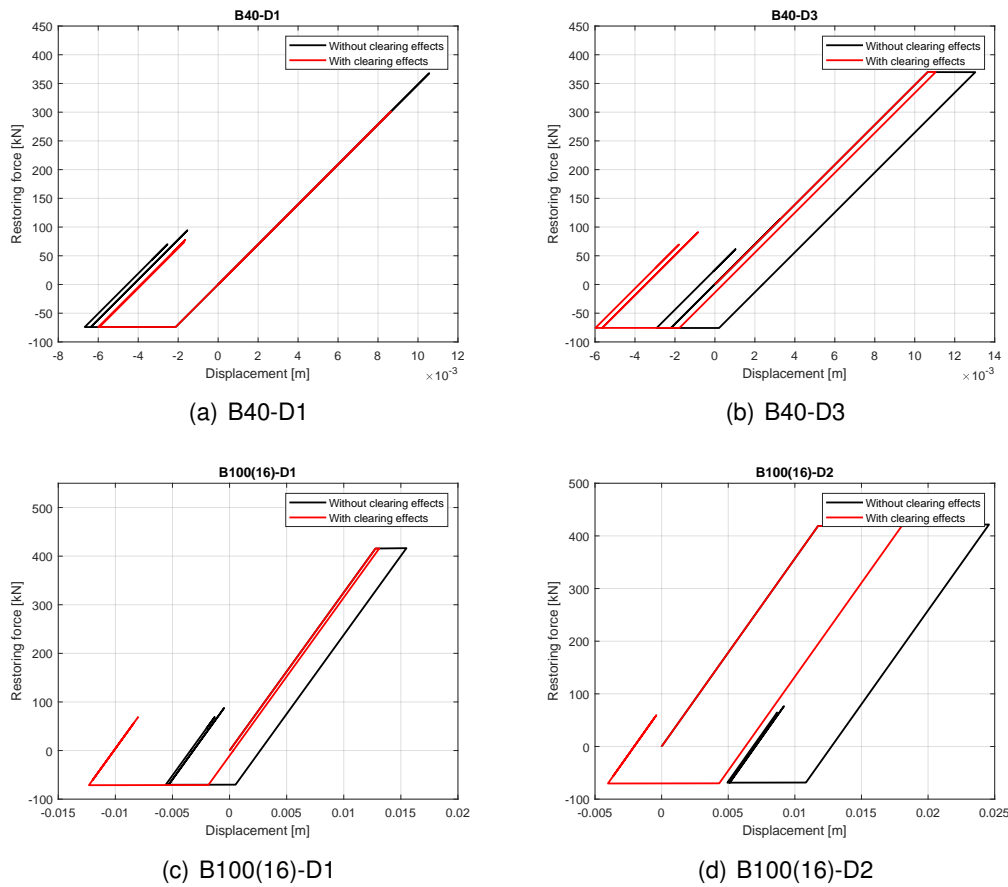
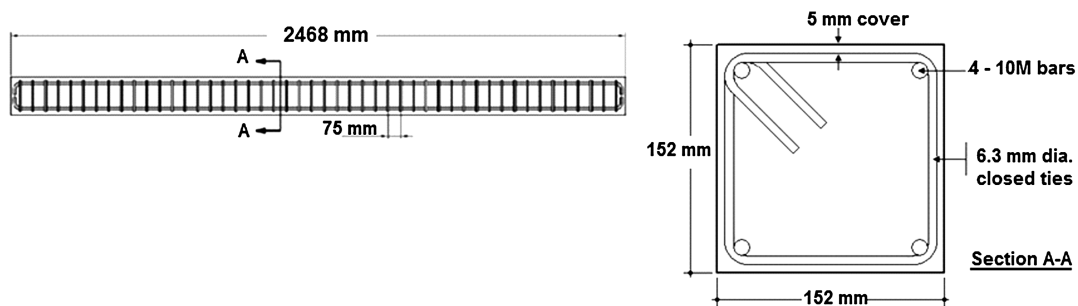Figure 5.16: Solved hysteretic loops of Magnusson beams

Figure 5.17: Longitudinal and transversal detailing of column SCC-0%-75, adapted from [12]

strength and Young's modulus of 51.6 MPa, 6.6 MPa and 37.75 GPa, respectively. The concrete's mechanical properties are indicated in Table 5.8.

Regarding the steel, the longitudinal reinforcement had a yield strength, ultimate strength and Young's modulus of 483 MPa, 675 MPa and 200 GPa, respectively. The shear ties have a yield strength of 604 MPa. The steel's properties are condensed in Table 5.9.

Table 5.8: SCC-0%-75 concrete properties

Concrete		
f_c [MPa]	f_t [MPa]	E_c [MPa]
51.6	6.6	37.75

Table 5.9: SCC-0%-75 steel properties

Steel			
ϕ [mm]	f_{sy} [MPa]	f_{su} [MPa]	E_s [GPa]
11.3	483	675	200
6.3	603	N/A	200

5.4.2 Shock tube

The blast load was simulated resorting to the University of Ottawa shock tube. The shock waves are produced by a compression chamber that releases compressed air into an expansion chamber, where the shock wave travels rapidly until it contacts with the specimen. The square test frame has a rectangular section of 2.033 m by 2.033 m.

5.4.3 Test setup

All columns in the experimental campaign were tested under axial load and lateral shock wave pressures. Figure 5.18 represents the test setup, in which the columns are partially restrained at the supports. A load-transfer device (LTD) is present under the form of a light gauge steel metal sheet connected to a series of steel beams, which collect and transfer the shock wave pressure as a uniformly distributed load acting on the face of the column.

The displacement history was recorded using three linear variable differential transducers (LVDTs), placed at 1/6th, 1/3rd and half the columns' span, enabling the interpolation of the displacements at any point in the specimens, in case that one of the LVDTs fail. The columns' free span was 1.98 m in length. The constant acting axial load of 294 kN was applied via a hydraulic jack.

5.4.4 Load conditions

As previously mentioned, three shock wave scenarios are to be tested: blasts 1, 2 and 3, acting on column SCC-0%-75. A summary of the shock wave's properties can be found in Table 5.10.

Table 5.10: Shock wave properties, adapted from [12]

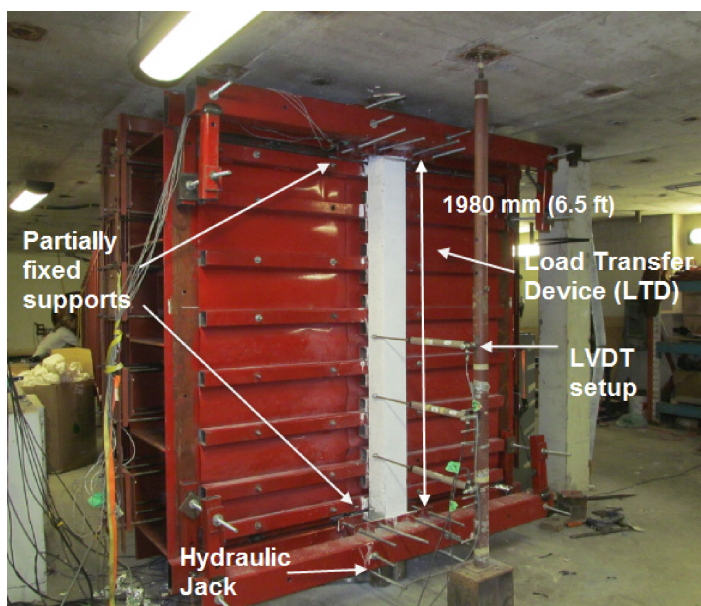| Blast nº	P_r [kPa]	$i_r^{(measured)}$ [kPa ms]	$i_r^{(used)}$ [kPa ms]	t_0^+ [ms]
1	13.7	130.0	113.1	22.2
2	42.4	381.0	361.6	22.2
3	87.9	780.7	776.7	25.4

Figure 5.18: Burrel column test setup, adapted from [12]

The acting shock waves were recorded. An idealized pressure profile was computed via the modified Friedlander equation and the shock waves were compared. The impulses for the recorded pressure time histories show slight discrepancies from the ones indicated by the authors. Therefore, the same procedure described in Case study 3 will be conducted and the idealized load histories will be adjusted to have the same impulse as the recorded pressure time histories. The initial idealized pressure, adjusted idealized and measured pressure profiles are illustrated in Figure 5.19.

5.4.5   Simplified model

The test's setup, consisting of the specimen and the test rig, had a combined mass of 315 kg, which is the mass of the SDOF model. The test's incident area for the shock wave is 4.129 m^2 (area of the shock tube opening).

Despite the authors indicating the support's partial restriction, the analysis will undergo assuming a simply supported beam.

The resistance-displacement relation was constructed from the geometric and material properties in the section file. The scaled distance Z equals -1. The DIF estimation routine `StrainRateEst` was used to predict the DIFs for tests 2 and 3 and the results are present in Table 5.11. Since in the test with blast 1 as acting load the element did not reach yield, estimating the DIFs for this scenario is impossible by using the iterative method. As such, the DIFs for blast scenario 1 will be the same as the ones used in blast scenario 2. Additionally, the effects of damping will not be considered. Therefore the damping ratio, ξ, is set to 0.

After running the resistance-deflection curve generating routine, the resulting curve is presented in Figure 5.20. The interaction diagrams for each
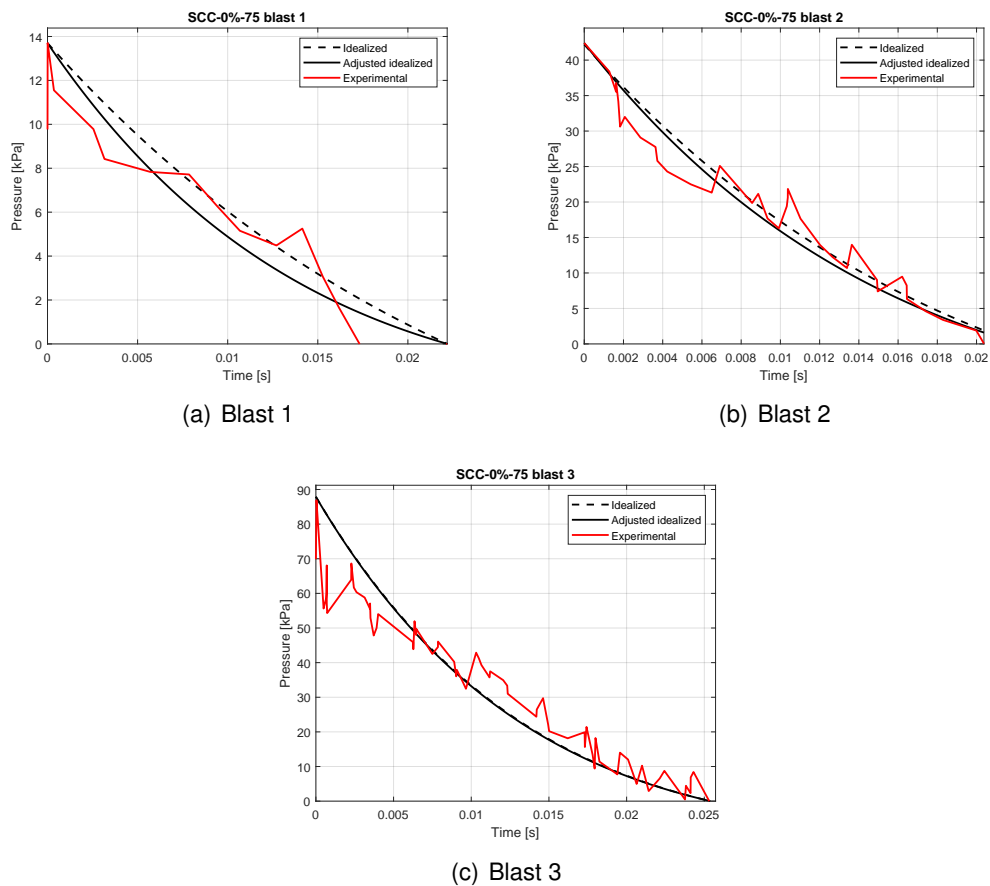
(a) Blast 1

(b) Blast 2

(c) Blast 3

Figure 5.19: Burrel pressure profiles for blast 1,2 and 3

Table 5.11: DIFs for blast 1,2 and 3

Blast nº	DIF_c	DIF_{sy}	DIF_{su}	E_{dy}/E_{cm}
1	1.371	1.241	1.072	1.27
2	1.371	1.241	1.072	1.27
3	1.388	1.254	1.076	1.28

specimen are displayed in Figure 5.21.

5.4.6 Results

Three shock wave scenarios were chosen, all acting on the same type of specimen: column SCC-0%-75. The chosen loads induced different deformation states. Three experimental results were provided after the tests were conducted: maximum mid-span displacement, the residual displacement and the maximum support rotation. In the present simulations, only the first and last ones of these parameters will be analysed. A summary of the recorded responses is present in Table 5.12. A graphical comparison between the experimental and numerical results, with and without load attenuation effects and energy balances for the three blast scenarios
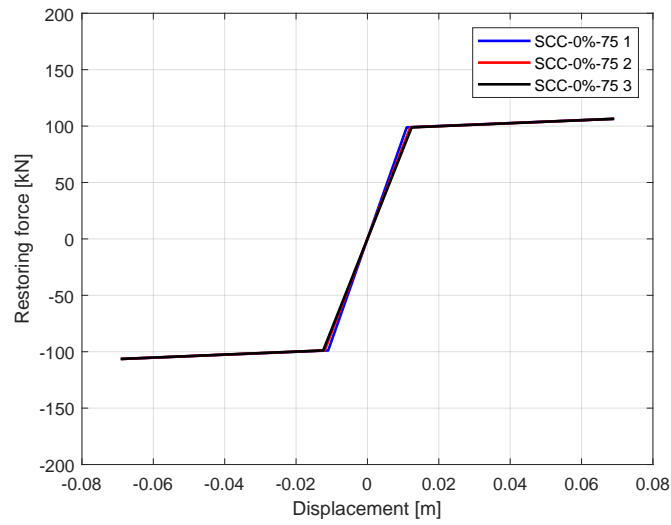
Figure 5.20: Resistance-deflection curves for column SCC-0%-75 blast 1, 2 and 3
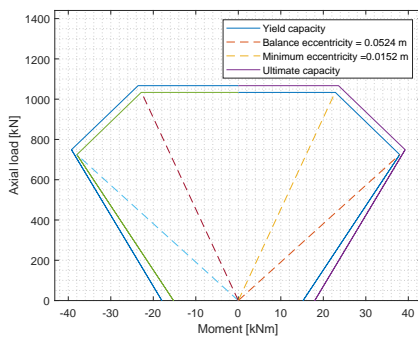
(a) Blast 1
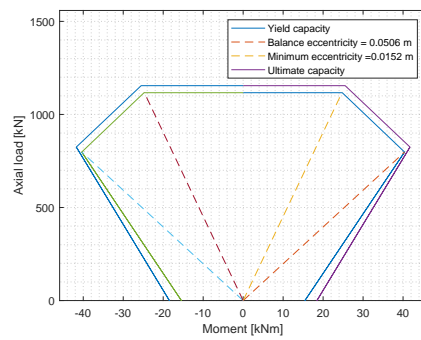
(b) Blast 2
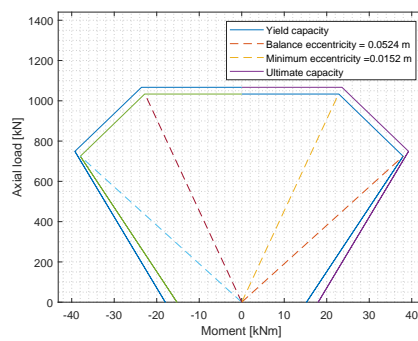
(c) Blast 3

Figure 5.21: Interaction diagrams for blast 1, 2 and 3

is illustrated in Figures 5.22, 5.23 and 5.24, respectively. The force-displacement (hysteretic loops) from the numerical simulations are presented in 5.25.
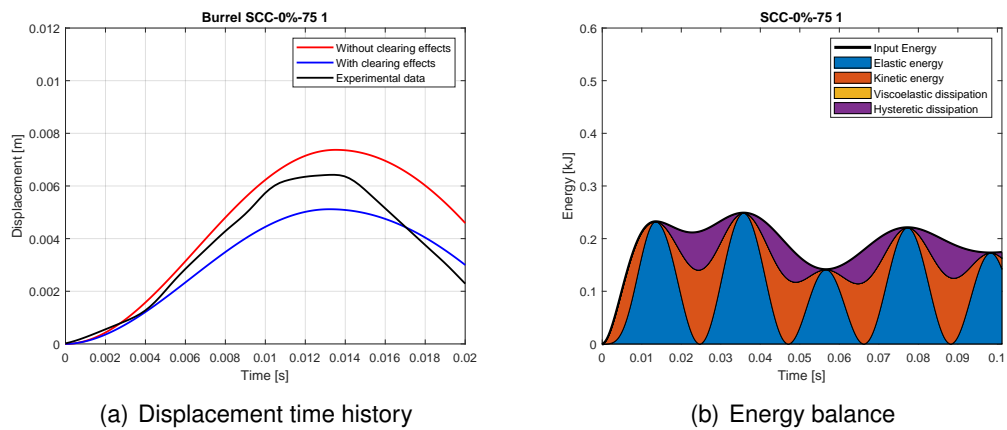
(a) Displacement time history

(b) Energy balance

Figure 5.22: Displacement time history and energy balance of blast scenario 1. Experimental data adapted from [12]

(a) Displacement time history
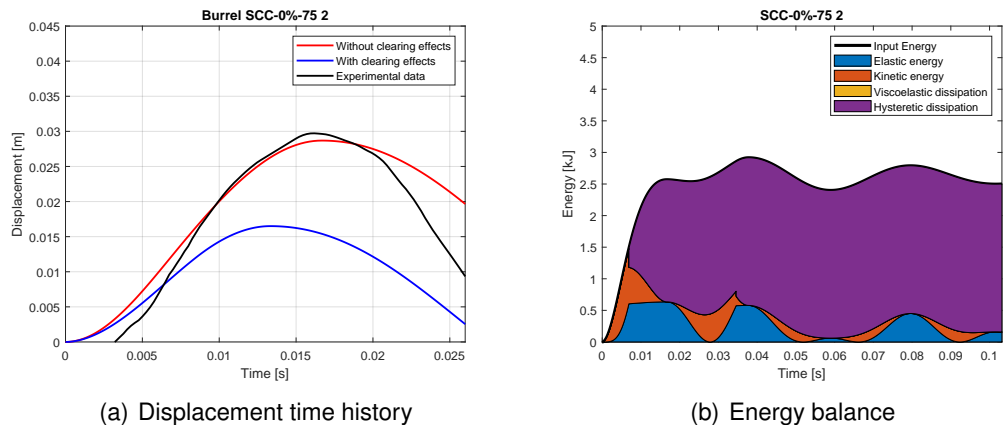
(b) Energy balance

Figure 5.23: Displacement time history and energy balance of blast scenario 2. Experimental data adapted from [12]

5.4.7 Discussion

Three blast scenarios were simulated, all acting on specimens SCC-0%-75. It's been shown the simplified numerical model predicts the response of the tests within a 25% error margin, on average. A possible origin for this discrepancy may come from the use of an idealized pressure profile. To investigate the validity of this assumption, blast case 1 was performed once again, this time with the real pressure profile as load input (seen in Figure 5.19(a)). This simulation was performed with no shock wave attenuation effects.

The numerical model retains the same properties as in the test with the idealized load. Running the simulation yielded a maximum displacement of 7.1 mm and a maximum support rotation of $0.60°$. Comparing with the experimental results, an error of 9.9% is registered for the maximum displacement. The resulting displacement history is presented in Figure 5.26.
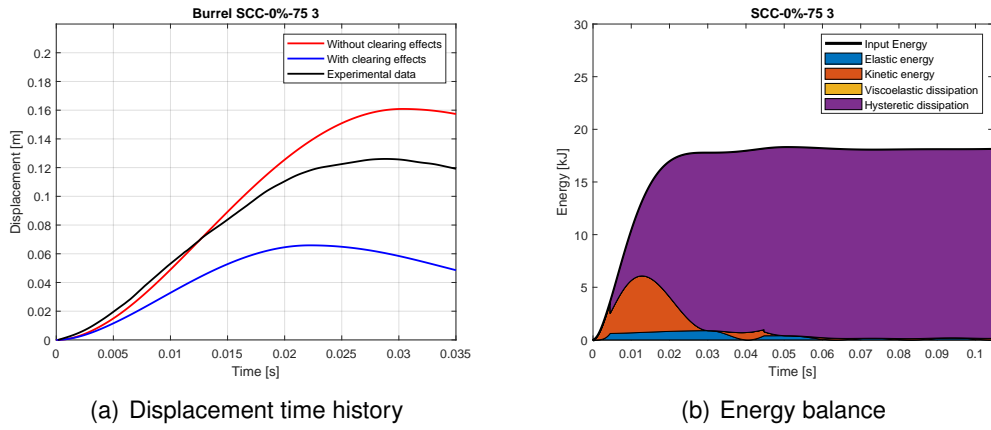
(a) Displacement time history

(b) Energy balance

Figure 5.24: Displacement time history and energy balance of blast scenario 3. Experimental data adapted from [12]
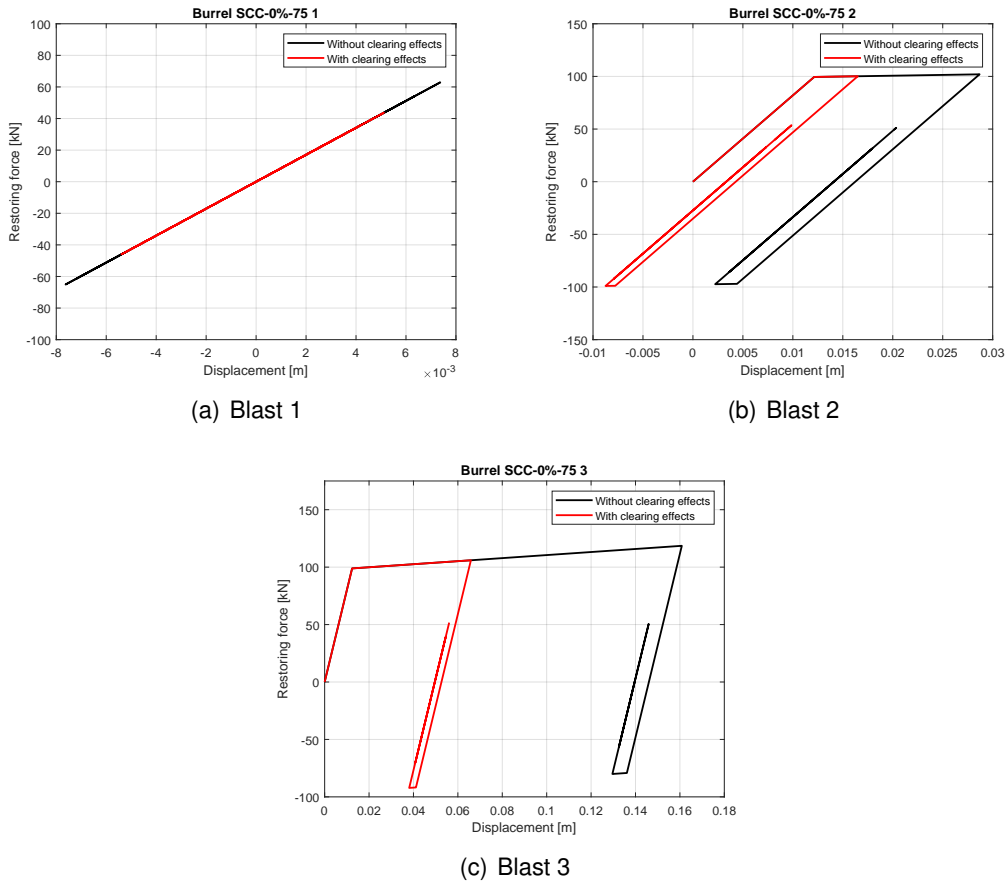

(a) Blast 1

(b) Blast 2

(c) Blast 3

Figure 5.25: Solved hysteretic loops for Burrel blast scenarios 1,2 and 3

These results illustrate the error introduced to the analysis by using an idealized pressure profile as input.

Table 5.12: Experimental [12] and simulated responses for Burrel columns

Blast	Attenuation effects	u_{max} [mm]	u_{exp} [mm]	Error(u) [%]	θ [°]	θ_{exp} [°]	Error(θ) [%]
1	No	7.37	6.40	13.16	0.44	0.37	15.91
	Yes	5.12		20.00	0.31		16.22
2	No	28.69	29.90	4.05	1.66	1.73	4.05
	Yes	16.50		44.82	0.95		45.09
3	No	160.86	126.20	21.55	9.23	7.26	21.34
	Yes	65.87		47.81	3.81		47.52
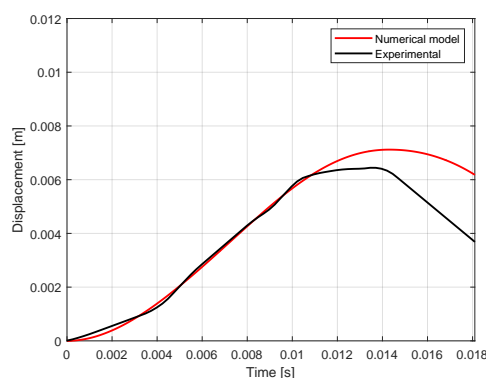
Figure 5.26: Results for blast scenario 1 with real load conditions

Another avenue for error may come from the way the specimens deflect in ongoing tests. As indicated by the authors, as the shock wave was applied to the column and it deflected horizontally, it resulted in a shortening of the specimens, leading to an instantaneous reduction in the axial compression until the axial load resumed its original level [12]. This behaviour was found to be representative of actual column performance under blast loads, where the rate at which the column deflects horizontally is higher under blast loads than the rate at which gravity loads can follow the columns. This phenomenon implies the numerical model wasn't as proficient at simulating P-δ effects acting on the column, likely affecting the final applied load and thus, the final result.

Additionally, the columns tested in this experimental campaign were partially fixed at the supports by means of steel rods. This implies that the resistance to rotation by the supports was not zero as idealized in this case study, making the boundary conditions assumed for the columns a new source for error.

5.5 Concluding remarks on the numerical results

The numerical model developed in the present study proves to be robust to output good approximations to real life blast scenarios on beam and beam-column structural elements. The model was also tested on three distinct support configurations: simply supported, fixed-fixed and fixed-simply supported.
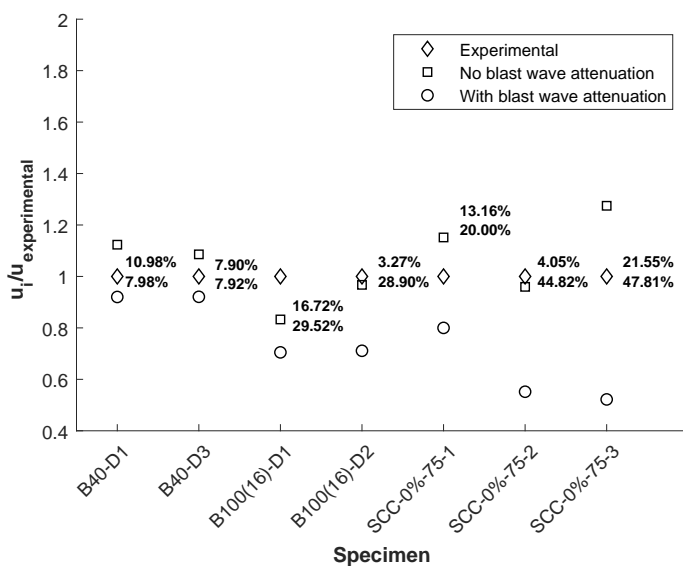
Figure 5.27: Present study's results normalized to experimental data. Percentages next to each data set represent the error between the results and experimental values.

The results for the more complete experimental data sets (Magnusson beams and Burrel columns) are illustrated in Figure 5.27. The numerical model was able to output an upper and lower bound of the response, for the majority of test cases, with a maximum upper and lower bound error of 17% and 30% for beams and 22% and 47% for beam-column elements. It was hypothesized that analyses conducted assuming an idealized load may be susceptible to error. To prove this claim, a second analysis was conducted on blast scenario 1 of the Burrel columns and the results differ roughly 10% from the experimental data, substantiating the claim.

Chapter 6

Conclusions and Future Work

6.1 Conclusions

The present work focused on the development of a numerical model with which to analyse the inelastic response of beam and beam-column elements subjected to blast loads. To do so, the literature regarding shock waves was reviewed, with a focus on the most prominent formulations for the definition of a blast wave's shape and parameters. Following this, a review on shock wave attenuation effects was conducted, with regards to shock fronts targeting finite elements, reflecting off of non-rigid surfaces.

To predict the blast response of RC beams and columns against blast-induced transverse loads the equivalent single-degree-of-freedom (SDOF) approach is used. The system is described by a spring-mass system in which the equivalent element mass, equivalent blast load and adopted resistance function are incorporated. To capture the full time-history response of the elements to dynamic loading the complete force-displacement is needed. To account for the combined axial load and blast-induced transverse loads, in case of the columns, the axial load - bending moment interaction diagram is considered. The damping effects are neglected in the simulations conducted in the present study as damping has little effect on the first peak of the structure's response.

The numerical solution of the non-linear SDOF system required special attention as the restoring force is a piecewise function of the displacement. To this end, the MATLAB ode45 numerical integration scheme based on an adaptive explicit Runge-Kutta formula is used. The integration scheme was expanded to allow for asymmetric resistance-displacement relationships to simulate equivalent systems with different positive and negative yield loads as well as different post yield stiffness values.

The developed numerical model is implemented in MATLAB environment. To facilitate the use of the resulting code a graphical interface was also developed.

The validation of the numerical model was done by analysing four case studies: two for beams and two other for beam-columns. The SDOF model and its implementation were validated by comparing the maximum displacements time history and maximum support rotation - when available - obtained from the SDOF analysis with experimental data reported in literature. It's inferred that the numerical

model developed in the present study is well-suited to simulate the structural response of RC beam and beam-column elements subjected to blast loads. It was found that the simulations on beam-column elements output results with a bigger offset, when compared with experimental data. It was then shown that a likely source for this discrepancy could come from the usage of an idealized pressure profile, as well as the rate at which the specimens deflected. A simulation with the real load was performed, and the resulting response differed roughly 10% from the experimental data - 25% less than the test with the idealized load. As such, these results are in accordance with the ones reported in the literature and deviations from the experimental data arise from simplifications used in the construction of the equivalent models and the load time histories.

6.2   Future work

The goals for the present study were accomplished. The resulting computational tool can be easily adapted to accommodate additional modules concerning the blast response of plates and walls. Suggestions for future work are listed below.

- Extension of the numerical tool for steel beam and beam-column analysis;

- Inclusion of the shear effects in the deflected shape;

- Inclusion of more blast load parameter formulations, other than the ones published by Kingery & Bulmash;

- Implementation of pressure-impulse diagrams;

- Inclusion in the analysis of shear-moment and shear-moment-axial load interactions.

Acknowledgment

References

[1] Unified Facilities Code (UFC). 2008. UFC 03-340-02. Structures to resist the effects of accidental explosions. United States of America Department of Defense, Washington, D.C.

[2] American journalism Review. Jumping to conclusions in Oklahoma City? https://web.archive.org/web/20101205081115/http://www.ajr.org/article.asp?id=1980, June 1995. Accessed on 13-02-2021.

[3] O. Aminer and B. Okelo. Wilson-theta algorithm approach to solution of dynamic vibration equations. *International Journal of Mathematics and Soft Computing*, 2014.

[4] W.E. Baker, Cox P.A., Kulesz J.J., Strehlow R.A., and Westine P.S. *Explosion Hazards and Evaluation*. ISSN. Elsevier Science, 2012.

[5] BBC. Beirut explosion: Port officials under house arrest as rescue efforts continue. https://www.bbc.com/news/world-middle-east-53670839, August 2020. Accessed on 13-02-2021.

[6] BBC news. Sri Lanka attacks: The family networks behind the bombings. https://www.bbc.com/news/world-asia-48218907, May 2019. Accessed on 13-02-2021.

[7] Beirut Today. Footage from the massive explosion in Beirut Port, Lebanon. https://twitter.com/bey_today/status/1290670725129371648, August 2020. Accessed on 13-02-2021.

[8] J. M. Biggs. *Introduction to structural dynamics*. 1964.

[9] P. H. Bischoff and S. H. Perry. Compressive behaviour of concrete at high strain rates. *Materials and Structures*, 1991.

[10] H. L. Brode. Numerical solutions of spherical blast waves. *Journal of applied physics*, 1955.

[11] L. F. L. Brálio. Modelos para a quantificação da deformação em vigas de betão armado. Master's thesis, NOVA School of Science and Technology, 2014.

[12] R. P. Burrell, H. Aoude, and M. Saatcioglu. Response of SFRC columns under blast loads. *Journal of Structural Engineering*, 141(9):04014209, 2015.

[13] E. Cadoni and D. Forni. Strain rate effects on reinforcing steels in tension. *The European Physical Journal Web of Conferences*, 94:01004, 09 2015.

[14] CBS news. Islamabad hotel blast. https://www.cbsnews.com/pictures/islamabad-hotel-blast/3/, February 2008. Accessed on 13-02-2021.

[15] Century Dynamics Inc. *AUTODYN, Theory Manual, Revision 4.0*. 1998.

[16] A. K. Chopra. *Dynamics of Structures: Theory and Applications to Earthquake Engineering.* N.J: Prentice Hall, 1995.

[17] W. G. Corley. Applicability of seismic design in mitigating progressive collapse. *Construction Technology Laboratories, Inc.*, 2002.

[18] C. Cranz. Lehrbuch der ballistik. springer, 1926.

[19] J.R. Dormand and P.J. Prince. A family of embedded Runge-Kutta formulae. *Journal of Computational and Applied Mathematics*, 6(1):19–26, 1980.

[20] D. et. al Dusenberry. Blast protection of buildings, ASCE/SEI 59-11, 2011.

[21] EN. *EN 1992-1-1 Erocode 2: Design of concrete structures - Part 1-1: General rules and rules for buildings*, Brussels, 2005. CEN.

[22] FIB. *Model Code for Concrete Structures 2010*. John Wiley Sons, Ltd, 2013.

[23] C. Gastaldi and T. Berruti. Competitive time marching solution methods for systems with friction-induced nonlinearities. *Applied Sciences*, 2018.

[24] Global Terrorism Database. National Consortium for the Study of Terrorism and Responses to Terrorism. https://www.start.umd.edu/gtd/, August 2020. Accessed on 13-02-2021.

[25] J. Henrych and R. Major. *The Dynamics of Explosion and Its Use*. Developments in civil engineering. Elsevier, 1979.

[26] B. Hopkinson. British Ordnance Board Minutes, Report No. 13565. British Ordnance Office, London. 1915.

[27] C. C. Hudson. Sound pulse approximations to blast loading (with comments on transient drag)" technical report SC-TM-191-55-51. 1955.

[28] International Federation of Red Cross and Red Crescent Societies. Lebanon: Beirut Port explosion. https://go.ifrc.org/emergencies/4660additional-information, August 2020. Accessed on 13-02-2021.

[29] E. Jacques, A. Lloyd, and M. Saatcioglu. Predicting reinforced concrete response to blast. *Canadian Journal of Civil Engineering*, 2013.

[30] JS. Pei et. al. On choosing state variables for piecewise-smooth dynamical system simulations. *Nonlinear Dynamics*, 95:1165–1188, 2019.

[31] M. J. Katona, R. Thompson, and J. Smith. Efficiency study of implicit and explicit time integration operators for finite element applications. Technical report, Civil Engineering Laboratory, California, 1977.

[32] C. N. Kingery and G. Bulmash. Airblast parameters from tnt spherical air burstand hemispherical surface burst. Tech. Rep. ARBRL-TR-02555. Technical report, 1984.

[33] K. Kinney, G. Graham. *Explosive shocks in air*. Springer Science + Business Media New York, 1985.

[34] F. D. Y Lin and L. L. Kuang, X. Strain rate behavior in tension of reinforcing steels HPB235, HRB335, HRB400, and HRB500. *Materials (Basel)*, 2016.

[35] Livermore Software Technology Corporation. *LS-DYNA User Manual: Volumes I & II (Version R10.1)*. California, 2018.

[36] J. M. Lourenço. *The NOVAthesis Template User's Manual*. NOVA University Lisbon, 2021.

[37] J. Magnusson and M. Hallgren. High performance concrete beams subjected to shock waves from air blast. *Defense Research Establishment*, 2000.

[38] L. Malvar and J. Crawford. Dynamic Increase Factors for Concrete, Twenty-Eighth DDESB Seminar Orlando, FL. 1998.

[39] L. Malvar and J. Crawford. Dynamic increase factors for steel reinforcing bars. *Proc. 28th DDESB*, page 18, 08 1998.

[40] MATLAB. *version 7.10.0 (R2010)*. The MathWorks Inc., Natick, Massachusetts, 2010.

[41] F. Mohee. The effects of strain rate on concrete strength under dynamic impact load. *Journal of Bangladesh Electronics Society*, 2016.

[42] National Research Council. *ISC Security Design Criteria for New Federal Office Buildings and Major Modernization Projects: A Review and Commentary*. The National Academies Press, 2003.

[43] C. E. Needham. *Blast Waves*. Springer Berlin Heidelberg, 2010.

[44] N. M. Newmark. A method of computation for structural dynamics. *Journal of the Engineering Mechanics Division*, 85(3):67–94, 1959.

[45] T. Ngo, P. Mendis, A. Gupta, and J. Ramsay. Blast loading and blast effects on structures - An overview. *Electronic Journal of Structural Engineering*, 7:76–91, 01 2007.

[46] NY Times. U.S. Beirut Embassy bombed; 33 reported killed, 80 hurt; pro-iran sect admits action. https://www.nytimes.com/1983/04/19/world/us-beirut-embassy-bombed-33-reported-killed-80-hurt-pro-iran-sect-admits-action.html, April 1983. Accessed on 13-02-2021.

[47] NY Times. 2008 Mumbai attacks plotter says Pakistan's spy agency played a role. https://www.nytimes.com/2016/02/09/world/asia/david-headley-mumbai-attacks.html, 2016. Accessed on 13-02-2021.

[48] NY Times. Sri Lanka attacks: What we know and don't know. https://www.nytimes.com/2019/04/24/world/asia/sri-lanka-easter-bombing-attacks.html, April 2019. Accessed on 13-02-2021.

[49] C. Oswald. Comparison of response from combined axial and blast loads calculated with SDOF and finite element methods. *Protection Engineering Consultants*, page 37, 07 2010.

[50] J. Pinto. Comportamento de estruturas de aço sob a ação de explosões conceção de dissipadores de energia. Master's thesis, Instituto técnico de Lisboa, 2018.

[51] H. Rebelo. Private publication: Blast Loading and Simplified Analysis Methods, Nova School of Sciences and Technology. October 2017.

[52] H. Rebelo. *Development and study of a high performance protective solution against blast loads.* PhD thesis, NOVA School of Science and Technology, Portugal, 2020.

[53] Reuters. Beirut port blast death toll rises to 190. `https://www.reuters.com/article/us-lebanon-crisis-blast-casualties-idUSKBN25Q08H`, August 2020.

[54] S. E. Rigby. *Blast Wave Clearing Effects on Finite-SizedTargets Subjected to Explosive Loads.* PhD thesis, University of Sheffield, 2014.

[55] A. R. F. Rodrigues. Método simplificado na análise de elementos estruturais solicitados a cargas explosivas. Master's thesis, NOVA School of Science and Technology, 2020.

[56] M. Smith. *ABAQUS/Standard User's Manual, Version 6.9*. Dassault Systèmes Simulia Corp, United States, 2009.

[57] M. Swisdak. Simplified Kingery Airblast Calculations; NAVAL SURFACE WARFARE CENTER INDIAN HEAD DIV MD: Indian Head, MD, USA. 1994.

[58] The Daily Iowan. 'it was never the same': Remembering the Oklahoma City bombing 25 years later. https://dailyiowan.com/2020/04/18/it-was-never-the-same-remembering-the-oklahoma-city-bombing-25-years-later/, April 2020. Accessed on 13-02-2021.

[59] NY Times. Mumbai terror attacks: 7 pakistanis charged. `https://abcnews.go.com/International/mumbai-terror-attacks-pakistanis-charged/story?id=9176592`, November 2009. Accessed on 13-02-2021.

[60] Times of India. Bomb rocks Islamabad hotel, at least 60 dead. https://timesofindia.indiatimes.com/world/pakistan/Bomb-rocks-Islamabad-hotel-at-least-60-dead/articleshow/3507428.cms, September 2008. Accessed on 13-02-2021.

[61] United States Geological Survey. M 3.3 Explosion - 1 km ENE of Beirut, Lebanon. https://earthquake.usgs.gov/earthquakes/eventpage/us6000b9bx/executive, August 2020. Accessed on 13-02-2021.

[62] U.S. Army Corps of Engineers. *Methodology Manual for the Single-Degree-of-Freedom Blast Effects Design Spreadsheets(SBEDS). PDC TR– 06–01, Rev 1, 2008.*

[63] U.S. Army Corps of Engineers. *Example problems for SBEDS (Single-Degree-of-Freedom Blast Effects Design Spreadsheets) PDC TR-08-03*, 2008.

[64] Us Dept. of State. Remembering the 1983 suicide bombings in Beirut: The tragic events that created the diplomatic security service. https://www.state.gov/remembering-the-1983-suicide-bombings-in-beirut-the-tragic- events-that-created-the-diplomatic-security-service/, 2018. Accessed on 13-02-2021.

[65] E. L. Wilson, I. Farhoomand, and K. J. Bathe. Nonlinear dynamic analysis of complex structures. *Earthquake Engineering and Structural Dynamics, vol. 1, 241.252*, 2018.

[66] WKYT. Video tribute honors Oklahoma City bombing victims amid outbreak. https://www.wkyt.com/content/news/Sunday-marks-25th-anniversary-of-Oklahoma-City-bombing-569768301.html?ref=301, April 2020. Accessed on 13-02-2021.

[67] J. P. Wright and JS. Pei. Solving dynamical systems involving piecewise restoring force using state event location. *Journal of Engineering Mechanics*, 138(8):997–1020, 2012.

Appendix A

User's manual

PrInCE 2.0 – User's manual
v. 2.0

A.1   Introduction

PrInCE 2.0 (Proteção de Infraestruturas e Sistemas Contra Explosões) is a simplified numerical analysis tool that is able to gauge the structural response of reinforced concrete (RC) beam and beam-column elements when subjected to blast loads. The PrInCE 2.0 tool was developed under the PROTEDES program from the Nova School of Sciences and Technology, Lisbon. The program comprises a simplified numerical model which allows for the estimation of a resisting capacity of RC one-way elements such as beams and beam-columns. Additionally, the program is capable of generating shock wave pressure time histories, given an explosive's mass and standoff distance. After running a simulation, several results may be consulted in the post-processing area in the GUI.

A.2   Acknowledgements

Contents

A.3 Installation and system requirements

The program described herein was created in the MATLAB framework, by Mathworks. As such, a copy of this software must be installed in order to run the model's GUI. The program was developed and tested on the 2018b release of MATLAB. It's unknown to the author whether the program is functional for other versions. The 2018b MATLAB release's system requirements may be consulted in the following link:

    `mathworks.com/content/dam/mathworks/mathworks-dot-com/support/`
`sysreq/files/system-requirements-release-2018b-windows.pdf`

A.4   Structure

The GUI consists of a single window, where all graphical objects such as buttons, axis and text-input boxes are featured. In this window, there exist three distinct stages: the pre-processing, processing and post-processing stages.
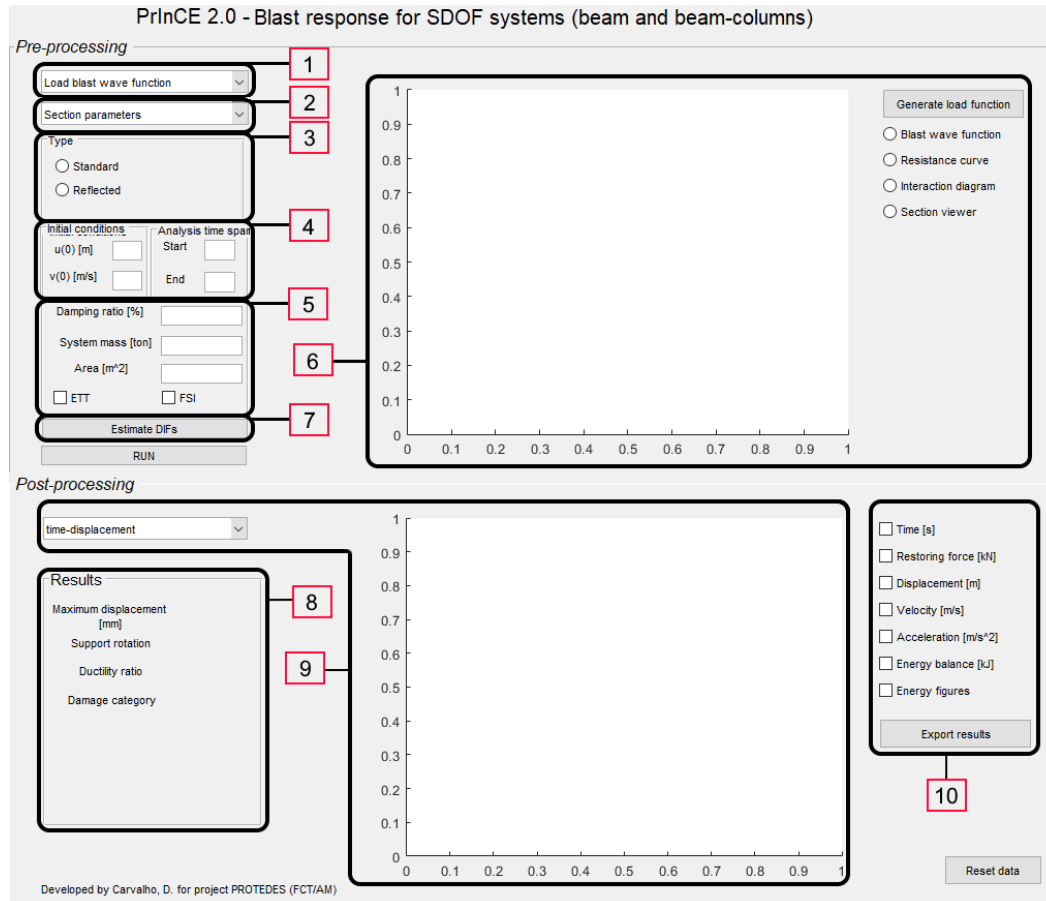
Figure A.1: Graphical user interface

A.5   Pre-processing

The pre-processing portion of the GUI enables the input of all files and variables required to run a simulation. It's divided into 4 different sections:

- A drop-down menu for the input or generation of a load time history;

- A drop-down menu for the input or generation of the equivalent system's resistance-deflection relationship;

- String-input boxes for various parameters;

- Graphical representation of pre-processing data.

On either instance of user file input, the files to be used have extension .txt (text files) and have the configuration described in the following sections. All variables, both strings and numerical data, are separated with commas, ",". Decimal values are separated with a dot ".", as is standard in MATLAB.

A.5.1 Load input

The theoretical bases that enable the generation of pressure time histories can be found in Chapter 2. The Kingery & Bulmash sets of polynomials are used to produce pressure profiles. During analysis, the user may choose to apply corrective effects to the pressure curve in the form of target clearing effects and fluid-structure interactions. The load time history to be considered in the analysis may be input in three different ways via the first drop-down menu, numbered **1** in Figure A.1:

- Direct input of the discrete load values at each time step, by choosing the `Load blast wave function` option. This in turn may be accomplished in two ways; the first option consists in inputting a text (.txt) file containing an n x 1 vector where the first value is the time step `dt` [s] and the remaining values are the discrete load values [kN] at times `dt(i+1)` at the `ith` entry in the input file. The second option involves the input of an n x 2 array consisting of time-load pairs (time [s] in first column and load values [kN] in the second);

- The `Load explosive parameters` option. Requires a user input of a .txt file containing a 2x6 array. The first row describes the required input variables and contains the string `dt,eEXP,wEXP,R,width,L`. The values of these variables are given in the second row: the time step dt [s], the explosive's specific energy `eEXP` [kJ/kg], the explosive's mass `wEXP` [kg], the blast standoff distance `R` [m] and the element's width and span, `b` and `L` [m]. The model computes the blast load's parameters via the Kingery & Bulmash polynomials which are then used in the modified Friedlander equation to compute the load time history;

- Input of a string function is also an available option, by selecting the `Input custom function`. To use this option, the user must provide a valid string in MATLAB which defines the load [kN] with respect to time [s].

A.5.2 Resistance-deflection relationship

The generation of resistance curves is done in accordance to the steps outlined in Chapter 3 for either reinforced concrete beam or beam-column structural elements. For the definition of the resistance curve, two options are available in field **2** in Figure A.1.

The first, named *Section parameters*, implies the input of a file containing the following structure:

```
SectionProperties.txt
Rows 1 through 13
L,b,h,c,phi_s,phi_t,phi_c,n_t,n_c,fc,fctm,Ecm,Es,
```

```
1.98,0.15,0.1,0.02,6.3,11.3,11.3,2,2,58,6.6,34.27,200,

Rows 14 through 25
fy,fys,fyu,N,Z,support,DIFc,DIFsy,DIFsu,spacing, SIFc, SIFs
483,604,675,350,-1,1,1.25,1.315,1.043,5,0,0
```

in which:

- `L` [m] is the element's span;

- `b` [m] is the element's width;

- `h` [m] is the section's depth ;

- `c` [m] is the section's cover;

- `phi_s` [mm] is the transversal reinforcement steel bars' diameter;

- `phi_t` [mm] is the longitudinal tension reinforcement steel bars' diameter;

- `phi_c` [m] is the longitudinal compression reinforcement steel bars' diameter;

- `n_t` is the number of longitudinal tension reinforcement steel bars;

- `n_c` is the number of longitudinal compression reinforcement steel bars;

- `fc` [MPa] is the concrete's static compression yield strength;

- `fctm` [MPa] is the concrete's static tensile yield strength;

- `Ecm` [GPa] is the concrete's Young's modulus;

- `Es` [GPa] is the reinforcement steel's Young's modulus;

- `fy` [MPa] is the longitudinal steel's static yield strength;

- `fys` [MPa] is the transverse steel's static yield strength;

- `fyu` [MPa] is the longitudinal steel's static ultimate strength;

- `N` [kN] is the acting axial force;

- `Z` [m/kg$^{1/3}$] is the scaled distance; Set to -1 if custom DIFs are to be used;

- `support` represents the desired support conditions; Available options are 1, 2, and 3 for simply support, fixed-fixed supports and simple-fixed supports, respectively. If the this variable is set to 0, then the mass transformation factors are both set to 1;

- `DIFc` is the concrete's dynamic increase factor;

- `DIFsy` is the reinforcement steel's dynamic increase factor in yield;

- `DIFsu` is the reinforcement steel's dynamic increase factor in its ultimate state;

- `spacing` [cm] is the spacing of the transverse reinforcement steel;

- `SIFc` is the concrete's strength increase factor; Set to 1 to use this factor, 0 otherwise; If set to 1, the concrete strength is multiplied by a factor of 1.21;

- `SIFs` is the reinforcement steel's strength increase factor; Set to 1 to use this factor, 0 otherwise; If set to 1, the steel strength is multiplied by a factor of 1.1.

The `SectionProperties.txt` file may be written as a 2 x 25 or a 25 x 2 array. If the explosive parameters aren't available and the blast load function is directly loaded in the GUI, thus, the value of the scaled distance Z is not known, the user must set $Z = -1$ and assign values to the three DIF's in the file in the section properties file.

Following the loading of the section's properties via the "Section properties" option, the routine `behaviour_curve.m` is launched automatically. This function starts by calculating the dynamic capacity of both concrete and steel. Next, it decides weather the the element is acting as a beam ($N = 0$) or a beam-column ($N \neq 0$).

In the case of a beam element, a sectional analysis is carried out to determine the loads and displacements that define the resistance curve. In particular, calculations for the elastic and elastoplastic stages involve determining the distance from the top of the section to the neutral axis x_I and x_{II}, respectively. The uncracked (I) and cracked (II) section's moment of inertia are computed next, to be used in calculating the stiffness k of each phase. The final loads are calculated for each stage using Bigg's methodology. The resulting tri-linear curve is bilinearized.

Conversely, if the element to be analyzed is a beam-column, then the function generates a P-M interaction diagram. The resistant moments are evaluated depending on the magnitude of the imposed axial load, and the function proceeds in the same fashion as if the element would be a beam.

Alternatively, if the user chooses to directly input the resistance curve, the file should contain two columns, the first containing displacements [m] and the second the resistant force [kN], as follows:

```
ResistanceCurve.txt
    -0.02,          -300
    -0.01,          -300
     0.0,            0.0
     0.01,           300
     0.02,           300
```

The flowchart of the pre-processing stage is presented in Figure A.2

A.5.3   Initial conditions and other material properties

The solving function requires the input of the system's initial kinematic conditions u_0 [m] and $\dot{u}_0$ [m/s] and time-span [s] in the section numbered **4** in Figure A.1.
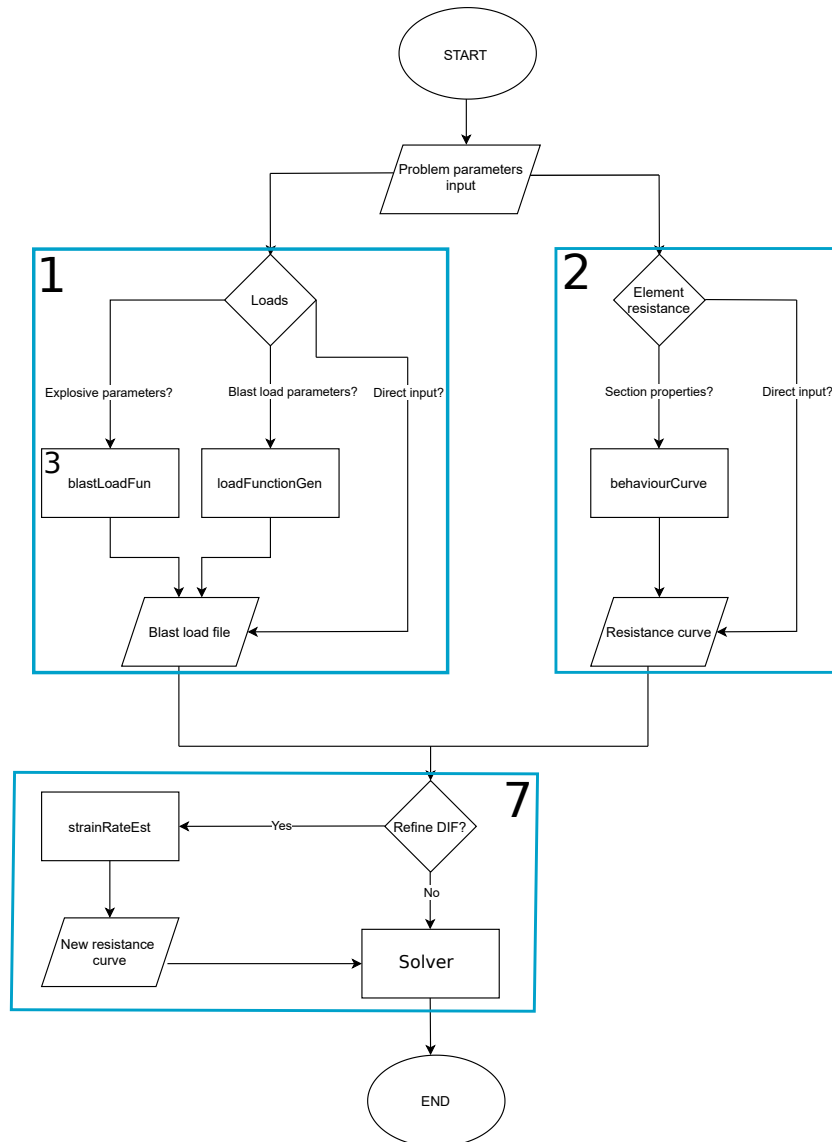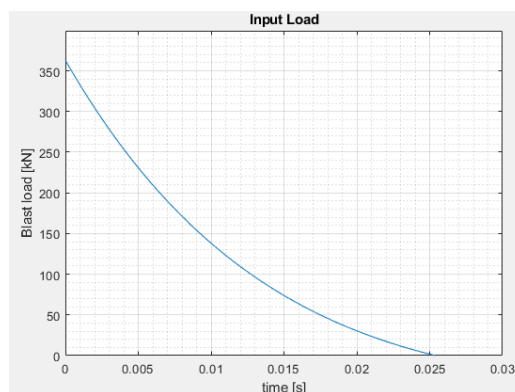
Figure A.2: Pre-processing stage flowchart

The remaining material properties not contemplated in the section numbered **2**, such as the damping ratio [%], the element's mass [ton] and shock wave incident area [m^2] are loaded in section **6**.

Additionally, if wave attenuation effects are to be accounted for, the check boxes *ETT* and *FSI* must be ticked for shock wave clearing and fluid structure interactions, respectively.

A.5.4 Graphical representation of pre-processing data

To visualize the input data, four different sets of pre-processing data can be selected, as seen in Figure A.3.

- Blast wave function - plots the time history of the blast load;

- Resistance curve - plots the displacement-resistance curve;

- Interaction diagram - plots the resultant interaction diagram for beam-column only; Otherwise, the string `No axial load detected. Element acts as a beam` is displayed;

- Section viewer - displays the element's cross-section; If no geometrical parameters were defined, the string `No material properties detected. Section view is unavailable.` is displayed.

(a) Input load
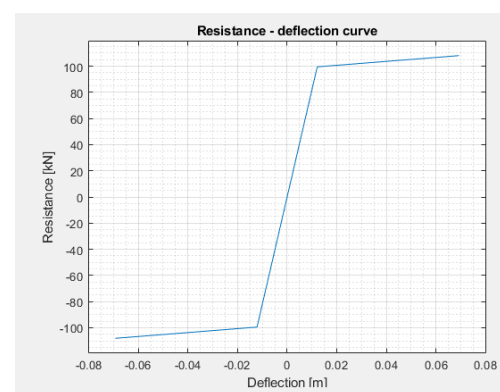
(b) Resistance-deflection curve
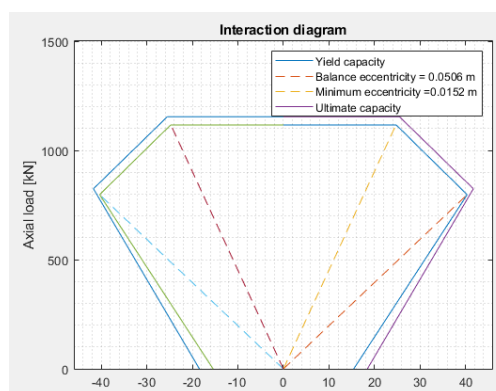
(c) P-M Interaction diagram
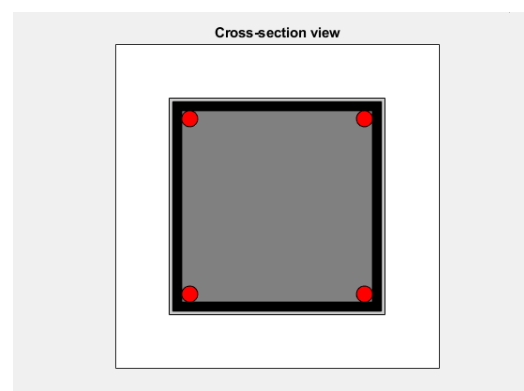
(d) Cross-section viewer

Figure A.3: Pre-processing graphical visualization options

A.5.5   Estimation of dynamic increase factors

The estimation of the DIFs is performed via the push-button numbered **7** in Figure A.1. By clicking this button, the user is prompted with a dialog box which requires a percentual tolerance value as input for the DIF estimation routine. If no value is input and the button *OK* is clicked, the program assumes the default tolerance as 1%. Next, the routine `StrainRateEst` is ran and the DIFs are computed. Following this, the program prompts the user with another dialog box indicating that the routine ran successfully and displaying the newly computed DIFs, as seen in Figure A.4.
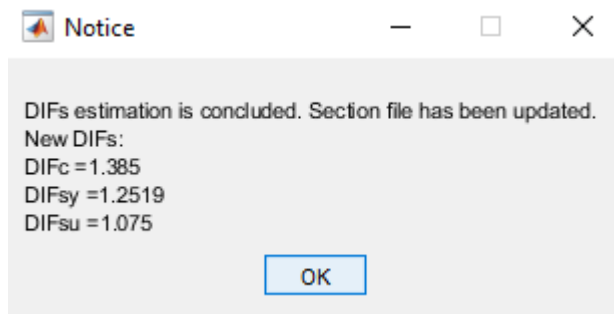
Figure A.4: Dialog box displayed after running StrainRateEst

The iterative algorithm for computing DIFs is detailed in section 3.2.1 and visually represented in Figure A.5. As the computation of the DIFs relies on the time to yield t_E to compute the strain rates for each material at each iteration, the routine can only run if the element yields.

A.6   Processing stage

The function that solves the equation of motion is named `Solver.m`. It contains all routines and nested functions necessary to simulate a blast scenario. The main solving scheme is described in Figure A.6.

Within the function `Solver.m`, several supporting sub-routines are present. Those are the following:

- `StructureODE` - Constructs the space-state vector that serves as input in the ode45 function;

- `EventFun` - Contains the event functions that detect changes in the deformation state and indicates ode45 to halt the analysis and reevaluate tag_2;

- `loadIdx` - Only used in cases where the input function is a non-blast load, custom function. Interpolates the input load function and outputs a load value for the desired time-step;

- `fetchParam` - Outputs the blast wave characteristics, provided the input load function is a blast load scenario;

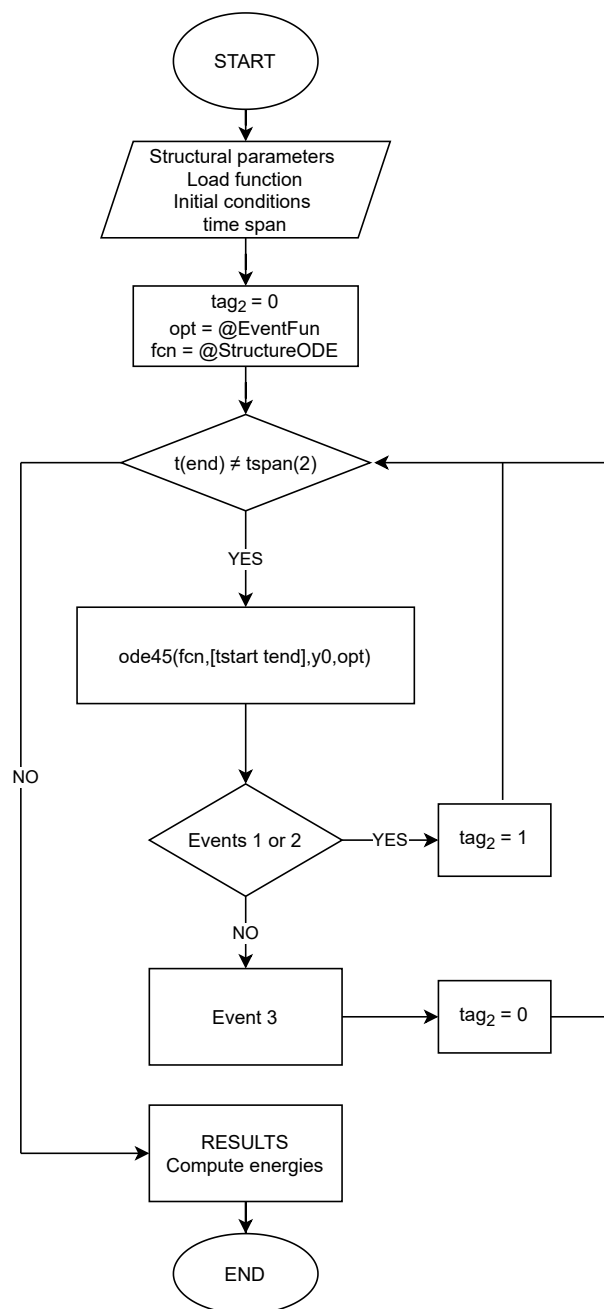Figure A.5: DIF estimating routine, `StrainRateEst.m`

Figure A.6: Solving function flowchart

- `load_history` - Outputs the complete load time history;

- `corrected_loads` - Outputs the corrected acting load time history (if load attenuation effects were considered);

- `EnergyBalance` - Computes the energy balance for the response;

- `monoDetect` - Detects whether the input load function is a strictly monotonic function;

- `ELL` - This is the equivalent lateral load function; it receives the previous displacement, the boundary conditions, the element's width and span and the acting axial load as input; outputs an equivalent lateral load at each time step to be added to the main load time history.

A.6.1 Dissipated energies

When the analysis is concluded, the energy balance is conducted. The computed energies are present in Table A.1.

Table A.1: Energy balance typology and corresponding expressions

Type	Expression ($i > 0$)
Total	$\sum \frac{1}{2}(u_{i+1} - u_i)(p_{i+1} + p_i)$
Elastic	$\frac{1}{2}R^2/k_y$
Kinetic	$\frac{1}{2}M_e v^2$
Visco-elastic	$\sum \frac{1}{2}c\,(u_{i+1} - u_i)(\dot{u}_{i+1} + \dot{u}_i)$
Histeretic	Total - Elastic - Kinetic - Visco-elastic

A.7 Post-processing stage

The software produces three types of outputs: a graphical representation of the evolution of a series of parameter with respect to time, the maximum values of the relevant parameters and solution files for spreadsheet manipulations.

A.7.1 Graphical results

In the numbered section **9** in Figure A.1 are the available graphical representations of results. Those are as follows:

- `displacement` - plots the displacement time history;

- `velocity` - plots the velocity time history;

- `acceleration` - plots the acceleration time history;

- `displacement-restoring force`;

- `displacement-velocity` - plots the phase plane;

- `Energy time history` - plots the energy balance;

- `Corrected load history` - plots the corrected acting load with shock wave attenuation effects, when available.

A.7.2   Final results

In section number **8** in Figure A.1, the relevant results regarding the analysis are displayed. Those are:

- `Maximum displacement;`

- `Support rotation;`

- `Ductility ratio` - the ratio between the maximum displacement and the maximum elastic displacement;

- `Damage category.`

These are the most relevant results for the structural design elements intended to sustain blast loads as they allow for the verification of limit states.

A.7.3   Exporting results

In the section numbered **10** in Figure A.1, the program allows for the exportation of several outputs, generated in the analysis. Those are the following:

- `Time [s]` - prints an n x 1 time vector, where n is the number of time steps;

- `Restoring force [kN]` - prints an n x 1 restoring force vector, where n is the number of time steps;

- `Displacement [m]` - prints an n x 1 displacement vector;

- `Velocity [m/s]` - prints an n x 1 velocity vector;

- `Acceleration [m/s^2]` - prints a n x 1 acceleration vector;

- `Energy balance [kJ]` - prints an n x 5 array containing all computed energies.

- `Energy figures` - prints the energy balance plot to a figure file;

The results are readily available to export by checking the relevant checkboxes and pressing the *Export results* button.

A.8   Examples

There exist several ways of running simulations in PrInCE 2.0, all differing in the way the pre-processing is handled i.e., how data is input. This appendix will specify all possible data input avenues in the form of example simulations.

A.8.1 Example 1

Example 1 consists of a simply supported beam element whose properties are defined via the *Section properties* option. The load originates from a blast scenario and is input via the *Load blast wave function* option. The blast load was defined as having a peak overpressure, positive phase duration and impulse of 650 kPa, 23 ms and 3.76 kPa s, respectively.
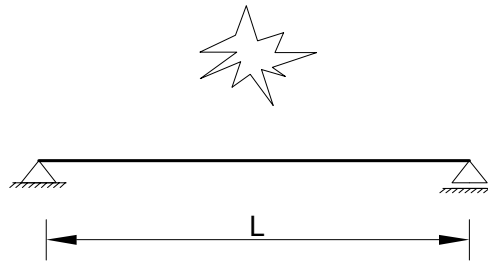
Figure A.7: Blast scenario for example 1

The data in the section properties text file is as follows:

```
SectionProperties.txt
Columns 1 through 13
L,b,h,c,phi_s,phi_t,phi_c,n_t,n_c,fc,fctm,Ecm,Es,
1.500,0.29,0.16,0.025,8.27,15.37,10,5,2,53.8,4.6,57.135,210,

Columns 14 through 25
fy,fys,fyu,N,Z,support,DIFc,DIFsy,DIFsu,spacing, SIFc, SIFs
604,501,703,0,-1,1,1.351,1.230,1.068,7.5,0,0
```

Procedure

1. Input load file by choosing *Load blast wave function*
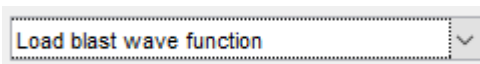
2. Input element's mechanical and geometric properties by choosing *Section properties*
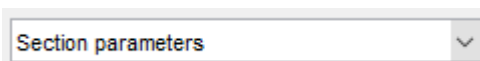
3. Define the initial conditions as null. Since no alternative time-span was prescribed, there's no need to edit the text boxes under *Analysis time span*. Define the element's damping ratio, mass and incident area.

4. Press the RUN button

5. Check the non-graphic results. (Optional)

6. Check the post-processing graphical data (Optional).
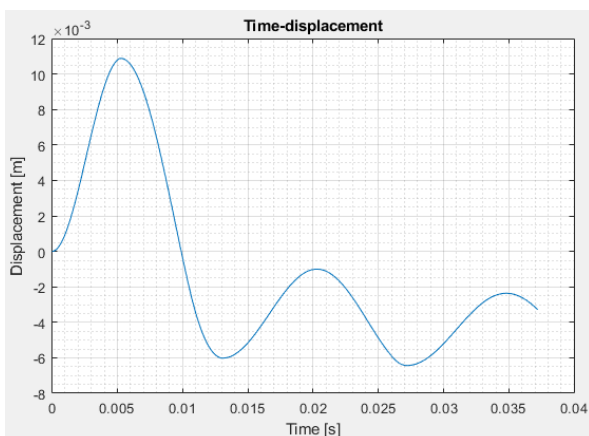
7. Tick the check-boxes for the desired results and press the $\boxed{\text{Export results}}$ button (Optional).

A.8.2 Example 2

Example 2 comprises a fixed-fixed beam element subjected to a blast wave originating from a 3 kg C4 charge placed at an offset distance of 3 m. This example will feature initial conditions of 1 mm and 5 m/s for initial displacement and velocity, respectively.
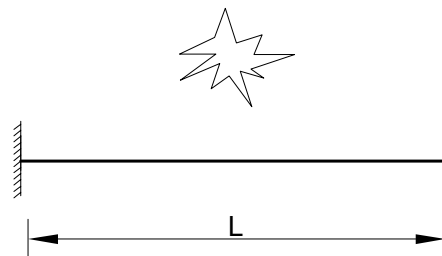
Figure A.8: Blast scenario for example 2

The specimen has a mass of 100 kg, a width of 0.3 m and a span of 3 m. Damping is set to 0. The resistance curve used in this example is the following:

```
ResistanceCurve.txt
-0.01, -50
-0.002, -45
0, 0
0.002, 45
0.01, 50
```
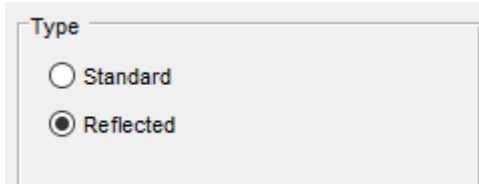
Procedure

1. Choose between standard or reflected blast wave to be computed with the explosive parameters.
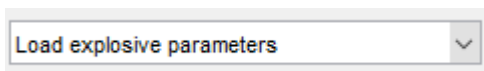
   ┌─ Type ─────────────────────────────┐
   │   │
   │   ○ Standard   │
   │   │
   │   ● Reflected   │
   │   │
   └────────────────────────────────────┘

2. Input blast scenario specifications by choosing the *Load explosive parameters* option.
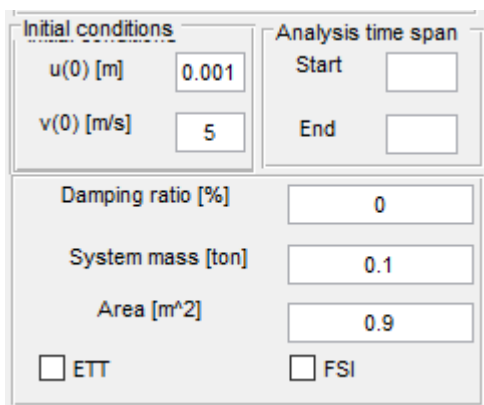
   ┌──────────────────────────────────┬─────┐
   │ Load explosive parameters   │ ∨ │
   └──────────────────────────────────┴─────┘

3. Input the resistance-deflection curve via the *Resistance curve* option.
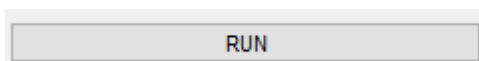
   ┌──────────────────────────────────┬─────┐
   │ Resistance curve   │ ∨ │
   └──────────────────────────────────┴─────┘

4. Define the initial conditions as 0.001 and 5 for the initial displacement and velocity, respectively. Define the element's prescribed damping ratio, mass and incident area.

   ┌─ Initial conditions ──┐┌─ Analysis time span ─┐
   │   u(0) [m]   [0.001] ││ Start   [   ] │
   │   ││   │
   │   v(0) [m/s]   [5] ││ End   [   ] │
   └───────────────────────┘└──────────────────────┘
   │   Damping ratio [%]   [0   ]   │
   │   │
   │   System mass [ton]   [0.1   ]   │
   │   │
   │   Area [m^2]   [0.9   ]   │
   │   ☐ ETT   ☐ FSI   │

5. Press the ⟦RUN⟧ button to run the analysis.

   ┌──┐
   │   RUN   │
   └──┘

6. Input the undetected variables.

7. The steps that follow are identical to step 5 and onward from Example 1.

A.8.3 Example 3

Example 3 features a simple-fixed beam-column element subjected to a half-sinusoidal pulse load defined by the following expression:

$$p(t) = \begin{cases} 500\sin(\pi t/9) & , t < 9 \text{ ms} \\ 0 & , t \geq 9 \text{ ms} \end{cases}$$

This load will be imparted on the same specimen contemplated in Example 1, with the only difference being the boundary conditions. This example will feature the DIF estimation routine. Additionally, damping will be accounted for with ξ equaling 5%.
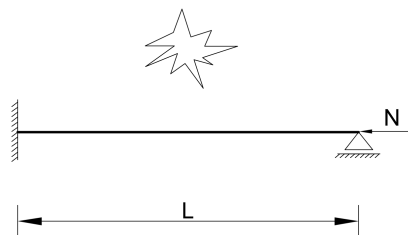
Figure A.9: Blast scenario for example 3

Procedure

1. Choose the *Input custom function* option.

Input custom function ⌄

2. Input the function's string in the correct format.

◢ User-input fun... — ☐ ✕

Input the custom function as a string

(t<0.009).*(500*sin(pi*t/0.009)) + (t >=0.009).*0|

OK Cancel

3. Input the element's mechanical and geometric properties by choosing *Section properties.*

Section parameters ⌄

4. Define the problem's initial conditions, time-span and remaining variables.

Initial conditions

u(0) [m]   0

v(0) [m/s]   0

Analysis time span

Start

End

Damping ratio [%]   5

System mass [ton]   0.174

Area [m^2]   0.435

☐ ETT   ☐ FSI

5. Run the DIF estimation routine by clicking on the [DIF estimation] button.

Estimate DIFs

6. Choose a tolerance for the algorithm. Simply clicking *OK* will have the routine use the default tolerance value of 1%.

◢ Tolerance for DIF estimati... — ☐ ✕

Define tolerance limit (click OK for default value)

OK Cancel

7. Inspect the resulting DIFs.
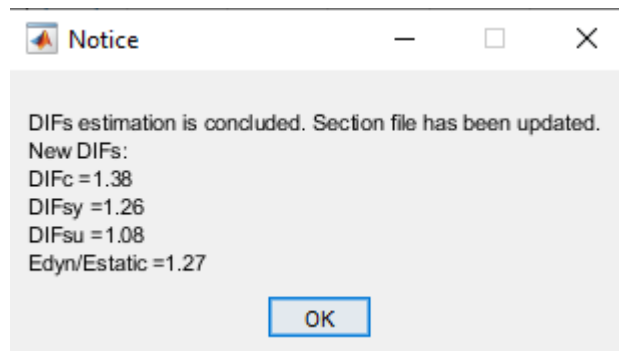
8. Click on the RUN button to start the analysis.
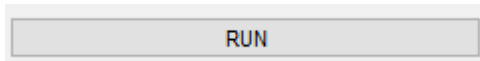
9. The remaining steps are identical to steps 5 and onward from Example 1.

A.9   Troubleshooting and other issues

This section details possible issues that might arise in using PrInCE 2.0. Naturally, not all malfunctions will be presented here as the software has only been tested by the author. However, if any bugs or issues are detected, the user can be contacted via email and this section will be expanded.

A.9.1   "Error" after failing to input a data file or canceling an operation

When the load/Resistance curve options are selected and the program requests the user to provide a file and the this operation is canceled, the command window in MATLAB will display the following error:

Figure A.10: Error message displayed after canceling any data input operation

This is not impeditive in any way to the performance of the program. The data input may be restarted after this error shows up.

Appendix B

Validation of the integration scheme

The validation of the hysteretic model was done by comparing results from the algorithm with those present in [30]. Two different case studies were assessed. These comprise a SDOF system with mass and elastic stiffness both equal to 1. The remaining resistance parameters can be inferred from Figure B.1.
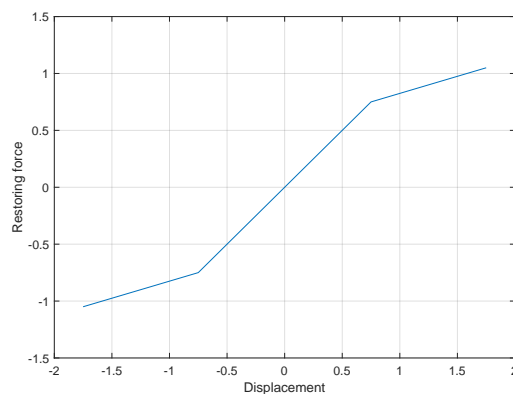
Figure B.1: Resistance curve for bilinear hysteretic examples, adapted from [30]

The difference between case studies are the external excitation force. In the first case, the load time history is described by a sine wave with constant amplitude throughout the response, seen in Figure B.2. The second consists in a modulated sine wave with varying amplitude, illustrated in Figure B.3. The results are illustrated in Figures B.4(a) through (h). A close inspection of the results reveals a good approximation between each data set. However, the second test displays some deviation as the analysis time increases. This is due to the fact that the results displayed in black were obtained by using the accuracy parameter *RelTol* in the ode45 option set equal to 10^{-3}, while the response in red used *RelTol* $= 10^{-12}$. Since the response at a given time step is dependent on the results that precede it, result deviation increases as time progresses.
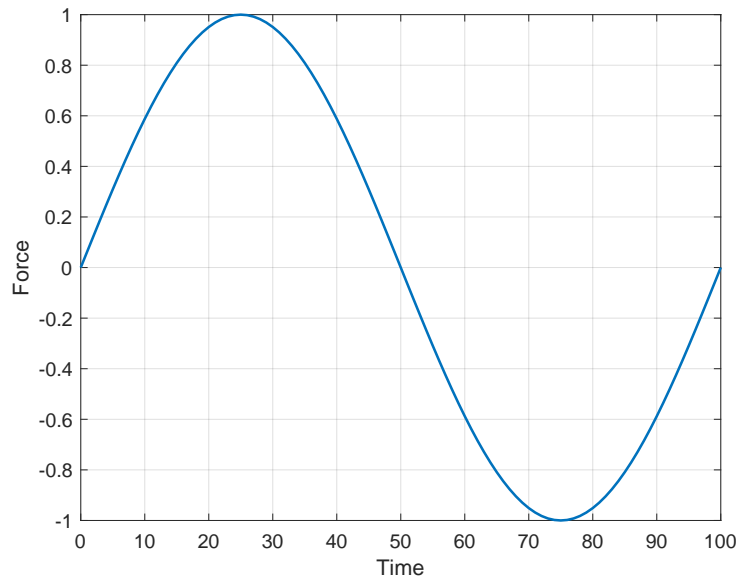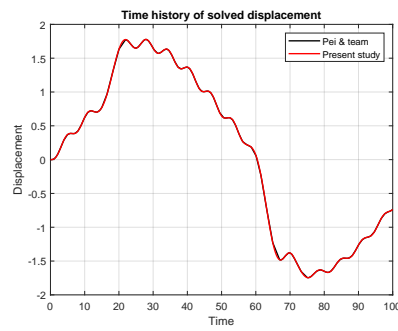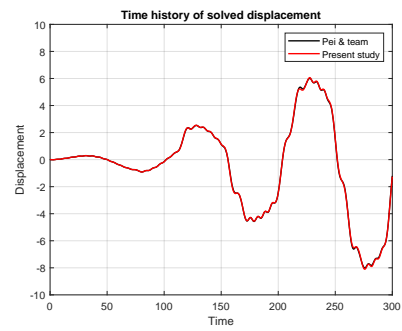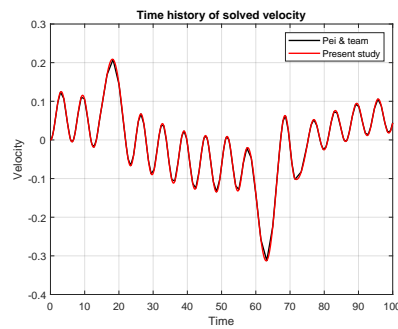
Figure B.2: Load for case study 1
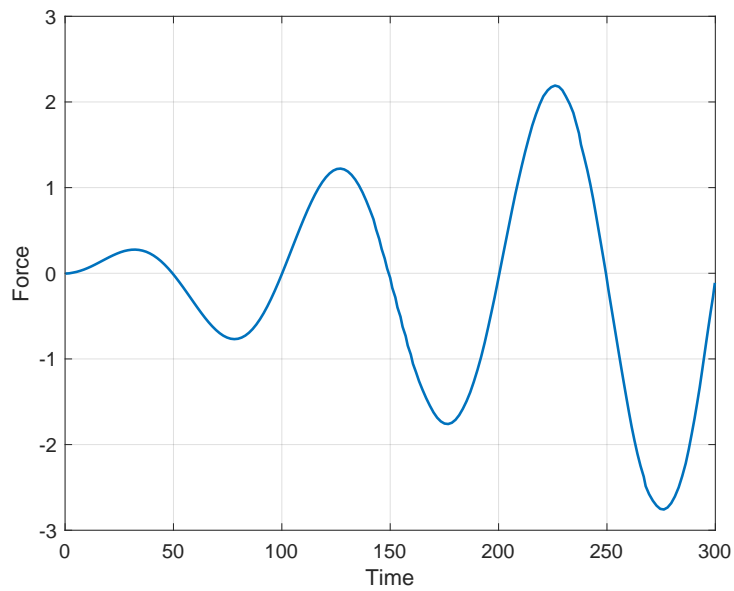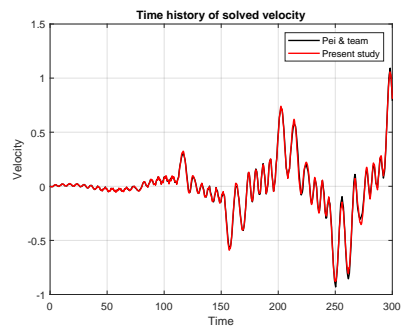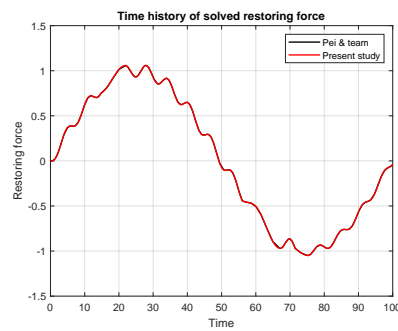

Figure B.3: Load for case study 2

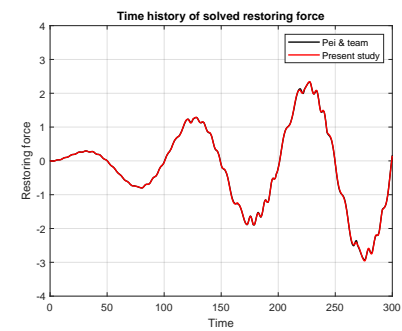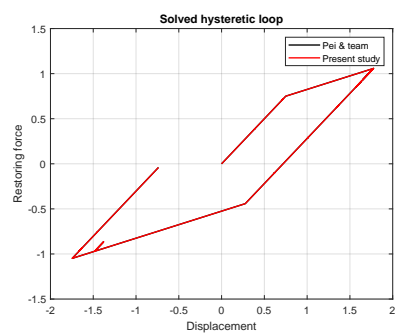(a) Displacement
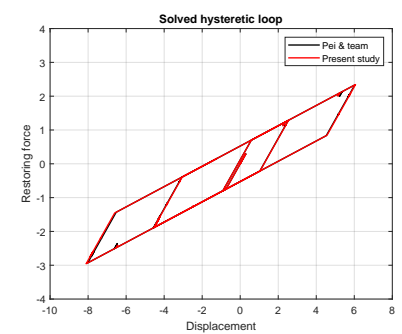
(b) Displacement

(c) Velocity

(d) Velocity

(e) Restoring force

(f) Restoring force

(g) Hysteretic loop

(h) Hysteretic loop

Figure B.4: Time history of displacement, velocity, restoring force and hysteretic loops for case studies 1 and 2